



EUROPEAN
COMMISSION

Community research

PAMINA

Performance Assessment Methodologies in Application to Guide the Development of the Safety Case

(Contract Number: **FP6-036404**)



Radionuclide migration in the near field (clay rock): sensitivity analysis on “Kd” and “solubility limit” models / geochemical transport **DELIVERABLE (D-N°:4.1.3)**

Author(s): D. COELHO (ANDRA) with contributions of:
ANDRA: B. COCHEPIN, I. MUNIER
CEA: E. PIAULT, L. TROTIGNON
IRSN: F. MARSAL, C. SERRES
JRC: K.F. NILSSON, S. PRVAKOVA
SCK-CEN: E. WEETJENS, E. MARTENS AND D. JACQUES

Date of issue of this report : **18/12/09**

Start date of project : **01/10/2006**

Duration : **36 Months**

Project co-funded by the European Commission under the Euratom Research and Training Programme on Nuclear Energy within the Sixth Framework Programme (2002-2006)		
Dissemination Level		
PU	Public	X
RE	Restricted to a group specified by the partners of the [PAMINA]	
CO	Confidential, only for partners of the [PAMINA] project	



Foreword

The work presented in this report was developed within the Integrated Project PAMINA: **Performance Assessment Methodologies IN Application** to Guide the Development of the Safety Case. This project is part of the Sixth Framework Programme of the European Commission. It brings together 25 organisations from ten European countries and one EC Joint Research Centre in order to improve and harmonise methodologies and tools for demonstrating the safety of deep geological disposal of long-lived radioactive waste for different waste types, repository designs and geological environments. The results will be of interest to national waste management organisations, regulators and lay stakeholders. The work is organised in four Research and Technology Development Components (RTDCs) and one additional component dealing with knowledge management and dissemination of knowledge:

In RTDC 1 the aim is to evaluate the state of the art of methodologies and approaches needed for assessing the safety of deep geological disposal, on the basis of comprehensive review of international practice. This work includes the identification of any deficiencies in methods and tools.

In RTDC 2 the aim is to establish a framework and methodology for the treatment of uncertainty during PA and safety case development. Guidance on, and examples of, good practice will be provided on the communication and treatment of different types of uncertainty, spatial variability, the development of probabilistic safety assessment tools, and techniques for sensitivity and uncertainty analysis.

In RTDC 3 the aim is to develop methodologies and tools for integrated PA for various geological disposal concepts. This work includes the development of PA scenarios, of the PA approach to gas migration processes, of the PA approach to radionuclide source term modelling, and of safety and performance indicators.

In RTDC 4 the aim is to conduct several benchmark exercises on specific processes, in which quantitative comparisons are made between approaches that rely on simplifying assumptions and models, and those that rely on complex models that take into account a more complete process conceptualization in space and time.

The work presented in this report was performed in the scope of RTDC 4.1.B (Clay).

All PAMINA reports can be downloaded from <http://www.ip-pamina.eu>.



Table of contents

1	BENCHMARK OBJECTIVES.....	4
1.1	INTRODUCTION.....	4
1.2	GENERAL COMMENTS.....	4
1.3	CONSIDERED WASTE TYPE AND RADIONUCLIDES.....	5
1.4	MODEL ASSUMPTIONS.....	7
2	BENCHMARK SPECIFICATIONS.....	8
2.1	ORGANISATION.....	8
2.2	INPUT DATA.....	10
2.3	REQUIRED OUTPUT DATA.....	15
2.4	INVOLVED PARTICIPANTS AND PROGRESS OVERVIEW.....	16
3	CONCEPTUAL MODEL AS DEFINED BY EACH PARTICIPANT.....	18
3.1	CONCEPTUALIZATION AND MODELLING PERFORMED BY ANDRA.....	18
3.2	CONCEPTUALIZATION AND MODELLING PERFORMED BY CEA.....	25
3.3	CONCEPTUALIZATION AND MODELLING PERFORMED BY IRSN.....	29
3.4	CONCEPTUALIZATION AND MODELLING PERFORMED BY JRC.....	36
3.5	CONCEPTUALIZATION AND MODELLING PERFORMED BY SCK*SEN.....	37
3.6	GENERAL COMMENTS.....	44
4	¹³⁵Cs TRANSFER MODELLING USING Kd/SL AND THERMODYNAMIC MODELS.....	46
4.1	AXIAL Cs TRANSFER IN THE BENTONITE PLUG OBTAINED WITH Kd/SL AND THERMODYNAMIC MODELS.....	47
4.2	RADIAL Cs TRANSFER IN CLAYSTONES OBTAINED WITH Kd/SL, LANGMUIR AND THERMODYNAMIC MODELS.....	59
4.3	2D CYLINDRICAL Cs TRANSFER AT THE HEAD OF THE DISPOSAL CELL (I.E. CLAYSTONES AND BENTONITE).....	75
5	CONGRUENT RELEASE AND COMPETITIVE / ADDITIVE EFFECTS BETWEEN RADIONUCLIDES.....	91
5.1	AXIAL Zr AND AM TRANSFER IN THE BENTONITE PLUG OBTAINED WITH Kd/SL AND THERMO DYNAMIC MODELS.....	92
5.2	1D OR 2D RADIAL AM TRANSFER AT THE HEAD OF THE DISPOSAL CELL (I.E. CLAYSTONE AND BENTONITE).....	105
6	GENERAL DISCUSSIONS.....	123
6.1	PARTICIPANTS' CONCLUSIONS.....	123
6.2	GENERAL COMMENTS.....	126



1 Benchmark objectives

1.1 Introduction

This report deals with the work of Project PAMINA, RTDC-4, WP4.1B: “Radionuclide migration in the near field (clay rock) - Sensitivity analysis on “Kd” and “solubility limit” models / geochemical transport”. It gives an overview of the benchmark results. This report is constructed as follows:

- The first section recalls the context and objectives of the benchmark
- The second section gives a synthesis of the benchmark characteristics (chemical, physical and geometrical input data), as well as participants and milestones. More details are available in the benchmark definition document (M4.1.2)
- This benchmark led to various interpretations and models. These differences and related consequences are summarized in section 3
- Section 4 is devoted to the first exercise of the benchmark: Cs transfer around a HA vitrified waste disposal cell. All participants’ results are shown one after another then similarities and discrepancies are discussed
- Section 5 deals with Am and Zr transfer. Again, results are discussed and compared
- Some conclusions and perspectives are proposed in the last section

1.2 General comments

Most performance assessment (PA) exercises represent radionuclide geochemical behaviour in terms of two parameters: Solubility Limit (SL) and distribution coefficient (Kd). The objective of this benchmark is to assess the sensitivity of PA calculations with regard to other geochemical models. It was applied to a test-case that considers the French concept for deep geological disposal of high-level waste in the Callovo-Oxfordian formation.

Kd are usually deduced from batch measurements solid/solution partitioning in well-controlled water/solid systems. Uncertainty in Kd value estimation can be represented in terms of average and extreme Kd values. Kd values are operational in that they are representative of the particular chemical conditions used for their measurement (i.e. pH, ligand concentrations...) and, in certain cases, Kd can vary as a function of radionuclide concentration for otherwise constant system parameters, Cs being the most common example.

Solubility limits are measured under well-defined conditions and saved into databases as constant values. These data are used for speciation calculations, assuming that radionuclide’s aqueous concentrations are controlled by the solid phase of highest stability with respect to the porewater composition. The relevance of such a calculation directly depends on:

- the quality of the thermodynamic database,
- the understanding of the porewater system,
- the steady state definition in time and space,



- and obviously the expertise of the modeller.

For the purpose of PA calculations, solubility limits can be estimated as constant values, if the porewater composition is also well defined and constant. Such statement is assumed for global volumes (meter magnitude), but can't expect to be relevant at shorter distances:

- If a constant SL value is defined in the whole computation domain, precipitation only takes place very close to the source term. It is then impossible to assess such model results
- Porewater composition undergoes interactions between the waste disposal components. It is therefore poorly defined in the near-field of the waste packages
- The Engineered Barrier System (EBS) degradation leads to the release of a large list of chemical elements which can interact with radionuclides. Solid-solution or co-precipitation might control the aqueous concentration of several radionuclides

These complex processes can be accounted for by performing a complete reactive transfer model. Thermodynamic models have been developed for single minerals (montmorillonite) or "simple" materials such as bentonite MX80. Solid surfaces are defined as mass concentrations of reactive sites and surface chemistry is calculated according to the overall speciation (using the mass action law). When applied to clayey systems, thermodynamic sorption models cause both surface complexation (site specific) and ionic exchange (structural charge) processes.

It is possible to model chemical evolutions (radionuclide concentration, pH or ionic strength) in the range of conditions studied for the model definition. Application of such an approach to bentonite and Callovo-Oxfordian claystone is quite limited though, because of the lack of available data. It is therefore important to show how important are the discrepancies between a fully thermodynamic approach and a K_d / SL model.

It must be highlighted that the selection of chemical models is mostly sensitive where significant disturbances are occurring. From a PA point of view, it is clear that the accuracy of a sophisticated chemical model only affects the near-field; no relevant effort is necessary for the far field, where water/rock interactions are correctly defined using a steady equilibrium state.

1.3 Considered waste type and radionuclides

Vitrified wastes (so called High Activity (HA) waste in French inventory) are sufficiently well characterized and homogeneous to define a reference test case, especially with regard to radiological and chemical inventory. C1 (HA) waste type is selected for the purposes of this exercise (see Figure 1.1).

Disposal cells and the overall design for HA wastes were defined in (Andra, 2005c). Note that this cell design isn't definitive. The main characteristics of the head part of the disposal cell and some waste packages are defined hereafter, in order to simulate both claystone and bentonite contributions to radionuclides' transport (cf. Figure 1.1). It must be highlighted here that some components of the disposal design were simplified for the benchmark:

- Intercalation blocks (designed for thermal purposes): their presence make the radionuclides flux heterogeneous along the cell axis. In a first approximation, it is proposed to attribute to the corresponding volumes the same transfer properties as those of the backfill material.
- Iron steel plug (designed for biological protection before closure): for the purposes of this exercise, we consider a direct contact between the bentonite plug and the last radwaste package.
- Iron steel containers and overpack components are not accounted for in the benchmark. They prevent from radionuclides release before 4000 years.

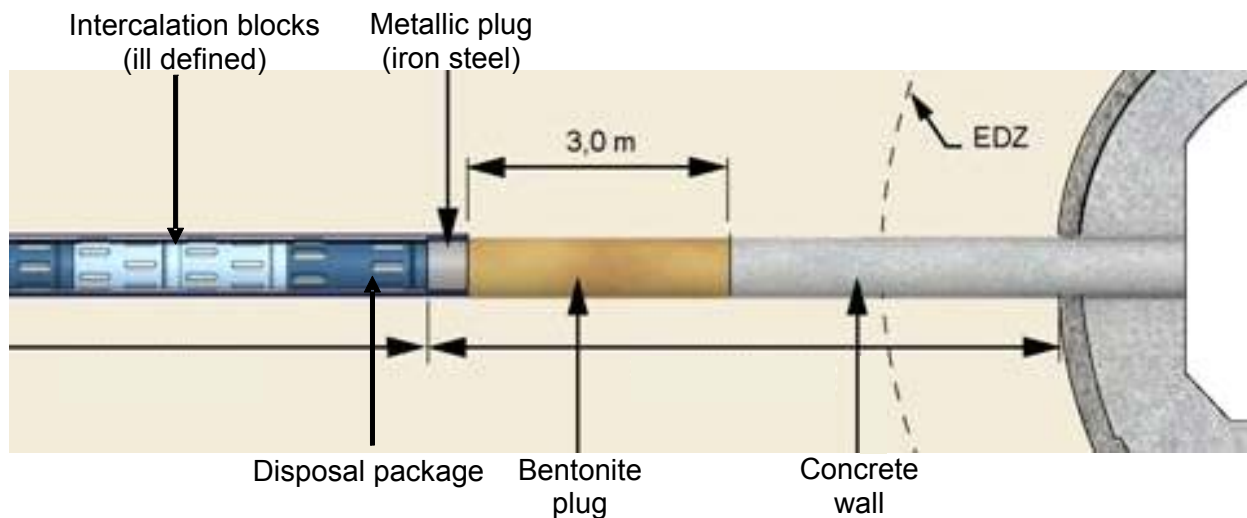


Figure 1.1: HA waste disposal cell design

The first element of interest is Caesium:

- High quantities of caesium are present in C1 (HA) wastes;
- Its solute concentration is not limited by solubility limit;
- Its transfer might be sensitive to major cations in water (Na, Ca, Mg, K, Cs, Sr);
- Its transfer might be influenced by another released cation: Rubidium;
- Its sorption isotherm has widely been measured in bentonites and a thermodynamic model is available in montmorillonite (Montmorillonite is the main reactive surface in bentonite) (Grambow et al., 2006);
- The sorption properties of Callovo-Oxfordian claystones have also been extensively measured; selectivity coefficients (Cs/Na) of illite (Illite is the main reactive surface in claystone) can be implemented;
- As far as the objective is comparison between models, these sorption models can be implemented in simplified geometries: Cs transport through bentonite (1D axial), claystones (1D radial) and in a simplified 2D geometry.

Americium and zirconium were also selected:

- The actual state of knowledge limits the application of such an exercise to the bentonite system (1D axial). However a 2D geometry is also tested;



- For zirconium, the mass ratio between stable and radio-isotope is around 20. This ratio can be estimated for Am by analogy between trivalent lanthanides and trivalent actinides: it is around 80;
- All of these elements/radionuclides will compete together for surface sites of clay minerals (especially for 'strong edge' sites);
- The aqueous concentration of all of these elements/radionuclides is limited by precipitation processes. Solubility limit can be defined by constant solubility values or calculated using a thermodynamic database (considering co-precipitation processes or not).

1.4 Model assumptions

The aim of the benchmark was dedicated to model comparison with regard to radionuclide behaviour focusing on the near-field of a disposal cell. Calculations are performed in 1D (radial and axial) and 2D (cylindrical). The recommended conceptual approach considers:

- Diffusion as the main transfer process;
- No advection nor coupled effects with mechanical phenomena;
- Fully water saturated conditions;
- Homogeneous and isotropic clayey systems (claystones and bentonite plug). However, claystones are damaged around the borehole: the excavation damaged zone (EDZ) has altered transfer (hydraulic and diffusive) properties;
- The modeled cell design is cut off in order to simplify the chemical system: there is no steel (waste package, intercalation block, overpack and metallic plug) nor concrete (plug and drift) in the benchmark model;
- Waste packages are the only source terms of the elements of interest (no consideration of the background inventory that might be defined from backfill materials or host rock);
- Radionuclides are released after the steel overpack failure at 4000 years, the temperature elevation is then negligible ($< 20^{\circ}\text{C}$);
- No radioactive decay for radionuclides (for systems to be studied). However, the radioactive decay and corresponding daughters (e.g. ^{243}Am) can be taken into account as an open option (in order to assess differences on tested outputs);
- No kinetic constraint (they are important in natural systems, but the lack of available model/data would harm the exercise). All chemical reactions are considered following an equilibrium state, with respect to significant residence time of solutes;
- All solutes have the same effective diffusion coefficient. However, ions diffuse at different rates but this can only be handled by few numerical tools. As an open option for 1D calculations, participants can carry out calculations with different diffusion coefficients for each ion.



2 Benchmark specifications

2.1 Organisation

The benchmark (WP 4.1.B - Clay) was divided into 3 parts including 2 exercises:

- Reference case: radionuclide transport modeled using Kd/SL models;
- Exercise 1: sorption of Cs with simple and thermodynamic models;
- Exercise 2: congruent release and competitive / additive effects between radionuclides.

2.1.1 ***Exercise 1: sorption of ¹³⁵Cs as a function of competing isotope (element) inventory***

Cs transfer is mainly controlled by ionic exchange. Such a mechanism is highly sensitive to aqueous concentration of the element (*i.e.* of the sum of all isotopes) and the water composition. Other competitive effects can also take place, considering the aqueous concentration of other elements such as Rb or major cations:

- C1 (HA) vitrified waste have the lowest Cs135 isotopic ratio among HA waste;
- One isotope of interest for PA: Cs135 and several isotopes included in the waste matrix: Cs133, Cs134, Cs137¹;
- Other elements also included as competitor: Rb87 for instance.

2.1.2 ***Exercise 2: congruent release and competitive/additive effects between radionuclides***

The chemical and radiological inventory of C1 (HA) waste is mainly defined with a few elements / radionuclides in the benchmark. Among this list, several chemical elements have similar behaviour with regard to sorption processes. Corresponding Kd values have been measured in batch experiments, with the groundwater composition defined in the benchmark.

The aqueous concentration of these elements / radionuclides is limited by precipitation processes. Solubility limitation can be described by three models:

1. Constant solubility values, provided from speciation calculations for the aqueous conditions of interest. The reference values were provided in the benchmark using the ThermoChimie Thermodynamic DataBase (TDB) of Andra and the reference groundwater composition;
2. Aqueous speciation, directly deduced from chemical-transfer calculations, where the stability of pure element/radionuclide phases is verified at each step. It was recommended to perform such calculations with ThermoChimie TDB;
3. Solubility limits of elements / radionuclides can be calculated as in stage 2, but considering co-precipitation processes. Such a development is associated to Am solubility, with respect to co-precipitation with lanthanides.

¹ Cs134 and Cs137 are neglected because of their half-life (considering steel overpack containment)

The exercise can be defined as:

- Comparison between Kd approach and thermodynamic sorption model, with regard to several levels of analogy / competition;
- Solubility limits (SL) analysis, with regard to several kinds of chemical analogy and with respect to co-precipitation process. Comparison with constant SL approach.

The actual state of knowledge limits the application of Exercise 2 to the bentonite plug system.

2.1.3 List of tasks and milestones defined in the benchmark

A precise list of tasks was defined in order to allow a step by step inter-comparison between every participant's results. Results reported in the next chapters refer to their corresponding task number. Test cases are independent and can be solved in one or two dimensions of space or for both.

Table 2.1.1: List of tasks defined in the benchmark

Exercises	Task	Objective	Expected results
Conceptual model	Task 0	Definition of the general framework from the benchmark's input data (geometry, boundary conditions, ionic diffusion, porosity...)	Model geometry, geochemical model
Reference cases	Task 1	Glass alteration / RN source term modelling and geochemical effects on porewater composition – 1D radial	Source term: B concentration profiles
	Task 2	RN (Cs, Zr, Am) transfer modelling with constant Kd/SL – 1D radial	Concentration profile and RN fluxes obtained with the reference PA model and parameters
	Task 3	RN (Cs, Zr, Am) transfer modelling with constant Kd/SL – 1D axial	Allows comparison with thermodynamic results in the bentonite plug
	Task 4	RN (Cs, Zr, Am) transfer modelling with constant Kd/SL – 2D cylindrical	Validity of the 1D assumption: are results along the bentonite plug and across the claystone in agreement with those from tasks 2 and 3
Exercise 1	Task 5	Cs135 transfer modelling using isotherms (including competitive effects with Cs isotopes and Rb (same data to be applied) – 1D radial	Langmuir isotherm. Comparison with task 2
	Task 6	Cs135 transfer modelling using thermodynamic model (including competitive effects and Task 1 results) – 1D radial	Comparison with tasks 2 and 5
	Task 7	Cs135 transfer modelling using thermodynamic model (including competitive effects and Task 1 results) – 1D axial	Transfer model in the bentonite plug
	Task 8	Cs135 transfer modelling using thermodynamic model (including competitive effects and Task 1 results) – 2D cylindrical applied at the head of the disposal cell (i.e. claystone and bentonite)	Validity of the 1D assumptions; comparison with task 4

Exercise 2	Task 9	Zr93 transfer modelling using thermodynamic sorption model and SL for a pure Zr solid phase (including sorption competitive effects with respect to chemical elements included in Table 2.2.3 and Task 1 results) – 1D axial	Different models for solubility limit and precipitation. Competition with trivalent and tetravalent elements.
	Task 10	Am243 transfer modelling using thermodynamic sorption model and SL for a pure Am solid phase (including competitive effects with respect to chemical elements included in Table 2.2.3 and Task 1 results) – 1D axial	Merged with task 9 because those tasks are similar and there is no coupling between Am and Zr
	Task 11	Am243 transfer modelling using thermodynamic sorption model and SL for a mixed Ln(III) solid phase (including competitive effects with respect to chemical elements included in Table 2.2.3 and Task 1 results) – 1D axial	Competition with lanthanides
	Task 12	Tentative of an overall modelling on Am243 transfer – 2D cylindrical	Application to the 2D geometry, extending to claystones the properties of bentonites.

2.2 Input data

The main data and parameters defined in the benchmark report (Milestone M4.1.2) are recalled here.

2.2.1 Transport

Data set for Callovo-Oxfordian claystones:

- Thickness = 130 m (disposal at the center)
- Dry density = 2.3 g.cm^{-3}
- Porosity for anion diffusion = 5%
- Porosity for cation diffusion = 18%
- $De(\text{anions}) = 5.10^{-12} \text{ m}^2.\text{s}^{-1}$
- $De(\text{cations}) = 2.5 \cdot 10^{-10} \text{ m}^2.\text{s}^{-1}$

Data set for EDZ: Two zones (fractured / fissured) defined as:

Extension: $0.1 \cdot \text{radius}$ (disposal cell)

- Porosity for anion diffusion = 15%
- Porosity for cation diffusion = 20%
- $De(\text{anions}) = 10^{-11} \text{ m}^2.\text{s}^{-1}$
- $De(\text{cations}) = 5 \cdot 10^{-10} \text{ m}^2.\text{s}^{-1}$

Extension: $0.7 \cdot \text{radius}$ (disposal cell)

- Porosity for anion diffusion = 5%
- Porosity for cation diffusion = 18%
- $De(\text{anions}) = 5.10^{-12} \text{ m}^2.\text{s}^{-1}$
- $De(\text{cations}) = 2.5 \cdot 10^{-10} \text{ m}^2.\text{s}^{-1}$



Data set for the bentonite plug:

- Dry density = 1.75 g.cm⁻³
- Porosity for anion diffusion = 5%
- Porosity for cation diffusion = 36%
- De(anions) = 5.10⁻¹² m².s⁻¹
- De(cations) = 1.5 10⁻¹⁰ m².s⁻¹

2.2.2 Geochemistry

The pore water composition in the near field of the waste packages will be influenced by the chemical degradation processes occurring in the cell (glass alteration, steel component corrosion, temperature elevation...). The evolution of this pore water composition can be deduced from modelling exercises. Aqueous boundary conditions are obviously defined by the geological host rock itself. Table 2.2.1 gives the groundwater composition to be considered for the far field. This water composition is deduced from geochemical modelling at 22°C, considering:

- Ionic exchange: Na/Ca, Na/Mg, Na/Sr, Na/Fe, Na/K;
- Equilibrium stability state with quartz, illite, chlorite, pyrite, calcite (+ siderite, dolomite) and celestite.

Exchangeable cations composition and solid stability constants are also given in the benchmark (M4.1.2).

Table 2.2.1: Groundwater composition

pH	pe
7.11	-2.85

mMol/L											
Al	Fe	Si	Sr	K	Mg	Ca	Na	Cl	S(6)	TIC	S(-2)
4.7.10 ⁻⁶	0.034	0.18	0.20	1.03	6.67	7.36	45.6	41.0	15.6	3.34	2.6E-7

2.2.3 C1 (HA) waste properties

Dimensions of disposal cells are given in table Table 2.2.2

Table 2.2.2: Dimensions (meter scale) of disposal cells for C1 (HA) wastes

Waste	Radius	0.35
	Length	1.587
Cell	Distance between cells	12
	Waste package number/cell	8
	Length of one cell	30
	Length of one spacer	2.472
	Length of the concrete wall *	3.3
	Length of the bentonite plug	3
	Length of the metallic plug *	0.7
	Cell length	37
	Module	Total number of waste packages
Total number of cells		580.0
Number of modules		3

(*) not represented in the benchmark

C1 (HA) waste contents, per waste form:

- Mass of the glass matrix: 400 kg
- Mass of Cs₂O: 5 kg
- Total mass of Cs: ~ 4.72 kg
- glass composition is the following (R7T7):

Oxides	Si	B	Na	Al	Ca
Weight %	45.5	14.0	9.9	4.9	4.0

Cs/Rb inventory and isotope ratios and glass composition are given in Table 2.2.3.

Table 2.2.3: C1 (HA) waste form inventory for trivalent and tetravalent elements/radionuclides

Elements	Stable isotope content (g/waste form)	Radio-isotope content (g/waste form)
Zr(IV)	$2.1 \cdot 10^{+04}$	Zr93f: $1.2 \cdot 10^{+03}$
Tc(IV)*	-	Tc99f: $1.4 \cdot 10^{+03}$
U(IV)*		U235f: $9.3 \cdot 10^{+00}$ U236f: $1.3 \cdot 10^{+01}$ U238f: $9.9 \cdot 10^{+02}$
Np(IV)*		Np237f: $2.2 \cdot 10^{+03}$
Am(III)		Am243f: $2.2 \cdot 10^{+02}$
La(III)	$2.3 \cdot 10^{+03}$	
Ce(III)*	$4.44 \cdot 10^{+03}$	
Pr(III)	$2.05 \cdot 10^{+03}$	
Nd(III)	$7.63 \cdot 10^{+03}$	
Sm(III)	$1.46 \cdot 10^{+03}$	

(*) considering reducing conditions and equilibrium assumption

Dissolution rate of C1 (HA) waste forms

Several models have been defined for glass matrix dissolution. It must be highlighted here that validity of these models are out of the scope of this sensitivity work. The source term model would be defined for C1 (HA) waste as:

- Initial stage of alteration: high dissolution rate (V_0) for 4% of the glass. The fraction of altered glass (τ) is defined as a function of glass cells characteristics.
For simplification, one can take into account an instantaneous release of radionuclides, considering proportionality between mass of dissolved glass that of released radionuclides (*i.e.* 4% of the radionuclide inventory);
- Long term stage of alteration: low residual dissolution rate (V_r). The fraction of altered glass (τ) is defined as a function of glass cells characteristics. The residual rate of dissolution $V_r(T)$ can be defined as a constant value, considering 50°C as reference temperature.

2.2.4 Sorption models

2.2.4.1 Linear isotherms

The reference case consists in modelling the transport of radionuclides (^{135}Cs , ^{93}Zr and ^{243}Am) with a Kd/SL model. Sorption of Cs is clearly a function of [Cs] in solution. It is then difficult to define properly a reference value:

- In claystones, minimum Kd values are measured around $10^{-2} \text{ m}^3.\text{kg}^{-1}$ for high [Cs] values (*i.e.* 10^{-2} Mol/L) and higher Kd values (up to $1 \text{ m}^3.\text{kg}^{-1}$) are measured with lower [Cs] (*i.e.* 10^{-8} Mol/L).
- In the bentonite plug, a reference value is defined as $\text{Kd} = 0.1 \text{ m}^3.\text{kg}^{-1}$; a conservative value is defined as $\text{Kd} = 6.10^{-2} \text{ m}^3.\text{kg}^{-1}$.

Kd reference values for Cs, Zr and Am are recalled in Table 2.2.4

Table 2.2.4: $\text{Kd} (\text{m}^3.\text{kg}^{-1})$ of radionuclides of interest in claystones and bentonite

	claystones	bentonite
Cs	0.3	0.06 or 0.1
Zr(IV)	10^{2^*}	10^{2^*}
Am(III)	$10^{1.7}$	$10^{1.7}$

* These values have been corrected from the benchmark definition

2.2.4.2 Langmuir isotherm

A Langmuir model is defined for Cs sorption in claystones.

$$C_{ads} = \frac{A.C_{aq}}{B + C_{aq}}$$

Where C_{ads} is the sorbed concentration in $\text{mol}\cdot\text{g}^{-1}$ and C_{aq} is the aqueous concentration at the equilibrium state, in $\text{mol}\cdot\text{l}^{-1}$.

Isotherm parameters are defined for two concentration ranges:

Model A: for $[\text{Cs}^+] \leq 10^{-5}$ M in solution,

$$A=1.8462 \cdot 10^{-7} \text{ mol}\cdot\text{g}^{-1}$$

$$B=4.7552 \cdot 10^{-7} \text{ mol}\cdot\text{l}^{-1}$$

Model B: for $[\text{Cs}^+] \geq 10^{-5}$ M in solution,

$$A=0.00012 \text{ mol}\cdot\text{g}^{-1}$$

$$B=0.00492 \text{ mol}\cdot\text{l}^{-1}$$

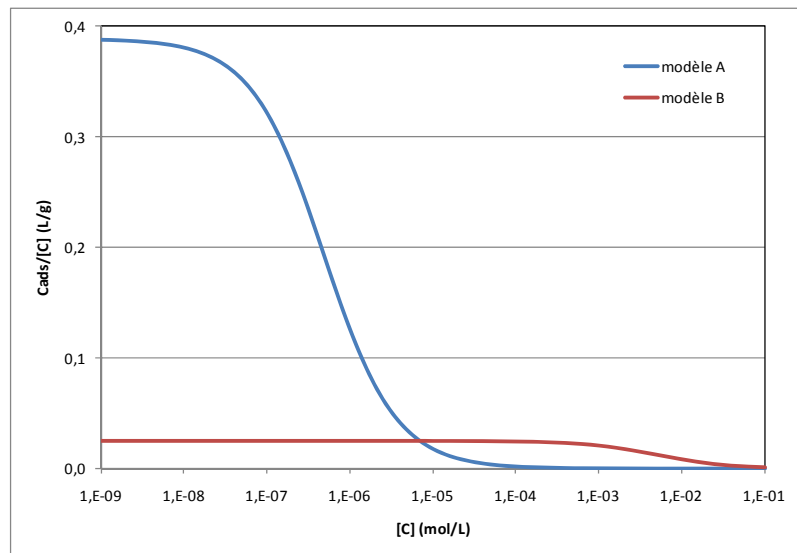


Figure 2.2.1: *Cs sorption isotherms calculated from simplified Langmuir models A and B*

2.2.4.3 Thermodynamic model

A non electrostatic surface complexation / ion exchange model was defined for montmorillonite (which is considered as the main reactive surface in the bentonite), by Grambow et al. (2006) involving 1 strong site and 2 weak sites.

The understanding of the surface sorption processes on claystones is poorly acquired at the present state of knowledge. For the caesium exercise, some approximations can be applied:

- Caesium is only sorbed by ionic exchange (no specific site)
- Selectivity coefficients can be used for major cations
- A rough estimation is proposed for Cs selectivity coefficient, using typical observations for illite. $K(\text{Na}/\text{Cs})$ is a function of $[\text{Cs}]$: The selected value corresponds to an average of Cs concentration applied to one exchange site



That leads to define Table 2.2.5, associated to characteristics of claystones at the level of the Meuse / Haute Marne (MHM) Underground Research Laboratory (URL).

Table 2.2.5: Selectivity coefficients to be used on claystones (Gaines-Thomas)

Log K(Na/Ca)	Log K(Na/Mg)	Log K(Na/Sr)	Log K(Na/Fe)	Log K(Na/K)	Log K(Na/Cs)
0.7	0.7	0.7	0.7	1.23	2
S _{BET} ^{N₂} = 37.3 m ² /g			CEC = 18.8 meq/100g		

Thermodynamic data sets for elements of interest (Zirconium, Technetium (IV), Americium (III), Uranium (IV) and Lanthanides (III)) are provided in the benchmark (M4.1.2 report). The reference database is ThermoChimie, developed by Andra.

2.3 Required output data

The following information was asked to participants in order to compare the tested models and numerical codes. Prior to addressing test cases, an optimization of mesh spacing and time stepping should have been driven. Furthermore, the computation time of each driven case gives an indication of the computational cost of the various models. Participants were asked to explain their geochemical models in details (including solved equilibriums and related solutes and solid phases).

In order to allow comparison between models, all participants had to draw the same output:

- Plots of radionuclide concentrations (Cs, Zr and Am), relevant species (B) and parameters (pH) over the domain at different times. Considering estimated transfer times, plots should be drawn 100, 1 000, 5 000, 10 000 and 50 000 years after the radionuclide release (*i.e.* after 4000 years from the waste packages setting). These plots are drawn (see Figure 3.5.4):
 - For axial 1D and cylindrical 2D models, along the axis of the bentonite plug (from the waste cell to the end of the 3 meters long plug). Note that the next component (concrete plug) is not accounted for in the model
 - For radial 1D and cylindrical 2D models, along a 10 meters long line perpendicular to the disposal cell, this axis crosses the middle of the disposal cell.
- For 2D cylindrical dimensions, iso-concentrations of radionuclide concentrations (Cs, Zr and Am), relevant species (B) and parameters (pH) over the domain should also be given 100, 1 000, 5 000, 10 000 and 50 000 years after the radionuclide release
- Plots of the evolution with time (from 0 to 50 000 years) of Cs (exercise 1) or Zr and Am (exercise 2) concentrations, at 4 points (located 0 and 1m (Cs) / 0.1m (Zr, Am) from the waste along the 2 axis defined above)
- Plots of radionuclide isotherms (solid vs. solution) if relevant for interpretation.



2.4 Involved participants and progress overview

Five organizations were involved in this benchmark: Andra, CEA, IRSN, JRC and SCK*CEN.

The benchmark specifications (M.4.1.2 Milestones report) were delivered by Andra (Eric Giffaut and Alain Dimier) in July 2007.

- First calculations were achieved in February 2008 by JRC who completed constant Kd/SL models. This work was done by a post-doctoral grant (Slavka Prvakova) who left JRC just after, so JRC couldn't take part in the scientific meetings held with all other participants during the last year of the project (from September 2008 to September 2009).
- IRSN (François Marsal) already did part of the work before September 2008, these preliminary results could be presented at the meeting at Hyères. Their experience allowed to point out some errors and missing data in the benchmark definition and to suggest some assumptions to be applied by the other participants. They also shared the draft version of their milestones report (M4.1.19) with other participants in April 2009.
- Andra started their calculations in August 2008 (Benoit Cochepin and Isabelle Munier). Their objective was to achieve a complete geochemical model, including mineral transformations. They faced many difficulties for solving the geochemical model because the glass waste dissolution rate yields very high solutes concentrations.
- SCK*CEN involved 3 engineers for this project: Eef Weetjens, Evelien Martens and Diederik Jacques. Their models focused more on the two-dimensional radial transport within the host formation than on the axial transport within the bentonite. The thermodynamic models included various degrees of competition for sorption sites and the simple sorption models (Kd and Langmuir) were systematically benchmarked with other numerical codes. Their work was completed by May 2009 (including Milestones report M4.1.17).
- CEA (Emmanuel Piault) started in May 2009. They could however achieve most tasks by the end of the project.

The current report is a synthesis of all these contributions summarized in Table 2.4.1. This edition was handled by Andra (Daniel Coelho) thanks to all participants' involvement.



Table 2.4.1: Progress overview

Exercises	Task	Andra	CEA	IRSN	JRC	SCK*CEN
Reference cases: Kd/SL transfer modeling	Task 2: 1D radial	done	done	done	done	done
	Task 3: 1D axial	done	done	done	done	done
	Task 4: 2D cylindrical		done	done	done	done
Exercise 1: Cs transfer	Task 5: Langmuir isotherm, 1D radial	done	done	done		done
	Task 6: Thermodynamic model, 1D radial	done	done	done		done
	Task 7 Thermodynamic model, 1D axial	done	done	done		
	Task 8 Thermodynamic model, 2D cylindrical		done	done		done
Exercise 2: Am/Zr transfer	Tasks 9 - 10: Thermodynamic model, 1D axial	done	done	done		
	Task 11: competing lantanides	done	done	done		done
	Task 12: 2D cylindrical		done	done		done



3 Conceptual model as defined by each participant

The geochemistry in the near field (claystone and bentonite plug) is influenced by the alteration of glass and this must be accounted for in the thermodynamic model. For that reason, the first task of the benchmark consisted in modelling the geochemistry near the glass source term.

The specifications given in the benchmark were numerous and it was necessary to introduce some further assumptions in order to perform the calculations with the various numerical codes. Therefore the models implemented by participants are not strictly identical, they are described and compared to each other in this section. In addition, some minor modifications were applied to the benchmark definition since its edition (M.4.1.2): for instance, Zr's Kd values and the glass dissolution rate had to be adjusted.

As discussed with participants, boron concentration profiles can be used in order to illustrate the results of the source term's model (hydraulic + chemistry). If some, pH spatial and temporal variations (and its impact on mineralogy alteration) must be discussed. Some additional information was asked for:

- Model general statements:
 - Numerical code used for every simulation, limitations and additional assumptions related to the code and consequences, calculation duration times
 - Geometry and void volumes, mesh construction / discretization, boundary conditions, differences between 1D and 2D models
 - Porosity, transport models and parameters
- Geochemical model:
 - Water chemistry fixed or related to equilibrium with minerals (calcite ...), mineral and clay definition. Solid/solution equilibrium
 - Methods for the chemical model, such as electroneutrality obtained with a free Cl concentration
- Radionuclide's thermodynamic model:
 - Sorption defined by fictive resin or by real sorption surfaces. Definition of sorption surfaces
 - Glass chemistry and alteration model, release kinetics
 - Implemented thermodynamic database

3.1 Conceptualization and modelling performed by Andra

The chemical-transport simulation tool used to perform this study is Phreeqc v2.16 (64bits Linux version). The radial transport has been set in Phreeqc enabling the fulfilment of tasks 1, 2, 5 and 6 (see Table 2.1.1). However, due to a lack of time to set the 2D in Phreeqc, 2D cylindrical simulations have not been performed (tasks 4, 8 and 12). The 2D simulation initially considered in task 12 is substituted by a simulation in radial 1D.

3.1.1 Geometry

The radionuclide release is supposed in these simulations to start after the steel overpack failure (i.e. after 4,000 years).

The glass waste package is represented by a unique mesh holding all the radionuclides present in the waste package. The waste package is also supposed to be in contact with the host rock, thus neglecting the chemical interactions of the glass with the steel overpack and with metal plug in the storage cell head. The simulated system considers a direct contact of the glass waste package with 3 linear meters of the bentonite plug in the axial direction, discretized in 60 cells with a length of 5 cm (Figure 3.1.1.a). In the radial direction, 20 m of claystones are divided in 2 zones: the first 28 cm (discretized in 2 cells) are the EDZ and 19.72m of undisturbed claystones (discretized in 100 cells of 20 cm) (Figure 3.1.1.b).

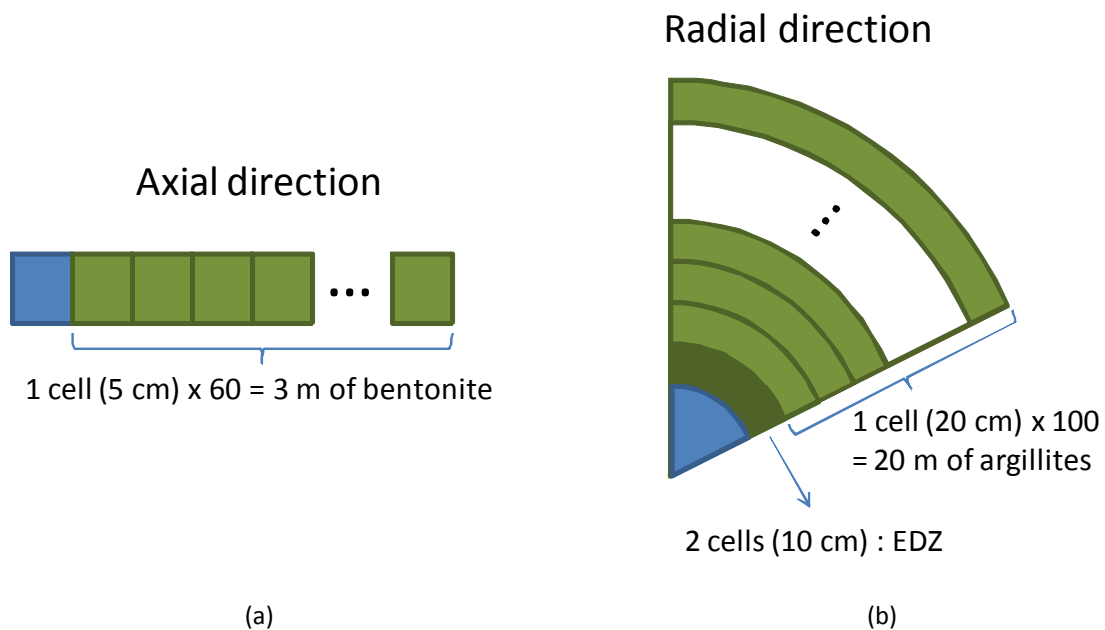


Figure 3.1.1: Schematic view of the numerical discretization in axial (a) and radial directions (b)

3.1.2 Transport

The simulated system is supposed to be initially fully saturated. The only transport phenomenon authorized is the diffusion of aqueous species (Table 3.1.1). The effective diffusion coefficient of aqueous species is supposed to be identical for each species and imposed by the crossed material.

Table 3.1.1: Transport properties in the bentonite plug and in the host rock

	Bentonite	Claystones	EDZ
Porosity (-)	0.36	0.18	0.20
$D_{\text{eff}} (\text{m}^2 \cdot \text{s}^{-1})$	1.5×10^{-10}	2.5×10^{-10}	5×10^{-10}
Density ($\text{g} \cdot \text{cm}^{-3}$)	1.75	2.3	2.3

3.1.3 Geochemistry

The database used to perform these simulations is the Thermoddem database developed by the BRGM and available online (<http://thermoddem.brgm.fr/>). For exercise 2, the benchmark suggests to consider new aqueous and mineral species defined in the Thermochimie database and manually introduced in the input scripts. The thermodynamic equilibrium approach is always considered in this study with a constant and homogeneous temperature of 25°C.

The benchmark's definition report didn't contain enough information about mineral phases and proportions to model both bentonite and the host rock, so most participants (Andra, CEA, IRSN, SCK*CEN) decided to use the mineralogical assembly described by the BRGM (see Gaucher et al., 2004).

3.1.3.1 Callovo-Oxfordian claystones

The retained model to represent the claystone's mineral composition comes from the study performed by the BRGM for Andra's Simulations Program. The constitutive mineral phases of the claystone were defined in the update of the THERMOAR model (Gaucher et al., 2006a; Gaucher et al., 2006b; Gaucher et al., 2007). The mass fraction of each phase comes from the mineralogical database of the BRGM (Lerouge et al., 2006) and is extracted from the C2b2 level of the experiment performed in the Bure URL (Table 3.1.2).

Table 3.1.2: Mineral phases considered to represent the Callovo-Oxfordian claystones

Minerals	Structural formula	Mass content	log K @ 25°C
Calcite	CaCO ₃	0.22	1,847
Célestine	SrSO ₄	0.01	-6,6
Chlorite	Fe ₅ Al(AlSi ₃)O ₁₀ (OH) ₈	0.02	51,0
Dolomite	CaMg(CO ₃) ₂	0.04	3,5
Illite	K _{0,85} Mg _{0,25} Al _{2,35} Si _{3,4} O ₁₀ (OH) ₂	0.34	10,8
Feldspath	K(AlSi ₃)O ₈	0.03	0,0438
Pyrite	FeS ₂	0.01	-104,7
Quartz	SiO ₂	0.24	-3,7
Sidérite	FeCO ₃	0.01	-0,5
Smectite	(Ca _{0,01} Na _{0,434} K _{0,026})(Si _{3,612} Al _{0,388})(Al _{1,608} Fe _{0,222} Mg _{0,228})O ₁₀ (OH) ₂ ·5.441H ₂ O	0.08	5,445

The pore water model is calculated using:

- Ion exchange only on the smectite phase;
- The consideration of Daphnite-14 Å / Illite Mg couple to represent the chlorite / illite couple;

- The interstratified Illite/smectite is supposed to be suited by separated illite and smectite poles whose relative proportions respect the abundance values in the host rock.

The pore water composition in equilibrium with the mineralogical assembly and exchange sites is presented in Table 3.1.3.

The equilibrated water presents few differences with that of the benchmark definition (see Table 2.2.1). These differences must at least partially come from the choice made in the selection of mineral phases to represent the claystone material. The host rock appears to be stable during the radionuclide release and no mineral transformation is observed.

The secondary mineral phases (saponite, zeolites) do not pretend to stand for representing the glass-claystone interaction. However, it enables the initial phases to dissolve if the equilibration with the injected water requires it.

Further information about secondary mineral phases (necessary for the initial glass-claystone-mineral equilibrium) is given in the M4.1.18 report.

Table 3.1.3: Composition of the claystone's porewater equilibrated with minerals and exchange sites

	Unit	Values
Temp	°C	25
pH	-	7.21
pe	-	-3.4
Al	mmol/L	7.10 ⁻⁶
Ca	mmol/L	8.8
Cl	mmol/L	41.0
Fe	mmol/L	0.0484
K	mmol/L	0.83
Mg	mmol/L	5.58
Na	mmol/L	45.8
S(VI)	mmol/L	16.3
Si	mmol/L	0.18
Sr	mmol/L	0.21
TIC	mmol/L	2.53

3.1.3.2 Bentonite plug

The plug contains 70% of swelling clay (MX80 bentonite) and 30% of siliceous sand (ESDRED sand). Its porosity is 36%. The mineral composition of the swelling clay presented in Table 3.1.4 comes from Sauzeat et al. (2001). The pore water composition (at equilibrium with this mineral assembly and considering the exchange sites) shown in Table 3.1.5 was calculated assimilating ankerite to dolomite and goethite to siderite. See M4.1.18 report for further details.

Table 3.1.4: Mineral composition of the swelling clay (MX80 bentonite)

Mineral	Structural formula	Mass fraction (g/g solid)	log K @ 25°C
Plagioclases	NaAlSi ₃ O ₈	0.065	2.74
Calcite	CaCO ₃	0.006	1.847
Chlorite	Fe ₅ Al(AlSi ₃)O ₁₀ (OH) ₈	0	51.0
Dolomite	CaMg(CO ₃) ₂	0.008	3.5
K Feldspath	K(AlSi ₃)O ₈	0.014	0.0438
Smectite	(Ca _{0.01} Na _{0.434} K _{0.026})(Si _{3.612} Al _{0.388})(Al _{1.608} Fe _{0.222} Mg _{0.228})O ₁₀ (OH) ₂ :5.441H ₂ O	0.559	5.445
Pyrite	FeS ₂	0.004	-104.7
Quartz	SiO ₂	0.32	-3.7
Siderite	FeCO ₃	0.004	-0.5

Table 3.1.5: Equilibration results of the bentonite porewater with minerals and exchange sites

	Unit	Values
Temp.	°C	25.
pH	-	8.4
pe	-	-4.85
Al	mmol/L	4.43e-5
Ca	mmol/L	0.0625
Cl	mmol/L	41.0
Fe	mmol/L	0.00843
K	mmol/L	0.346
Mg	mmol/L	0.0378
Na	mmol/L	101.
S	mmol/L	16.4
Si	mmol/L	0.192
TIC	mmol/L	26.6

When the radionuclide transfer is modelled using the K_d model, the injected water does not induce smectite dissolution during the simulations, but other minerals may dissolve or precipitate. When sorption is represented with the thermodynamic model, the mineral assembly may undergo some transformations. The dissolution of smectite occurs in the simulation of the task 9, as presented in Figure 1.1, thus decreasing the number of sorption sites.

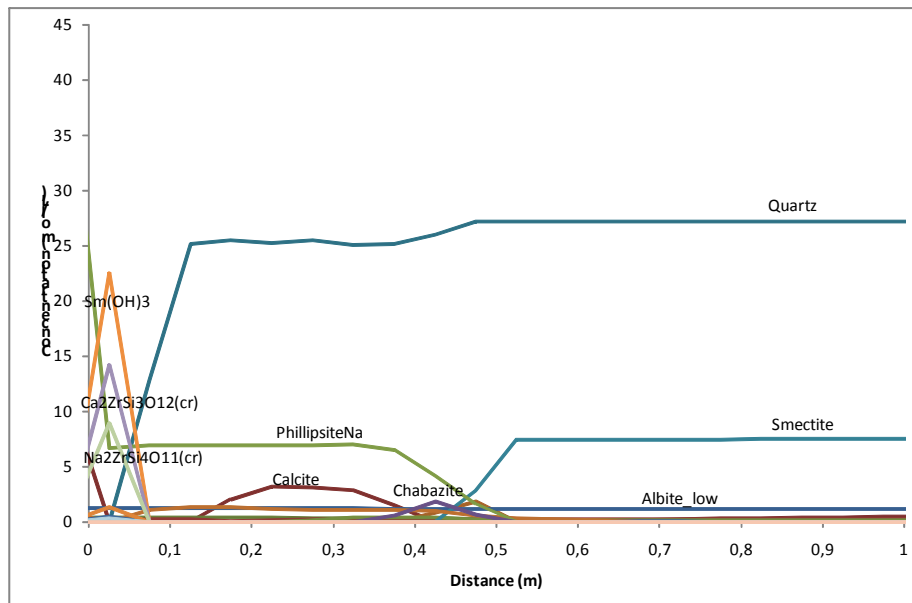


Figure 3.1.2: Mineral concentrations as a function of the distance from the glass waste after 50000 years (task 9 of the benchmark: axial coordinates)

3.1.3.3 Representation of the K_d/S_L and Langmuir models in Phreeqc

Neither the K_d model nor the Langmuir model are available as an option in Phreeqc. However, the use of surface sites can lead to an equivalent representation as the K_d model: If we suppose a K_d sorption model applied to an aqueous species 'Aq' and the definition of a sorption site 'Sor' in a huge amount (here set to 10100 moles), we can define the following equilibration equation: $Sor + Aq \leftrightarrow SorAq(\text{sorbed})$ such as the corresponding mass action law is: $\log(K) = -100 + \log(K_d)$ (see USGS internet site for more explanations). It is thus possible to impose the K_d values for Zr(IV), Tc(IV), U(IV), Ln(III) and Am(III). It is important to notice in that conditions of definition, it is possible to observe K_d variations with ionic strength or electrochemical potential variations.

The solubility of a radionuclide is set with the definition of fictive mineral such that its equilibrium constant is set to impose the desired solute concentration defined in Table 5.1.

Concerning the Langmuir model, the same method can be defined to represent the sorption in Phreeqc, excepted that two surface sites must be defined because two models are considered following the Cs concentration range (see section 2.2.4.2).

3.1.3.4 Source term

In the presented simulations, all the stock of radionuclides is supposed to be available and it diffuses in the unique direction defined by the 1D simulation. As a consequence, 1D cartesian (resp. radial) simulations cannot be considered as a longitudinal (resp. transversal) slice of 2D simulations.

The kinetics controlled dissolution of a radionuclide fictive mineral is used to simulate the radionuclide release with a kinetic rate (expressed in moles per unit of time) matching the imposed flux defined in the benchmark (expressed in moles per unit of time and surface) and recalled in section 2.2.3.

The use of the V_0 - V_r release kinetic rate recommended in the benchmark definition could lead to convergence difficulties. Moreover, the V_0 term leads to solute concentrations which would need the use of Pitzer or SIT correction model of activity. As a consequence, the whole tasks are treated with a unique V_r release rate from the glass dissolution ($V_r = 8.5 \cdot 10^{-9}$ /day at the reference temperature 323 K). The released aqueous species from the glass dissolution and their amount are listed in Table 3.1.6. For Caesium, only Cs133 and Cs135 are considered in the simulations, Cs134 and Cs137 isotopes being neglected because of their short half-life, in agreement with the benchmark instructions.

Table 3.1.6 : Oxide composition of the dissolved glass

Oxides	Mass Fraction (%)
SiO ₂	57.42
B ₂ O ₃	15.22
Na ₂ O	12.06
Al ₂ O ₃	3.45
CaO	5.40
Cs ₂ O	0.34
Rb ₂ O	0.05
ZrO ₂	4.6
Am ₂ O ₃	0.01
Ln ₂ O ₃	1.12
UO ₂	0.07
TcO ₂	0.27

The use of V_r dissolution rate leads to the consumption of 16% of the initial glass quantity after 50,000 years (see Figure 3.1.3).

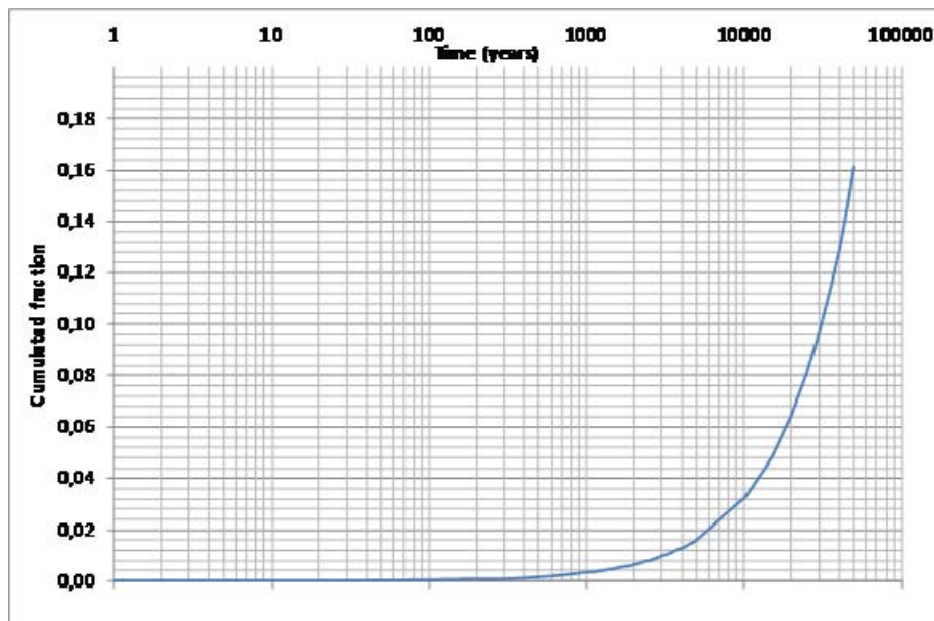


Figure 3.1.3: Cumulated mass fraction of dissolved glass

3.2 Conceptualization and modelling performed by CEA

3.2.1 Codes and Geometries

The Pamina exercise has been done with the Alliances platform developed by Andra, CEA and EDF. This platform allows different possibilities for generalized transport and for reactive transport. We chose to use the Cast3m code for generalized transport calculations and the coupled reactive transport code Alichess-Cast3m which is a reactive transport code based on the Chess chemistry solver (as in Hytec, and developed by the Mines school and “Pole Geochimie Transport”) and the Cast3m transport code.

Using these codes implies some restrictions as using 2D description with an angular sector for 1D radial calculation, and using 3D description with an angular sector for 2D radial calculation.

For the axial cases, we chose to represent three materials: Intercalation zone, Radwaste zone and Bentonite zone (Figure 3.2.1). In the same way, the radial cases take into account the radwaste, the EDZ zone and the claystone zone (Figure 3.2.2). For 2D calculations, the geometry takes into account the five materials previously used.

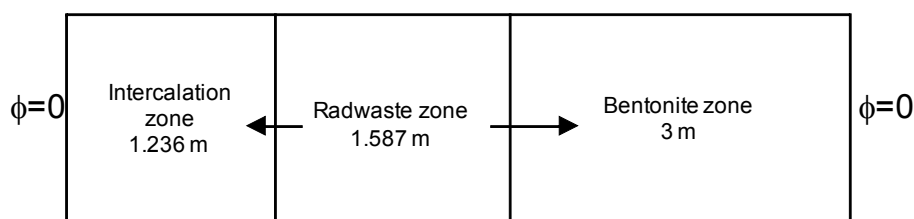


Figure 3.2.1: Overview of spatial zones distribution, axial case

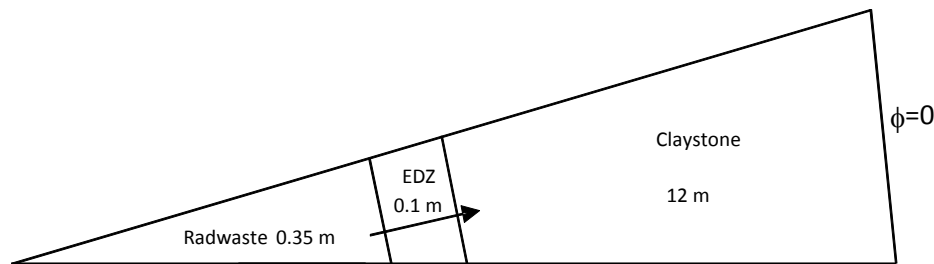


Figure 3.2.2: Overview of spatial zones distribution, angular sector (for radial cases)

3.2.2 Source term modelling

The source term is taken as described in appendix 3 of Pamina document (Andra, 2007) and recalled in section 2.2.3. The parameters used allow determining V_0 and V_r . As the duration time for V_0 is short, we made the following approximation: the release during V_0 is a labile part. This part is evaluated at 4% of the whole inventory. For the V_r flux, we could compute from the given formula at 50°C a yearly released fraction of $3.13 \cdot 10^{-6} \text{ y}^{-1}$.

For Cs, we took into account the 133 and 135 isotopes, and we neglected the radioactive decay during the time period considered in this benchmark (50,000 years).

3.2.2.1 Kd and Langmuir approaches

For the reference cases, a linear Kd approach is taken into account. For task 5, a Langmuir isotherm is considered. The code doesn't allow taking simultaneously the model A and B defined in the Pamina document. Then we arbitrary chose to conduct simulations with the model B.

For these cases, the way the different source terms are simulated depends on the geometrical approach. In the 1D axial case, the initial release is distributed over the cells representing the radwaste and afterwards a source term over the radwaste surface is taken into account. For 1D radial and 2D radial simulations, a similar approach is taken, the initial release and the source term being balanced by the angular surface or the angular volume.

Once the geometrical ratio is defined, the source term depends on the radionuclide transport to be simulated, namely Cs, Rb, Am or Zr. As an example, for Cs the initial release is of 0.869 mol (0.116 kg) and afterwards a flux of $6.54 \cdot 10^{-5} \text{ mol/year}$ is taken. This was computed from the yearly released fraction (see section 3.2.2).

3.2.2.2 Thermodynamic approach

Here, the source term is issued from the data provided in the benchmark definition and recalled in section 2.2.3. C1 (HA) vitrified waste (R7T7 glass) composition is given here by decreasing amount SiO_2 (45,5 %), B_2O_3 (14 %), Na_2O (9.9 %), Al_2O_3 (4.9 %) and CaO (4 %). These ratios enable to define the initial state for the radwaste equilibrium.



A kinetic term is used to simulate the influx induced by glass alteration. A tracer is introduced in the glass formula in order to check the mass balance; it shows that the kinetic definition of the glass dissolution rate fits V_0/V_R with less than 3% discrepancy.

Equilibrium constants for heterovalent reactions are corrected by the concentration of sites in the soil.

It is to note that simulations, apart from simulation CPU time, were difficult to get converged; the fixed point residual shows a “stochastic” evolution, that parameter making the choice of the residual level of convergence difficult. That is why a coarse residual convergence level has been used.

3.2.3 *Transport parameters*

We considered five zones in the simulations: bentonite, claystone, radwaste, intercalation and EDZ. Their properties are summed up in Table 3.2.1. All these values come from the section 2.2.1, except for the intercalation and the radwaste zones:

Table 3.2.1: *Transport properties for bentonite, intercalation, EDZ and claystone zones*

		bentonite	claystone	EDZ	radwaste	intercalation
Porosity	-	0.36	0.18	0.18	1	0.4
D_{eff}	m ² .s ⁻¹	1.5 10 ⁻¹⁰	2.5 10 ⁻¹⁰	5. 10 ⁻¹⁰	3. 10 ⁻⁹	2. 10 ⁻⁹
Density	g.cm ⁻³	1.75	2.3	2.3		1.75

3.2.4 *Initial equilibrium for thermodynamic approach*

Thermodynamic simulations are using three equilibriums, one for the radwaste zone, one for the claystone and one for the bentonite. The groundwater composition is defined in section 2.2.2.

Hereafter we give, for the main ions, the pore water description of the bentonite zone at equilibrium as issued from Chess (Table 3.2.2).

Table 3.2.2: *Bentonite pore water equilibrium description*

		Bentonite pore water
Temperature	°C	22
pH		7.7
Pe		-3.84
Ionic str.		0.085
Fe[2+]	mol/l	$1.889 \cdot 10^{-3}$
Sr[2+]	mol/l	$1.838 \cdot 10^{-3}$
K[+]	mol/l	$2.997 \cdot 10^{-2}$
Mg[2+]	mol/l	$1.76 \cdot 10^{-1}$
Ca[2+]	mol/l	1.794
Cl[-]	mol/l	$4.1 \cdot 10^{-2}$
SO4[2-]	mol/l	$1.25 \cdot 10^{-2}$
SiO2(aq)	mol/l	5.663
HCO3[-]	mol/l	0.9714

The chemistry of the zone bearing the canister is described hereafter (Table 3.2.3).

Table 3.2.3: *Canister pore water equilibrium description*

		Radwaste pore water
Temperature	°C	22
pH		7.
Pe		8.4338
Ionic str.		0.1494
H[+]	mol/l	$1.306 \cdot 10^{-7}$
Ca[2+]	mol/l	$2.056 \cdot 10^{-2}$
Na[+]	mol/l	$8.37 \cdot 10^{-2}$
SiO2(aq)	mol/l	$1.762 \cdot 10^{-4}$
Cl[-]	mol/l	0.127
Rb[+]	mol/l	$7.28 \cdot 10^{-4}$
Cs[+]	mol/l	$1.384 \cdot 10^{-3}$

3.2.5 *Mesh sensitivity study*

A grid sensitivity study has been carried out on the task 2 exercise. The results (Figure 3.2.3) show that spreading of ions also depends on mesh quality within the scope of a numerical study; it also gives an estimation of the error made on meshes used all along that study. The strong gradients induced by some high Kd values conducted to grid refinement within the scope of the present study

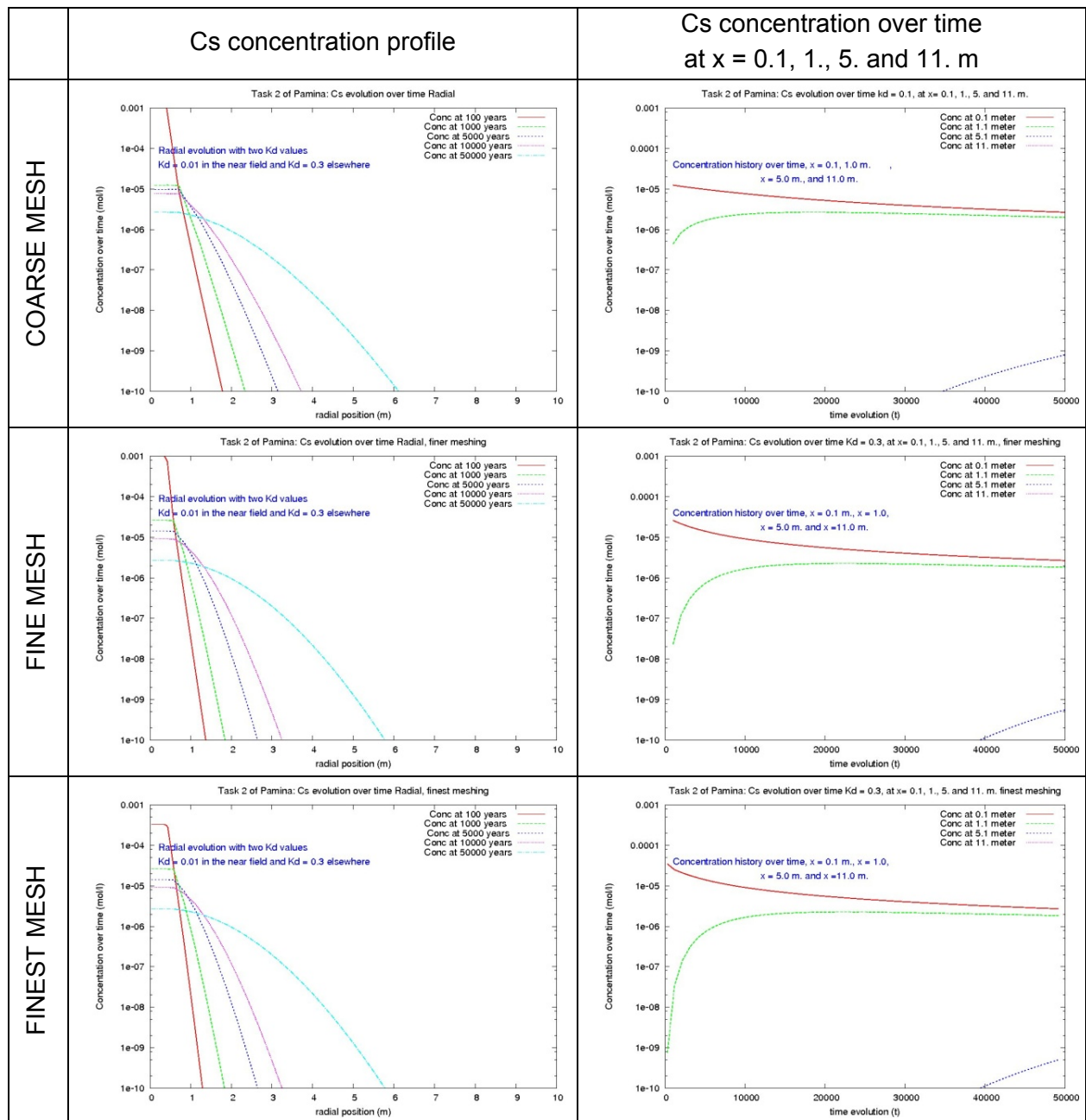


Figure 3.2.3 : Task2, Influence of the mesh size on the Cs concentration profile and the Cs concentration over time at x = 0.1, 1., 5. and 11. m

3.3 Conceptualization and modelling performed by IRSN

3.3.1 Codes and geometry

The whole set of benchmark tasks have been performed with HYTEC (van der Lee *et al.* (2003); van der Lee (2005)), which is a reactive transport code developed by ARMINES (<http://pgt.geosciences.enscm.fr/>) commonly used for transport in porous media under saturated and unsaturated conditions.

The MELODIE software, which is a numerical tool developed by IRSN (<http://net-science.irsn.org/scripts/net-science/publigen/content/templates/show.asp?P=3133&L=FR>) to model the transport of radionuclides in the context of radioactive waste disposal, has also been used to perform constant K_D /SL calculations in order to compare the results with the software specifically used by IRSN for performance assessment.

As advised in the benchmark definition, the present study does not consider the iron steel plug. The system simulated thus includes the 3 m long bentonite plug in direct contact with a radwaste package. For simplification, the concrete plug is also not considered. Two 1.5 m waste packages and two 2.5 m intercalation blocks complete the disposal cell simulated (1D-axial). In 1D-radial and 2D-cylindrical simulations, migration of radionuclides outside the primary waste package (radius = 35 cm) is modelled over about 5 m in the claystone, subdivided into 28 cm of excavated damaged (corresponding to 80 % of the disposal cell radius) and 4.37 m of undisturbed Callovo-Oxfordian claystone. The 2D-cylindrical simulation grid is pictured in Figure 3.3.1.

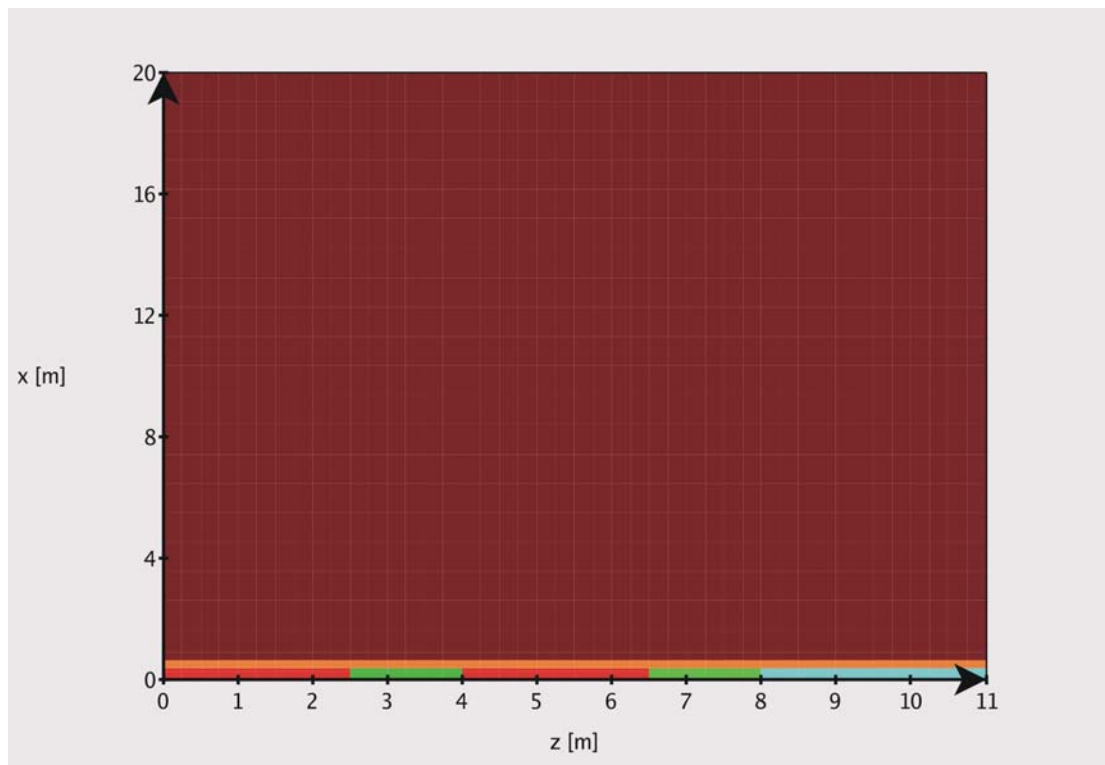


Figure 3.3.1: 2D-cylindrical grid used in the HYTEC calculations: host rock (brown), EDZ (orange), waste packages (green), MX-80 bentonite (blue), backfill (red)

3.3.2 Transport

As recommended for the benchmark, clayey systems are considered as homogeneous porous media and no coupled effects with regard to hydraulic mechanisms are accounted for. The whole system is assumed to be fully saturated in the calculations and diffusion is considered



as the predominant transport process. HYTEC being not able to consider a specific diffusion coefficient for each species in solution, all ions are supposed to diffuse at the same rate within each part of the simulated domain. Cation transport parameters selected for the present study (see section 2.2.1) are the most conservative values proposed in the benchmark definition (anionic exclusion is not taken into account in the present work).

3.3.3 Geochemistry

3.3.3.1 Host rock

No recommendation being given in the benchmark, the mineral composition of claystones taken into account in the calculations is, by wt. % decreasing order: clay minerals (50%), quartz (26%), calcite (17%), siderite (6%) and pyrite (1%). This composition is in a good agreement with values usually given for Callovo-Oxfordian claystones (Gaucher et al., 2004). The whole set of mineral proposed in the benchmark definition for the claystone modelling has not been exactly taken into account in order to match as well as possible with the host rock groundwater composition, also given in the benchmark definition. Thus, illite and chlorite are not explicitly accounted for: clay minerals take place in the simulation only for the sorption processes occurring on their surface and are represented by montmorillonite. The amount of calcite represents carbonate minerals (calcite and dolomite). Pyrite and siderite are taken into account in order to set the iron content properly. Finally, for convergence reasons, aqueous aluminium and K-Feldspars have not been taken into account in the groundwater chemistry.

Temperature is set to 22°C and the pH to 7.1. The calculated pore water is reported in Table 3.3.1. The equilibrium with the minerals mentioned above leads as expected to a Na-Cl-SO₄ water type and is in good agreement with the composition reported in the benchmark proposal. The pore water is also in equilibrium with the exchangeable cation population of montmorillonite, the modelled occupancy of exchangeable cations being as follows: Ca (41% in equivalent), Na (28%), Mg (18%), K (11%), Sr (2%) and Fe (0.1%). The simulations take into account the dissolution/precipitation of calcite, dolomite, quartz and pyrite only.

3.3.3.2 MX-80 bentonite

Simulations of bentonite/clayey host-rock interactions performed by IRSN in the framework of the BENIPA European project (2003) have shown that bentonite and host rock compositions are very similar, only slight changes in pH and aqueous concentrations being observed after 10⁵ y. Therefore, the bentonite porewater is assumed to be in first approximation equivalent to that of the surrounding host rock. The main difference with host rock groundwater concerns the exchangeable cation populations and the pH value.

The mineral composition is mainly represented by montmorillonite (93 %), but also takes into account the presence of quartz (5 %), calcite (1 %), siderite (0.5 %) and pyrite (0.5 %), according with the composition of MX-80 bentonite given by SKB (Arcos et al., 2006) (no specific recommendation in the benchmark).

Temperature is set to 22°C and pH to 7.7 in order to ensure the electroneutrality. The calculated pore water is reported in Table 3.3.1. The equilibrium with the minerals mentioned above leads as expected to a Na-Cl-SO₄ water type and is in good agreement with the composition advised in the benchmark proposal. In the absence of data concerning the exchangeable cation population in the benchmark definition, the modelled occupancy of exchangeable cations is taken from Arcos et al. (2006): Na (74% in equivalent), Ca (19.5%), Mg (5%), K (1.5%). The simulations reported take into account the dissolution/precipitation of calcite, dolomite, quartz and pyrite only.

Table 3.3.1: Calculated chemical composition of claystone and bentonite pore waters

		Benchmark	Claystone	Bentonite
Temp.	°C	22	22	22
pH	-	7.11	7.1	7.7
pe	-	-2.85	-2.81	-3.84
Al	mmol/L	4.7e-6	-	-
Fe	mmol/L	0.034	0.031	0.0056
Si	mmol/L	0.18	0.18	0.18
Sr	mmol/L	0.2	0.3	0.2
K	mmol/L	1.03	1.53	0.76
Mg	mmol/L	6.67	3.32	0.56
Ca	mmol/L	7.36	7.52	1.43
Na	mmol/L	45.6	66.5	88.5
Cl	mmol/L	41	41	41
S(VI)	mmol/L	15.6	11.2	12.5
TIC	mmol/L	3.34	2.56	3.26

3.3.3.3 Source term modelling

The source term is simulated from the data provided in the benchmark. C1 (HA) vitrified waste (R7T7 glass) simplified composition, *i.e.* considering the main oxides only, is given as follows by wt. % decreasing order: SiO₂ (45,5 %), B₂O₃ (14 %), Na₂O (9.9 %), Al₂O₃ (4.9 %) and CaO (4 %). The sum of weight percentages of these oxides is not equal to 100 % due to the fact that minor oxides are not taken into account in this composition. These proportions are however respected in the calculations performed in the frame of this work. In addition to this, and depending on the case computed, the waste content in radionuclides has also been considered (see glass composition with or without radionuclides in Table 3.3.2).

In order to take into account both the waste dissolution rates proposed by the benchmark and the recommended approximations in the benchmark definition, 4 % of the mass are assumed to dissolve instantaneously at the simulation start. The dissolution then occurs with a constant rate ($5 \times 10^{-5} \text{ g.m}^{-2}.\text{d}^{-1}$) over the simulation period. It is worth noting that unit of dissolution rate values given in the benchmark definition should be read in $\text{g.m}^{-2}.\text{d}^{-1}$ and not in $\text{g.m}^{-2}.\text{y}^{-1}$.

In order to understand and to compare the results obtained in the following sections, the migration of boron, which is considered to be equivalent to a tracer component of the radwaste, is simulated in 1D-radial, 1D-axial and 2D-cylindrical geometries (Figure 3.3.2). This

illustrates in particular the possible overestimation of the diffusion of species in 1D-axial geometry due to a so-called “channelization” effect (transport is allowed in only one direction).

Table 3.3.2: Glass composition

Oxides	Si	B	Na	Al	Ca	Cs	Rb	Am	Ln	Zr	Tc	U
Weight %	45.5	14.0	9.9	4.9	4.0	1.23	0.1	0.055	4.47	5.25	0.35	0.25

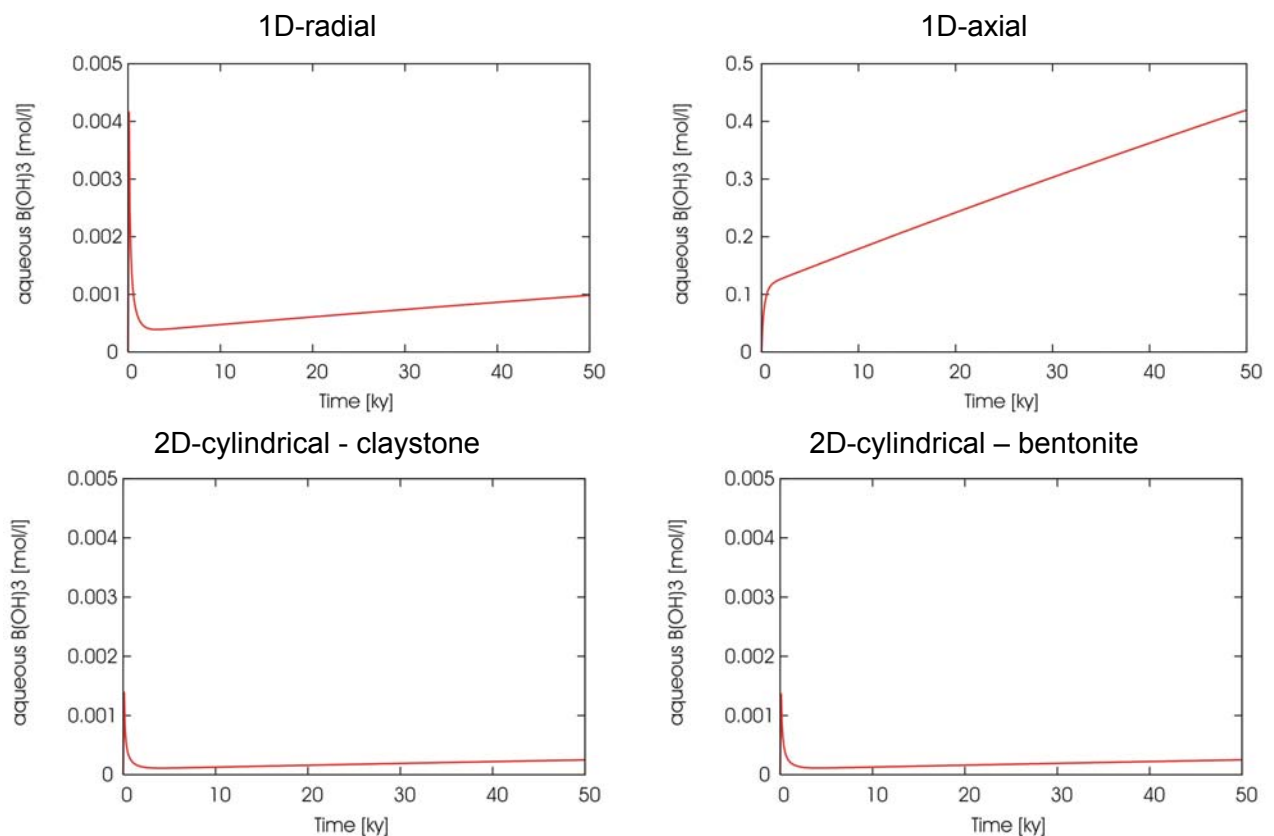


Figure 3.3.2: Evolution of aqueous concentration of $B(OH)_3$ released from the waste package at 2 m depending on the symmetry simulated

3.3.3.4 Geochemical effects of glass alteration on the near-field (task 1)

The geochemical effects of the source term on the claystone groundwater are modelled with HYTEC in 1D-radial geometry over 50,000 y of simulation. The steel overpack failure occurs at the beginning of the calculation and the dissolution proceeds as described in section 2.2 (initial release of 4% wt. of the glass matrix and then constant dissolution rate). Two cases have been treated so as to compare the geochemical effects of the glass dissolution on the claystones with and without the complete set of radionuclides composing the source term.

Two stages of geochemical modifications are observed: i) a strong perturbation due to the initial release of 4 % wt. of the glass at the steel overpack failure and ii) a continuous



perturbation over the simulation period due to the residual dissolution of the waste package. In both treated cases, the release of glass dissolution products does not lead to strong mineral modifications in the claystone (slight precipitation of calcite only, due to the dissolution of CaO composing the glass matrix, see Figure 3.3.3-a) and the global cation exchange population changes only slightly over the simulation period, due to the small release of Ca and Na from the waste package compared to the cationic pool in the claystone.

During the initial stage of alteration, the hydrolysis of the oxides contained in the glass induces a strong release of hydroxides in the groundwater, leading to an increase of pH at the steel overpack failure in the first 5 m of the host rock. This increase is more pronounced when radionuclides are taken into account because of the higher oxide content in the glass matrix: close to the waste package, the pH rises significantly from 7.1 to 8.9 in the case where radionuclides are not taken into account in the source term, and from 7.1 to 10 in the other case (Figure 3.3.3-b). Then, the out-diffusion of the hydroxides into the host rock leads to the decrease of pH close to the package and its subsequent increase farther in the host rock, and to a homogenisation at 5,000 y in the whole host rock around a pH value of 7.15 in the first case and 7.2 in the second one (Figure 3.3.3-c). Finally, the slight release of hydroxides corresponding to the long term stage of glass alteration leads to a small increase of pH in the 20 m of host rock over the simulation period: 50,000 y after the overpack failure, pH reaches 7.3 in the claystone when radioelements are not considered in the source term and 7.5 otherwise (Figure 3.3.3-d). In both cases, it is worth mentioning that the modification of argillaceous phases is not taken into account, silica chemistry being only controlled by quartz. The dissolution of montmorillonite at high pH could reduce the CEC and thus decrease the sorption of radionuclides.

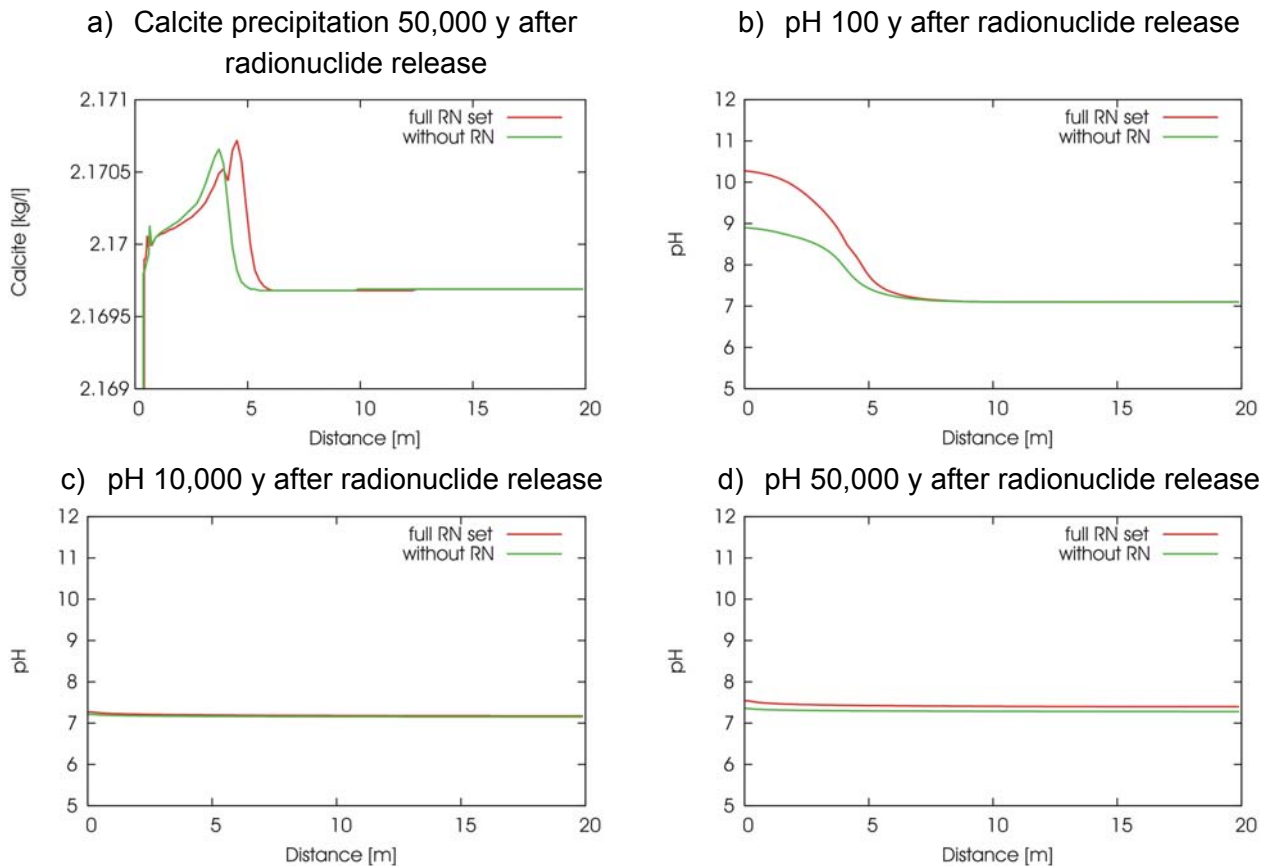


Figure 3.3.3: Geochemical evolution of the claystone after the waste package release

3.3.3.5 Constant K_D -SL modelling

Using constant solubility limits (SL) and sorption coefficient (K_D) is the common way for modelling chemical processes with the code MELODIE, but is not straightforward with HYTEC. Thus, the corresponding tasks have been modelled in three different ways: two different methods (so called methods A and B in this report) have been set up to adapt HYTEC to deal with constant SL and K_D , and a third set of simulations has been performed with MELODIE, so as to compare the results with the software specifically used by IRSN for performance assessment.

The set of K_D and SL values taken into account comes from the benchmark definition and are reported in M4.1.19 report (IRSN, 2009, Table 7) (see also Table 2.2.4 and Table 5.1). Values given for the radionuclides (Cs, Am, Zr) are consistent (same order of magnitude) with values given by Andra (2005a). Adimensional K_D values for Cs, Am and Zr have been calculated from the values given in the benchmark definition. The low K_D value of Cs in the claystone ($0.01 \text{ m}^3 \cdot \text{kg}^{-1}$) represents the behaviour of Cs close to the source term and is used for the EDZ in the present study, whereas the high value ($0.3 \text{ m}^3 \cdot \text{kg}^{-1}$) is used in the undisturbed Callovo-Oxfordian claystone, as recommended in the benchmark definition. Two different cases have been considered for the bentonite: a first one with the reference K_D value for Cs ($0.1 \text{ m}^3 \cdot \text{kg}^{-1}$) and a second one with the conservative value ($0.06 \text{ m}^3 \cdot \text{kg}^{-1}$). Same K_D values are used in



bentonite and claystones (in both the EDZ and undisturbed Callovo-Oxfordian claystone) for Am ($50 \text{ m}^3 \cdot \text{kg}^{-1}$) and Zr ($100 \text{ m}^3 \cdot \text{kg}^{-1}$). SL of Zr is taken from that controlled by ZrO_2 pure phase ($2 \cdot 10^{-8} \text{ mol} \cdot \text{l}^{-1}$) and SL of Am is taken from that controlled by AmOHCO_3 ($4 \cdot 10^{-7} \text{ mol} \cdot \text{l}^{-1}$), both in clayey systems. Cs is supposed to have no SL in the present work.

In the method A, both SL and K_D are simulated using an artificial mineral, without accounting for any other chemical reactions in the system but the sorption on this mineral. It is worth noting that the use of too high sorption coefficient leads to very long-time calculations and that task 4 simulations have not been successfully carried out with this method, due to the difficulties for HYTEC to deal with the combination of huge sorption values and a 2D-grid.

In the method B, no new chemical species is introduced. Constant K_D is accounted for with an adapted porosity ω' (see table 8 in M4.1.19 report), through retardation coefficient R:

$$\omega' = \omega \cdot R \quad \text{with} \quad \omega' = \omega + \rho_d \cdot K_D \quad \text{and} \quad \rho_d: \text{dry density of the porous medium.}$$

3.4 Conceptualization and modelling performed by JRC

The transport of radionuclides was performed using code GoldSim², a compartment mass transport model tool which is designed for simulation of contaminants migration within an environmental system. The code can be used for deterministic as well as for probabilistic analysis.

The transport of radionuclides in the considered concepts is diffusion dominant in fully saturated conditions.

According to the concept described in the benchmark definition (Andra, 2007), only part of the disposal cell is considered. In the axial direction:

- one waste package (radwaste),
- bentonite plug,
- no biological and intercalation block were considered due to the lack of input data.

In the radial direction:

- fracture zone (0.1 m),
- microfissure zone (0.7 m),
- claystone layer (1 m, 5 m, 10 m).

The discretisation of geometry is shown on Figure 3.4.1.

² GoldSim, User's Guide, GoldSim Technology Group, Issaquah, Washington, 98027 USA, www.goldsim.com

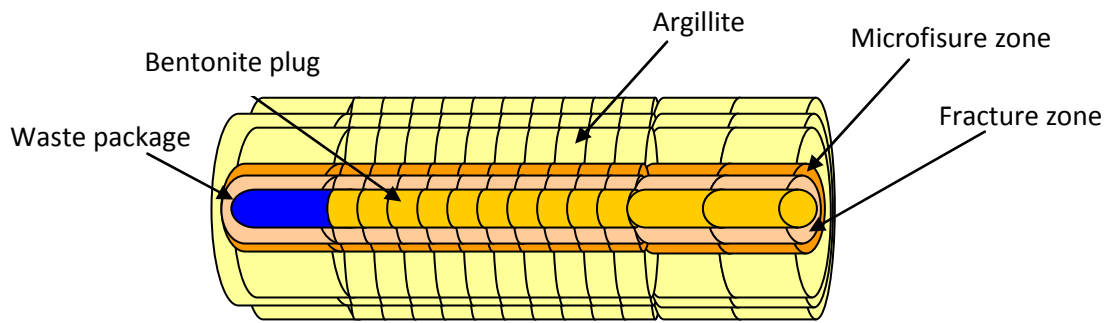


Figure 3.4.1: Geometry used in calculation

The bentonite plug, in axial direction up to 1 m length, is discretized into 10 equal disks with length of 0.1 m. The rest of the bentonite is discretized into two 1 m long parts.

The fracture and microfissure zone are not discretized in the radial direction. However, in the axial direction, the discretization follows the geometry of the bentonite.

In the radial direction, the undisturbed claystones are divided into 10 equal parts, each of 1 m radius. The discretization in axial direction follows again the geometry of bentonite.

The waste form is considered to be compact and homogeneous. All considered radionuclides are assumed to be cations.

The calculations have been performed with two different time-steps. The time-step up to 10,000 years is 10 years and beyond it has increased to 100 years. The computational times are:

- Exercise 1: 6s for 1D calculations and 180s for 2D calculations,
- Exercise 2: 5s for 1D calculations and 170s for 2D calculations.

3.5 Conceptualization and modelling performed by SCK*SEN

The details of the benchmark are defined in Milestone M 4.1.2 (clay case) of the PAMINA project (Andra, 2007). Because many different aspects are suggested in this benchmark (and correspondingly many calculation cases can be considered) and the benchmark definition leaves some room for interpretation, this paragraph clarifies which general assumptions are made by SCK.

3.5.1 Simplifications in the conceptual model

Two main assumptions made in exercise 1 and 2 are neglecting (i) the decay of the radionuclides and (ii) advective transport. The half-life of ^{135}Cs , ^{93}Zr and ^{243}Am is 2.3×10^6 , 1.53×10^6 and 7,380 years respectively, while the timescale of interest in this benchmark is limited until 50,000 years. Hence, decay would only have a noticeable effect on the evolution of the ^{243}Am concentration. However, since the focus of this study was on process modelling of sorption and solubility and there is no interaction with radioactive decay, the latter was not



considered. Advective solute transport can be excluded since diffusion is the main transport process in Callovo-Oxfordian claystone.

3.5.2 Radionuclide release

The release of radionuclides and other glass components from the vitrified waste form is based on a constant dissolution rate without any temperature or pH dependency: the whole glass block is assumed to be dissolved in 50,000 years. This approach was followed for most of the SCK calculations reported in this document.

However, the effect of a higher initial dissolution rate was also studied as a variant case. In this case, the initial and long-term dissolution rate were calculated as follows: the fraction of altered glass per year, τ , is given by:

$$\tau = \frac{V_0 \cdot S_0 \cdot \tau_0}{M}$$

where $V_0=1.7$ g/(m²·day) is the initial glass dissolution rate at reference temperature and pH, $S_0=1.7$ m² is the external surface of the waste form, $\tau_0=5$ is the initial cracking factor and $M=400$ kg is the mass of the waste form. This results in a glass alteration fraction (τ) of 3.613×10^{-5} day⁻¹. This rate is limited to 4% of the total mass, a limit that is reached after 3 years (see Figure 3.5.1). Thereafter, the altered glass fraction, defined as:

$$\tau = \frac{V_r \cdot S_0 \cdot \tau_r}{M}$$

drops down to 8.854×10^{-9} day⁻¹ using $V_r=5 \times 10^{-5}$ g/(m²·day) as the residual rate of glass dissolution at reference temperature and pH and $\tau_r=40$ the long-term cracking factor.

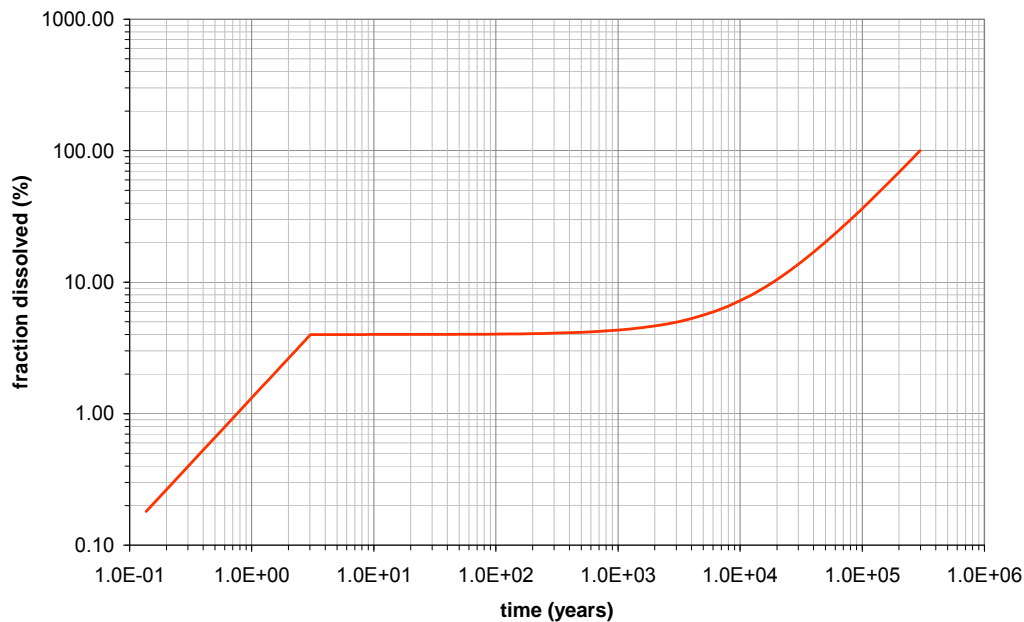


Figure 3.5.1: Fraction of the waste form dissolved as function of time for the variant case

3.5.3 Material properties

The material properties for the concrete plug and waste forms are not explicitly mentioned in the benchmark definition. They are assumed to be comparable as those of the backfill (intercalation blocks). The bulk density of the fractured EDZ was assumed to be slightly

lowered according to the increased porosity: $\omega = \left(1 - \frac{\rho_d}{\rho_g}\right)$. From the undisturbed Callovo-

Oxfordian claystone we derive $\rho_g = 2.805 \text{ g/cm}^3$ (with $\rho_d = 2.3 \text{ g/cm}^3$ and $\omega = 0.18$), and using the increased porosity of $\omega = 0.20$ we come to a bulk density ρ_d of 2.244 g/cm^3 for the fractured EDZ³.

3.5.4 Sorption models

3.5.4.1 Simple models

In a first case (case 1), sorption of ¹³⁵Cs on claystone and bentonite minerals is assumed to be adequately represented by a distribution coefficient, K_d (i.e. linear sorption). This is the common approach in classical performance assessment (PA) calculations, where the often complex geochemical transport behavior in the near field of a geological repository is necessarily simplified in view of the extreme timescales that need to be computed.

³ Note that measured solid density measured in argillites varies from 2,67 and 2,72 g/cm³ (see Andra, 2005 b)

For the bentonite plug, a reference K_d of $0.1 \text{ m}^3/\text{kg}$ was applied. An alternative case was tested using a conservative K_d value of $0.06 \text{ m}^3/\text{kg}$. For the host formation (Callovo-Oxfordian claystone), a reference K_d of $0.3 \text{ m}^3/\text{kg}$ was applied, except for the EDZ (both fissured and fractured) where the K_d is lower: $0.01 \text{ m}^3/\text{kg}$.

In a second case (case 2), non-linear sorption according to a Langmuir isotherm (model A as defined in the benchmark) was applied for the COX claystone:

$$C_{ads} = \frac{AC_{aq}}{B + C_{aq}}$$

with $A=1.8462 \times 10^{-7} \text{ mol/g}$ and $B=4.7552 \times 10^{-7} \text{ mol/l}$. These coefficients are valid as long as the Cs^+ concentrations remain smaller than 10^{-5} mol/l , which was verified during the calculation. Figure 3.5.2 compares the Langmuir and K_d isotherms for the Callovo-Oxfordian claystone and the EDZ. In the concentration range of interest, the two isotherms cross for the Callovo-Oxfordian claystone, while for the EDZ, sorption according to a linear K_d remains smaller than in the case of Langmuir sorption.

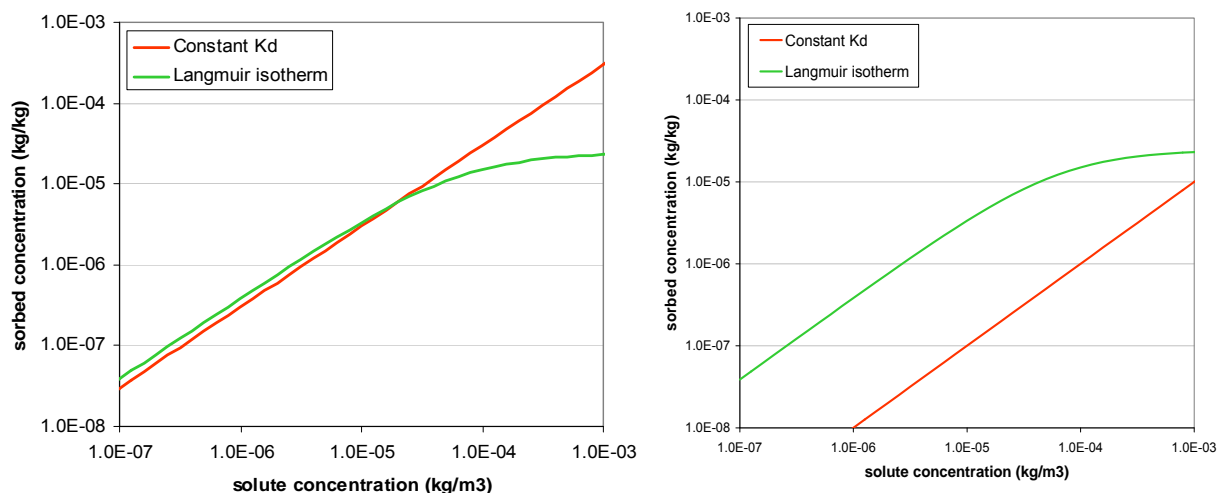


Figure 3.5.2: Comparison between Langmuir isotherm and constant K_d : sorbed concentration vs. solute concentration in Callovo-Oxfordian claystone (left) and in EDZ (right)

Sorption according to a constant K_d is modelled using PORFLOW, COMSOL Multiphysics and PHREEQC. Langmuir isotherms can be modelled with COMSOL Multiphysics and PHREEQC.

3.5.4.2 Thermodynamic model

Complex models take chemical processes into account. For bentonite, a non electrostatic surface complexation/ion exchange model is applied as defined in Table 3 of the benchmark definition. For the Callovo-Oxfordian claystone, only ion exchange is considered. The selectivity coefficients are given in Table 2.2.5.

These thermodynamic processes can only be modelled with PHREEQC. Three cases are implemented:

- Case 3a which considers only the presence of Cs and Na in the pore water and only Cs in the waste forms.
- Case 3b which is the same as case 3a, but also takes into account the presence of Na, Ca, Mg, Sr, Fe and K in the pore water (concentrations given in Table 2.2.1). These elements may then compete with Cs for occupation of the ion exchange sites
- Case 3c which is the same as case 3b, but which also considers the release of Na and Ca from the waste form (as defined in section 2.2.3).

The characteristics of the three cases are summarized in Table 3.5.1.

Table 3.5.1: Overview of models 3a, 3b and 3c

Case 3a	Case 3b	Case 3c
thermodynamic model for bentonite	thermodynamic model for bentonite	thermodynamic model for bentonite
thermodynamic model for claystones; only Cs and Na ion exchange	thermodynamic model for claystones	thermodynamic model for claystones
groundwater composition as defined in Table 2.2.1 for Na only	groundwater composition as defined in Table 2.2.1	groundwater composition as defined in Table 2.2.1
only Cs in waste (no Na and Ca)	only Cs in waste (no Na and Ca)	source term for waste as defined in appendix 3

Figure 3.5.3 compares the isotherms for the thermodynamic models with the Kd isotherm for the Callovo-Oxfordian claystone for the Cs concentration range of interest (*i.e.* the concentration range obtained around a waste disposal gallery) and the Na and Ca concentrations (where applicable) as calculated in the simulations for a position close to the waste zone. Case 3b and 3c give the same isotherm, indicating that the effect of the additional competing elements that are released from the waste (in case 3c) is negligible. Moreover, in the concentration range of interest, the cases with the highest process complexity (case 3b and 3c) show fairly linear isotherms. This suggests that a linear Kd model is an adequate representation of Cs' ion exchange process. However, the choice of the Kd value might not be appropriate in this benchmark. Figure 3.5.3 shows that, compared to case b and c, the selected linear Kd value in this benchmark overestimates (by approximately a factor 10) the amount of Cs that sorbs on the Callovo-Oxfordian clay minerals, which is not conservative in view of long-term radiological safety. For the EDZ however, the choice of the Kd is conservative.

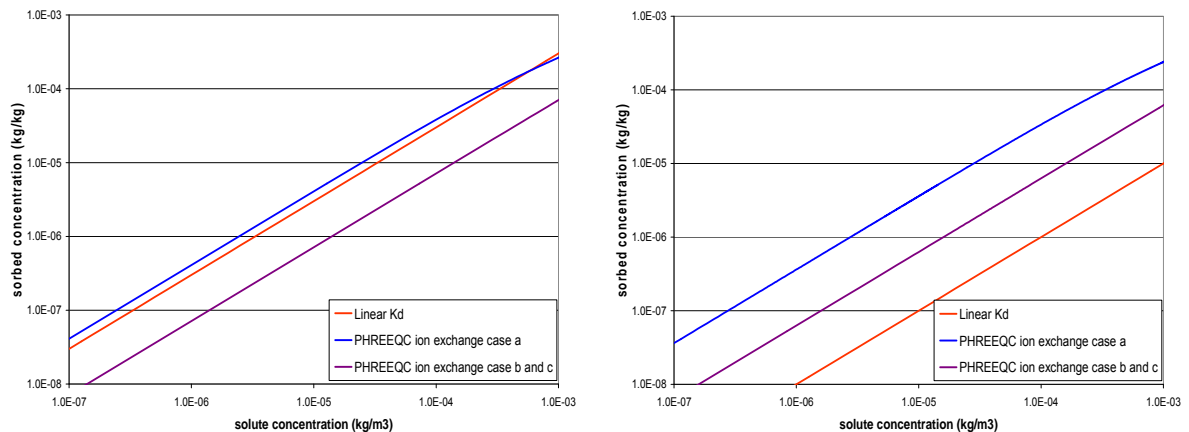


Figure 3.5.3: Comparison between isotherms for the thermodynamic cases and for the case with constant K_d . Sorbed concentration vs. solute concentration. Left : Callovo-Oxfordian claystone; right: EDZ

3.5.5 Model geometry, boundary conditions and output

The French repository concept for disposal of vitrified high-level waste is shown in Figure 1.1. The benchmark defines a number of transport calculations in the axial and radial direction, in both 1D and 2D. The geometries applied in the numerical models are shown in Figure 3.5.4. Because output is requested as far as 10 meters from the waste form (and since diffusion is the dominant transport process, isoconcentration lines are circular), we opted to include a second waste form in the model. Red lines in Figure 3.5.4 denote cross-sections for which output is plotted 100, 1,000, 5,000, 10,000 and 50,000 years after the start of radionuclide release; green dots represent calculation nodes in which the concentration evolution is recorded.

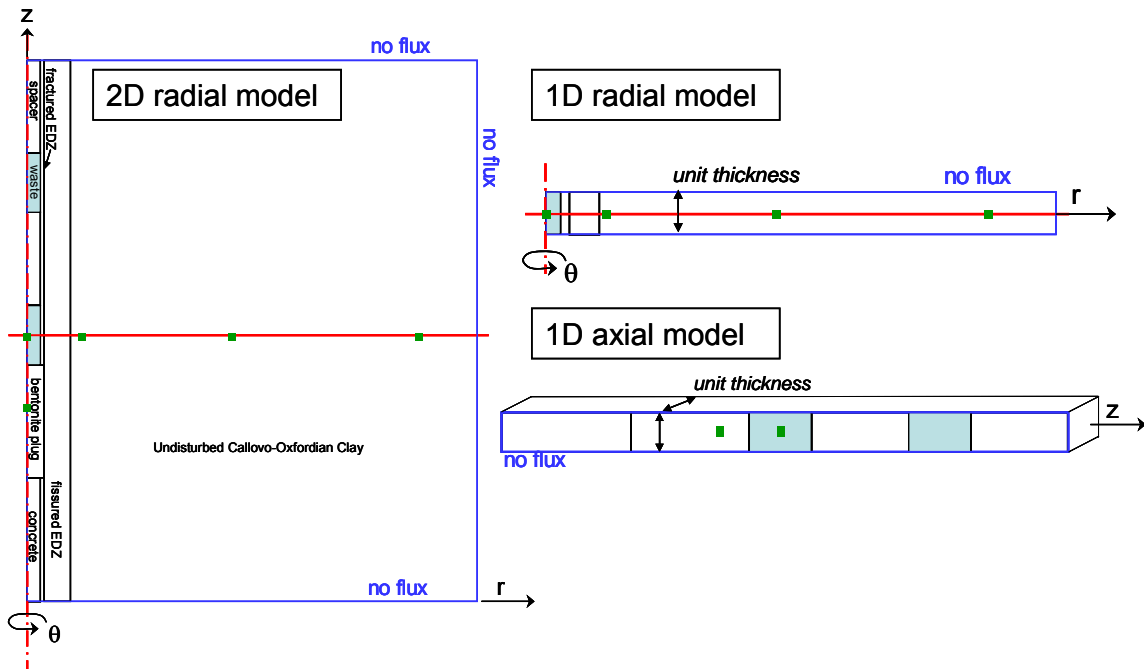


Figure 3.5.4: Geometry and boundary conditions applied in the numerical models. Zero r and z -axes are shown in red (they denote also the cross-sections for profile output); green points are the observation nodes for time series output

3.5.6 Overview of calculation cases

An overview of all calculation cases performed by SCK•CEN, indicating the geometry, the processes considered and the codes used is given in Table 3.5.2.

Table 3.5.2: Overview of calculation cases for exercise 1

Task	Case	geometry	sorption on bentonite	sorption on EDZ	sorption on undisturbed C-O Clay
Task 2	Case 1	1D radial		reference Kd: 0.01 m ³ /kg	reference Kd: 0.3 m ³ /kg
Task 2	Case 1	1D radial		reference Kd: 0.01 m ³ /kg	reference Kd: 0.3 m ³ /kg
Task 2	Case 1	1D radial		reference Kd: 0.01 m ³ /kg	reference Kd: 0.3 m ³ /kg
Task 5	Case 2	1D radial		Langmuir isotherm	Langmuir isotherm
Task 5	Case 2	1D radial		Langmuir isotherm	Langmuir isotherm
Task 3	Case 1	1D axial	reference Kd: 0.1 m ³ /kg		
Task 6	Case 3a	1D radial		ion exchange, Cs only	ion exchange, Cs only
Task 6	Case 3b & 3c	1D radial		ion exchange, all elements	ion exchange, all elements
Task 4	Case 1	2D radial	reference Kd: 0.1 m ³ /kg	reference Kd: 0.01 m ³ /kg	reference Kd: 0.3 m ³ /kg
Task 4	Case 1	2D radial	reference Kd: 0.1 m ³ /kg	reference Kd: 0.01 m ³ /kg	reference Kd: 0.3 m ³ /kg
Task 4	Case 1	2D radial	reference Kd: 0.1 m ³ /kg	reference Kd: 0.01 m ³ /kg	reference Kd: 0.3 m ³ /kg
Task 4	Case 1	2D radial	conservative Kd: 0.06 m ³ /kg	reference Kd: 0.01 m ³ /kg	reference Kd: 0.3 m ³ /kg
	Case 2	2D radial	reference Kd: 0.1 m ³ /kg	Langmuir isotherm	Langmuir isotherm
	Case 2	2D radial	reference Kd: 0.1 m ³ /kg	Langmuir isotherm	Langmuir isotherm
Task 8	Case 3a	2D radial	thermodynamic sorption model	ion exchange, Cs only	ion exchange, Cs only
Task 8	Case 3b & 3c	2D radial	thermodynamic sorption model	ion exchange, all elements	ion exchange, all elements

Legend:

- COMSOL Multiphysics 3.2
- PORFLOW 3.07
- PHREEQ-C

Figure 3.5.5 shows an excellent agreement between the COMSOL, PHREEQC and PORFLOW simulations results for the Cs concentration profiles. Differences in results are limited to the waste zone ($r < 0.35$ m) and are due to the fact that the waste zone is

represented by only one cell in PHREEQC. The diffusive transport in the radial direction is correctly modelled in PHREEQC.

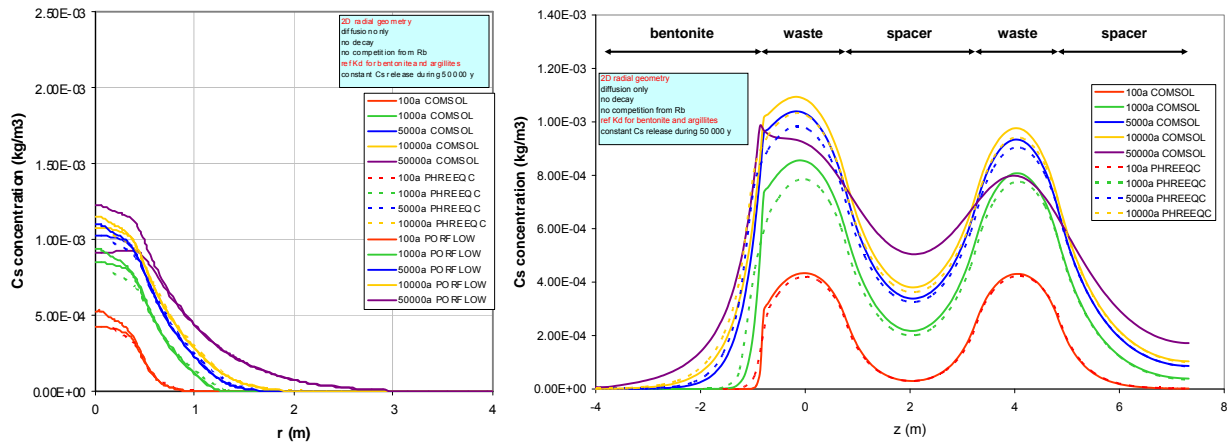


Figure 3.5.5: Radial (left) and axial (right) concentration profiles for the linear K_d model and constant C_s dissolution rate (2D simulations)

3.6 General comments

The model considered by each participant exhibit major differences. These differences were introduced by some freedom in the benchmark definition and specific constraints of the selected softwares:

Andra used phreeqc in order to complete the full geochemical simulation. This limited their simulations to 1D and revealed very high concentrations near the source term. Therefore it was necessary to ignore the initial dissolution rate (V_0). According to this model, 16% of the glass is dissolved after 50 000 years

CEA performed K_d /SL and Langmuir calculations with Cast3m (Chess/Cast3m for the thermodynamic model) in the Alliances platform. The initial source term is 4% of the waste, then 20% are released by 50,000 years. CEA used Langmuir model B, relevant for high C_s concentrations (thus conservative). The thermodynamic model only includes the most influent elements in ion exchange processes. Note that CEA has performed a mesh sensitivity study.

IRSN used Hytec and they handled the K_d /SL model with two different methods, fictive mineral (method A) and capacity factor (method B). They could validate their results thanks to Melodie. The main dissolved species were introduced in simulations. The glass dissolution rate is the one defined in the benchmark, including the initially 4% dissolved glass. IRSN's thermodynamic model considers ionic exchange and a simplified mineralogy.

JRC only performed K_d /SL calculations using GoldSim.



SCK•CEN performed their own comparison between codes. Most simulations were performed with a constant dissolution rate: 100% of glass is dissolved after 50 000 years and Cs concentration is drawn in kg/m^3 (all isotopes included). It is then necessary to convert their results knowing that 1kg Cs corresponds to 7,5 moles and their constant dissolution rate is about 5 times faster than that defined in the benchmark. Their Langmuir model is model A, relevant for low Cs concentrations. The thermodynamic models were solved in a 2D radial coordinate system considering all dissolution products from the waste forms but not including mineral phases to buffer the pore water concentrations.

4 ¹³⁵Cs transfer modelling using Kd/SL and thermodynamic models

Cs transfer is mainly controlled by ion exchange. Such a mechanism is highly sensitive to the aqueous concentration of the element (*i.e.* of the sum of all isotopes) and the water composition (see section 2.2.2). Other competitive effects can also take place, considering the aqueous concentration of other elements such as Rb or major cations. Some useful model assumptions were proposed in the benchmark definition:

- Application to C1 (HA) vitrified wastes
- Several Cs isotopes included in the waste matrix: Cs133, Cs134, Cs135 and Cs137
- One stable and one radioactive isotope of interest: Cs 133 and Cs135, respectively
- Cs134 and Cs137 are neglected because of their short half-life (considering steel overpack containment)
- Other elements also included as competitor: *e.g.* Rb87
- Starting point for radionuclides release: steel overpack failure at 4,000 years
- Temperature elevation at this moment is negligible (less 20°C higher than the geothermal temperature)
- Fully water saturated conditions

This chapter is structured according to the three studied geometries: axial transfer in the bentonite plug, radial transfer through claystones and 2D simulations (see Table 4.1). General comments end this chapter.

Table 4.1: Tasks involving Cs transfer

	Sorption model	N° Task in the benchmark
Section 4.1: Cs transfer modelling in the bentonite plug - 1D axial	constant Kd/SL	part of task 3
	thermodynamic model (including competitive effects and Task 1 results)	7
Section 4.2: Cs transfer modelling in the claystone - 1D radial	constant Kd/SL	part of task 2
	isotherms (including competitive effects with Cs isotopes and Rb)	5
	thermodynamic model (including competitive effects and Task 1 results)	6
Section 4.3: Cs transfer at the head of the disposal cell (<i>i.e.</i> claystones and bentonite): 2D cylindrical	constant Kd/SL	part of task 4
	thermodynamic model (including competitive effects and Task 1 results)	8

4.1 Axial Cs transfer in the bentonite plug obtained with Kd/SL and thermodynamic models

The following results and comments were asked to all participants:

- Plots of Cs concentration profile along the axis through the bentonite plug at 100, 1,000, 5,000, 10,000 and 50,000 years after the release
- Plots of the evolution with time (from 0 to 50,000 years) of Cs concentration, at points located 0 and 1 m from the waste
- Discussions about the Cs sorption models and differences between the 2 models
- If possible for interpretation, plots of Cs isotherms solid vs. solution

4.1.1 Results from Andra

The axial transfer of Cs in the bentonite plug was simulated by two different models: the Kd model and the thermodynamic model, corresponding respectively to the tasks 3 and 7 of the benchmark.

The Kd reference value used to model Cs sorption in bentonite plug is the one recommended in the benchmark ($K_d=0.1 \text{ m}^3/\text{kg}$). A smaller value of Kd, called conservative, is also tested ($K_d=0.06 \text{ m}^3/\text{kg}$).

The thermodynamic sorption model of Cs in the bentonite plug considered in the simulations is defined by an exchange site with the benchmark's parameters (table 3 of the benchmark, Andra, 2007). As mentioned in the benchmark, Cs and Rb compete on the same exchange sites with identical equilibrium constants for both species.

4.1.1.1 Kd/SL model

One of the Kd values used in the benchmark to model Cs sorption in the bentonite plug ($K_d=0.1 \text{ m}^3/\text{kg}$) is the one used for PA calculations. A smaller value of Kd, called conservative, is also tested ($K_d=0.06 \text{ m}^3/\text{kg}$).

Figure 4.1.1 shows the evolution of Cs concentration profiles with time. It can be noticed that the opposite boundary of the bentonite domain is quickly reached by the diffused Cs (before 5,000 years) with every models and it can lead to overestimate the aqueous species concentrations. It has been decided to impose a zero flux boundary condition in the concrete wall. A null concentration at the boundary would have been more realistic but it would have been impossible to detect that this boundary is reached by Cs.

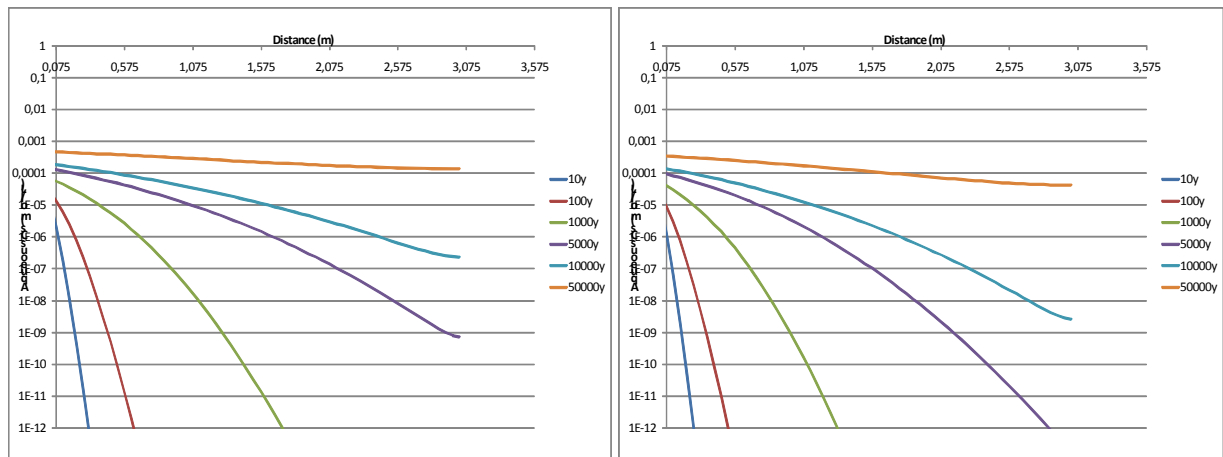


Figure 4.1.1: Evolution with time of Cs concentration profiles in bentonite, $K_d = 0,06 \text{ m}^3/\text{kg}$ (left) and $K_d = 0,1 \text{ m}^3/\text{kg}$ (right)

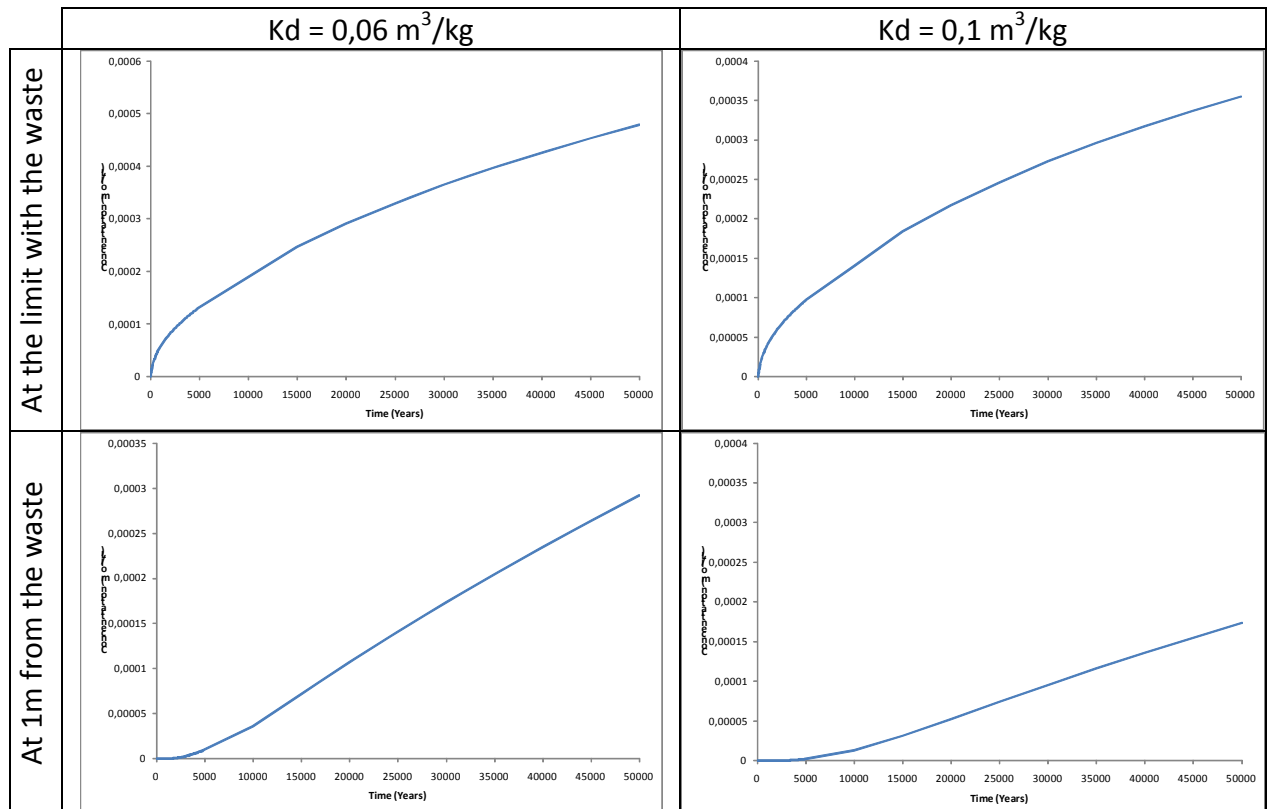


Figure 4.1.2 : Temporal evolution of Cs concentration at 0m (up) and 1m (down) in bentonite, K_d model (left : $K_d = 0,06 \text{ m}^3/\text{kg}$; right : $K_d = 0,1 \text{ m}^3/\text{kg}$)

K_d values are actually imposed by the solubility of a fictive mineral. There is however a little discrepancy between required results and obtained solid/solute ratios. This comes from a lack of precision in the equilibrium constant imposed for each fictive mineral to fulfil the solubility limit condition (see M4.1.18 report for more details).

4.1.1.2 Thermodynamic model

The thermodynamic sorption model of Cs in the bentonite plug considered in the simulations is defined by an exchange site with the benchmark's parameters. As mentioned in the benchmark, Cs and Rb compete on the same exchange site with identical equilibrium constants for both species.

Again, it can be noticed that the opposite boundary of the bentonite plug domain is quickly reached by the diffused Cs.

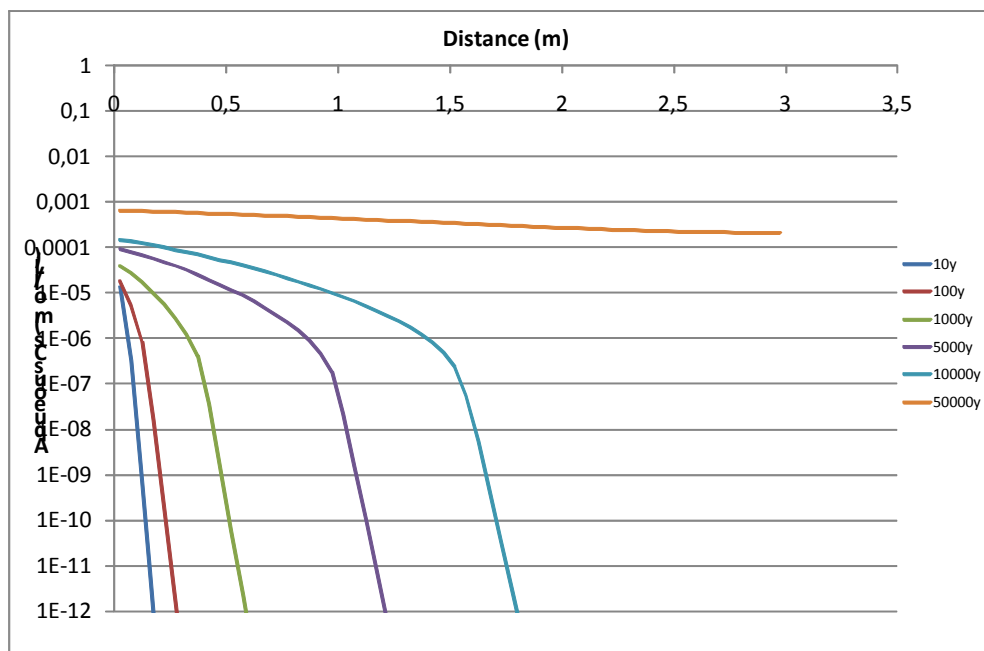


Figure 4.1.3: Evolution with time of Cs concentration profiles in bentonite, thermodynamic model

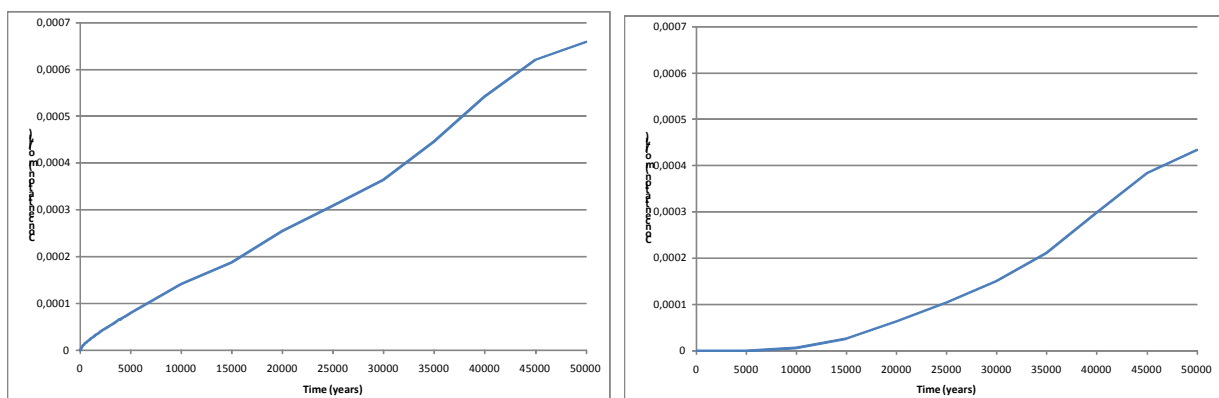


Figure 4.1.4: Temporal evolution of Cs concentration at 0m (left) and 1m (right) in bentonite, thermodynamic model

Figure 4.1.5 shows that the equivalent K_d calculated from simulations made with the thermodynamic model is not linear in the considered solute concentration range. That effect comes from the saturation of sorption sites available in the bentonite for relatively high Cs

solute concentration (*i.e.* higher than 10^{-6} mol/L). Thus the thermodynamic approach cannot be strictly represented by an equivalent K_d model on the whole C_s concentration range.

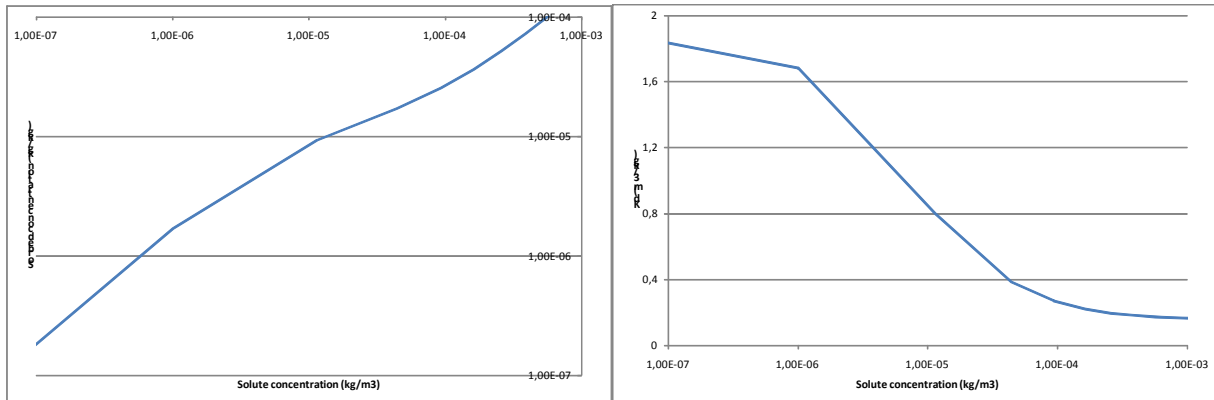


Figure 4.1.5: *Cs Sorption isotherm (left) and exchange coefficient (right) in bentonite, thermodynamic model*

4.1.1.3 Comparison of results in bentonite

Figure 4.1.6 shows the evolution of C_s concentration profiles with time considering the K_d approach (recommended and conservative values) and the thermodynamic approach.

The highest C_s concentrations are obtained with the conservative K_d model, the lowest with the thermodynamic model. The strong retention of C_s simulated by the thermodynamic model beyond a certain migration length is due to the most effective retention of C_s for small concentration (Figure 4.1.8).

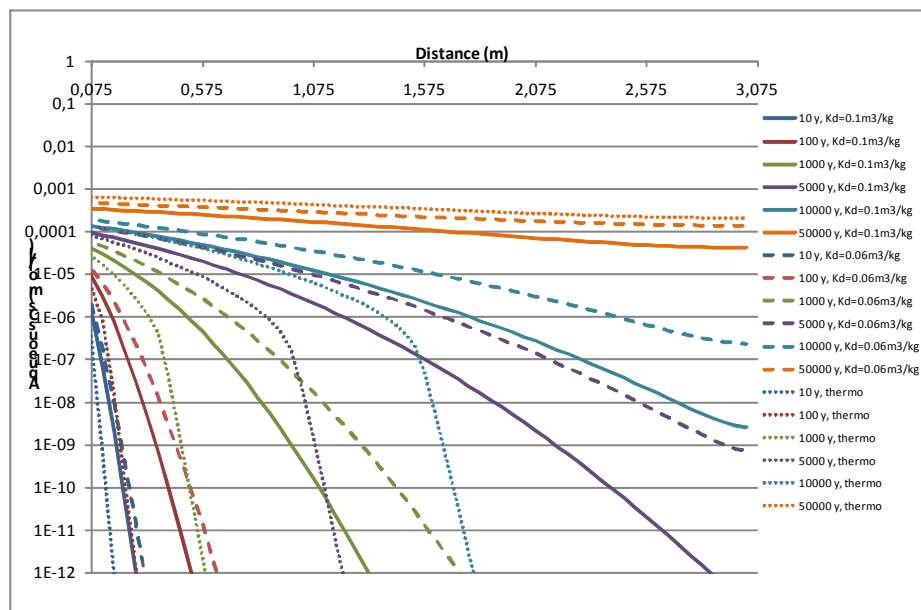


Figure 4.1.6: *Comparison of concentration profiles in bentonite with different models*

Figure 4.1.7 shows the increase of Cs concentration at the direct contact of the source term (=0m) and at 1m. The evolution of the Cs concentration simulated with the thermodynamic model (initially lower than with Kd model but increasing faster) is due to the mineralogy modification of the bentonite plug at the interface with the glass. The smectite is destabilized and dissolves leading to a decrease in the number of exchange sites (see Figure 3.1.2).

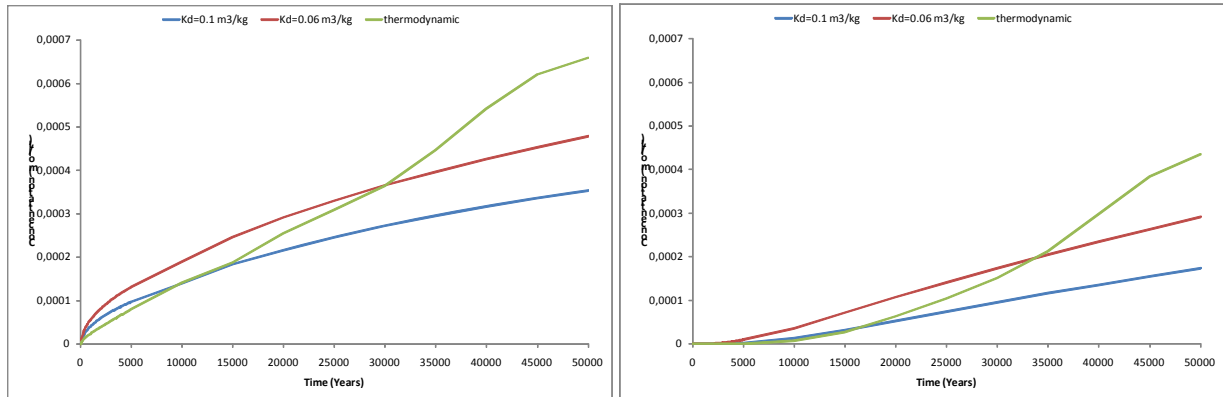


Figure 4.1.7: Comparison of Cs temporal evolution at 0m (left) and 1m (right) in bentonite with different models

Figure 4.1.8 shows the different sorption isotherms obtained with Kd and thermodynamic models with the initial mineralogy. Kd values (recommended and conservative) taken for performance assessment simulations in the bentonite plug are always lower in the considered concentration range than the one calculated from the thermodynamic model. Thus, from a performance assessment point of view, Kd models considered in this study allow us to simulate a “conservative” Cs migration. However, mineralogical changes decrease Cs sorption in the near field.

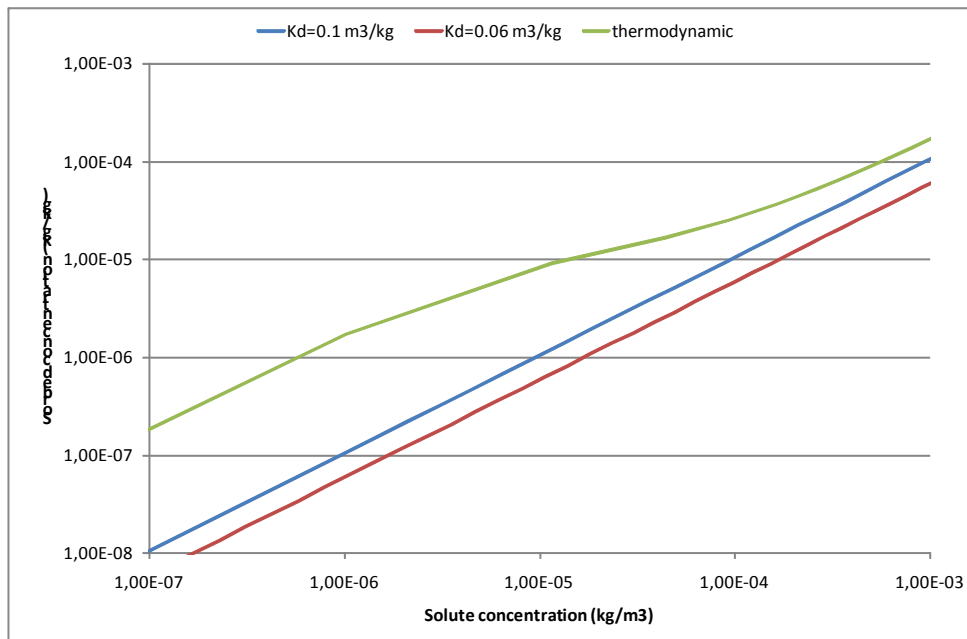


Figure 4.1.8: Comparison of Cs sorption isotherms in bentonite with different models

4.1.2 Results from CEA

Simulations for Cs 1D axial transfer show that the results of the thermodynamic model approach can be compared to the results of those obtained by the Kd approach (with 0.06 m³/kg and 0.1 m³/kg values) (Figure 4.1.9 to Figure 4.1.12).

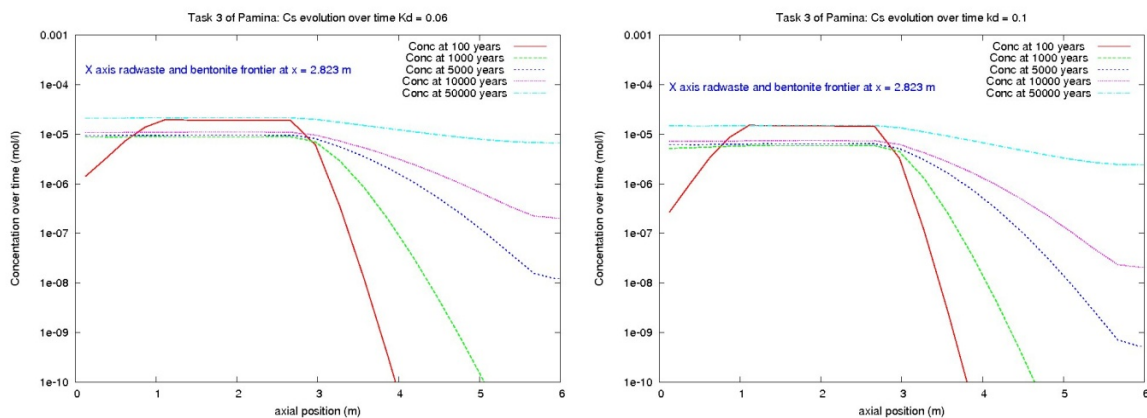


Figure 4.1.9: Cs axial evolution over time with $K_d = 0.06 \text{ m}^3/\text{kg}$ (left) and $K_d = 0.1 \text{ m}^3/\text{kg}$ (right)

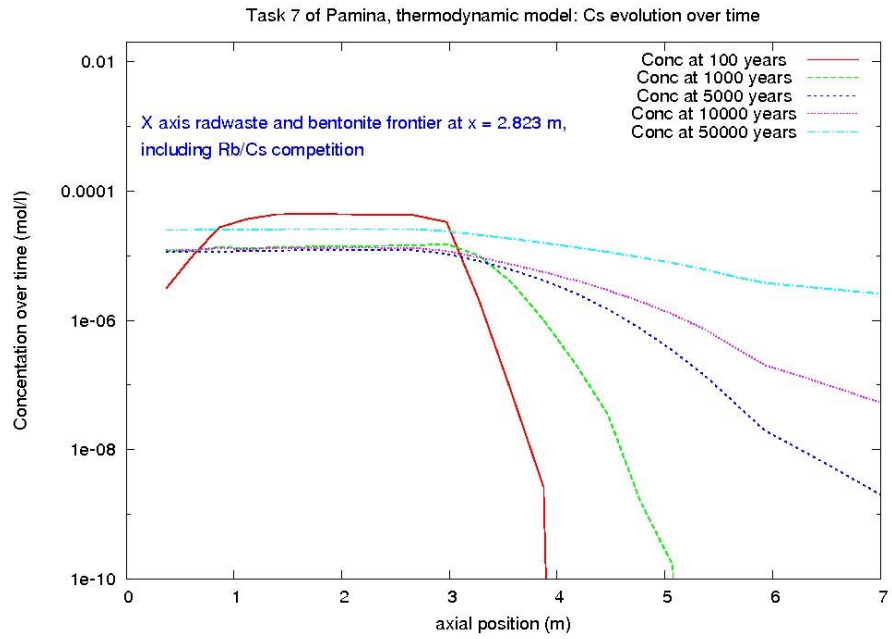


Figure 4.1.10: 1D axial thermodynamic simulation, Cs evolution over time

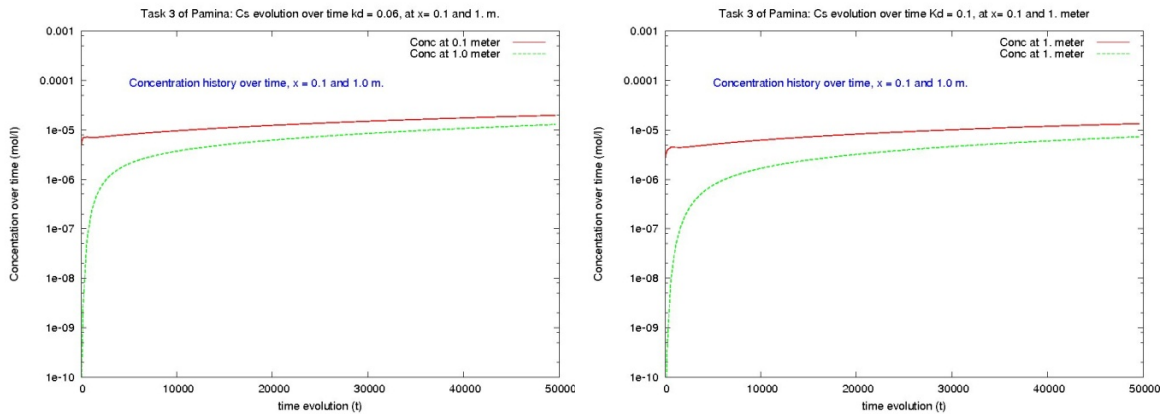


Figure 4.1.11: Task3, Cs concentration over time at $x = 0.1$ and 1.0 m for $K_d = 0.06$ m³/kg (left) and $K_d = 0.1$ m³/kg (right)

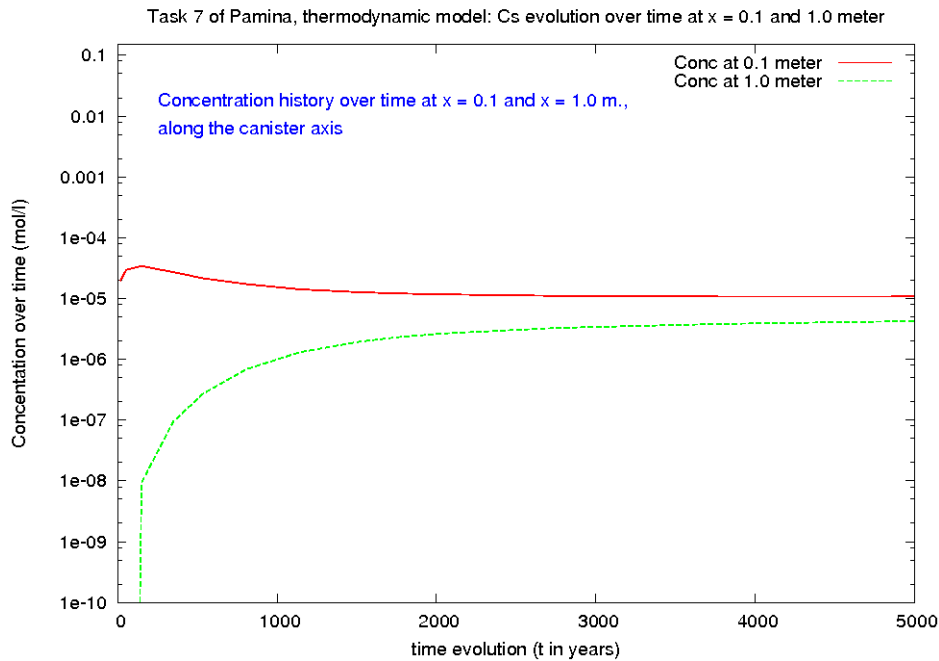
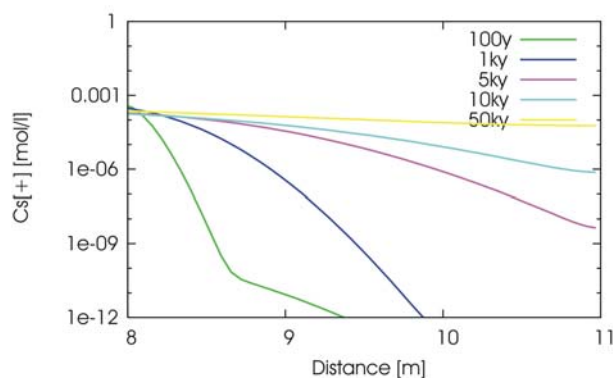


Figure 4.1.12: Task 7, 1D axial thermodynamic simulation, concentration over time at x = 0.1m and 1.0 m.

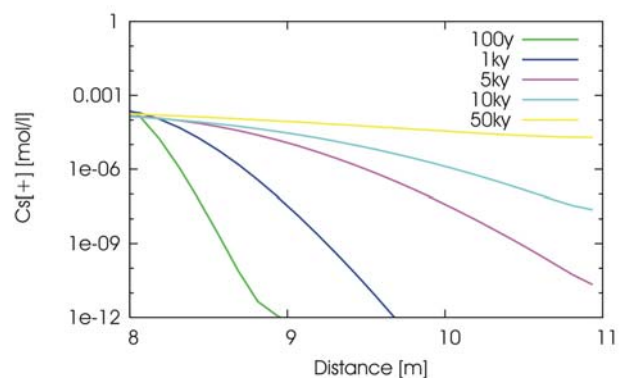
4.1.3 Results from IRSN

The modelling of Cs migration with constant K_D and SL with the different methods leads to comparable results: Cs migrates over the whole bentonite plug in both reference and conservative cases. Similar results are obtained with the full thermodynamic approach. The equivalent $\rho_d \cdot R_D$ (ρ_d is the dry density of the bentonite) coefficient in thermodynamic modelling is found to be constant at a value of 125 (Figure 4.1.13 to Figure 4.1.15).

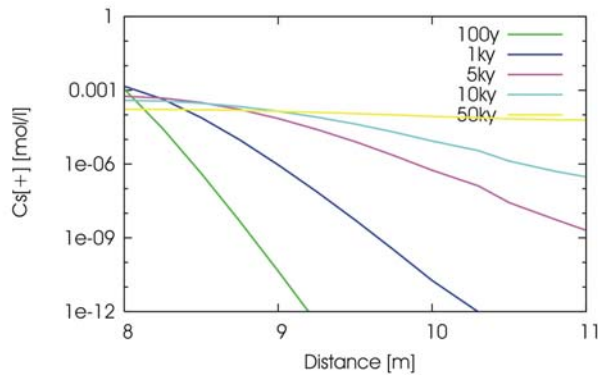
Method A – 100 to 50,000 y after release of source term (Cs) ($\rho_d \cdot K_D = 291$)



Method A – 100 to 50,000 y after release of source term (Cs) ($\rho_d \cdot K_D = 486$)



Method B – 100 to 50,000 y after release of source term (Cs) ($\rho_d \cdot K_D = 291$)



Method B – 100 to 50,000 y after release of source term (Cs) ($\rho_d \cdot K_D = 486$)

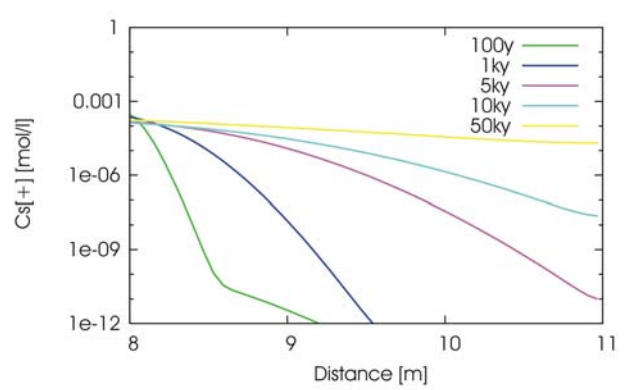
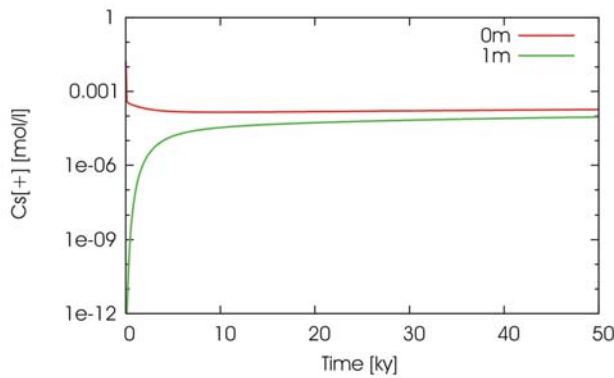


Figure 4.1.13: 1D-axial with constant K_D /SL. Cs concentration profile evolution over 50,000 years.

Method A



Method B

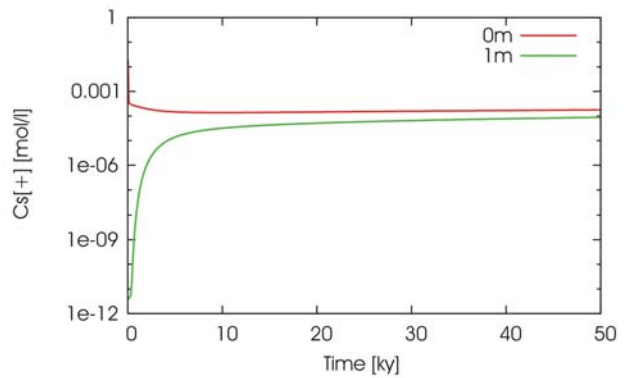
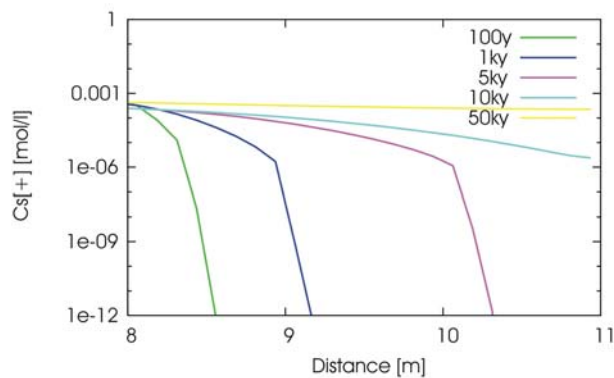
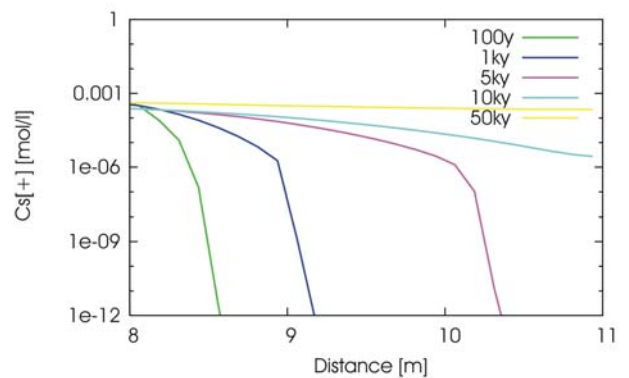


Figure 4.1.14: 1D-axial with constant K_D /SL. Cs concentration over time at $x = 0$ m and $x = 1$ m.

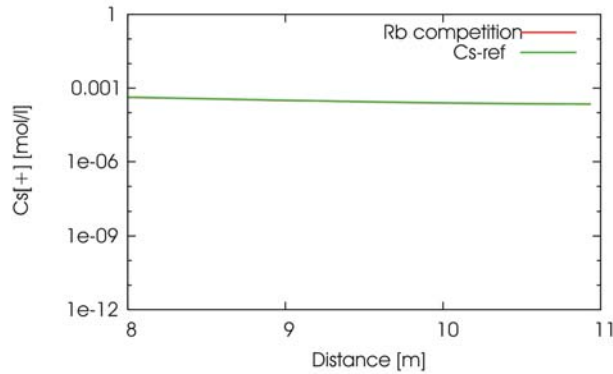
Cs evolution without Rb competition



Cs evolution with Rb competition



Comparison of Cs concentration over the bentonite plug at $t = 50,000$ y with and without Rb competition



Cs concentration over time at $x = 0$ m and $x = 0.1$ m

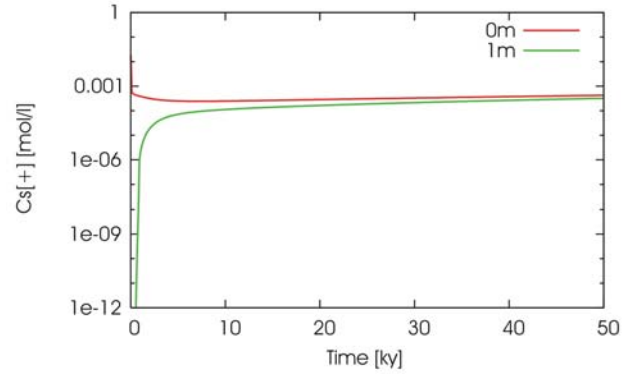


Figure 4.1.15: Cs Concentration profiles after 50,000 y (left) and temporal evolution of Cs aqueous concentration (right) in the bentonite plug. 1D-axial calculations with thermodynamic sorption model.

4.1.4 Results from JRC

The Exercise 1 considers migration of ^{135}Cs and the associated competing isotopes. However, the results are presented only for the nuclide ^{135}Cs . The radioactive decay is taken into account and as regards the sorption model, only linear isotherm was considered. For Cs sorption on bentonite, two cases were applied, one for a reference value $K_d = 0.1 \text{ m}^3 \cdot \text{kg}^{-1}$ and one for a conservative value $K_d = 6 \cdot 10^{-2} \text{ m}^3 \cdot \text{kg}^{-1}$.

In this exercise, the solubilities of all radionuclides were assumed to be unlimited.

Figure 4.1.16 shows the concentrations of ^{135}Cs in 1D axial direction, in the bentonite plug 1 m from the waste package. Two cases are distinguished; the blue curve corresponds to the reference value of bentonite sorption coefficient and the red curve to the conservative value.

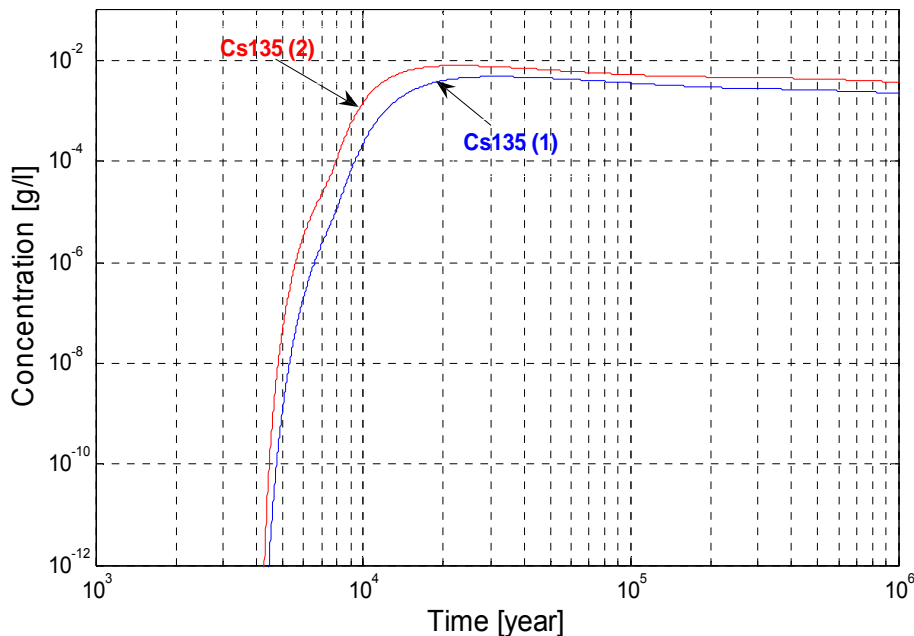


Figure 4.1.16: Concentration of ^{135}Cs in 1D axial direction, in the bentonite plug 1 m from the waste package:
 (1) reference distribution coefficient for bentonite $K_d = 0.1 \text{ m}^3 \cdot \text{kg}^{-1}$,
 (2) conservative distribution coefficient $K_d = 6 \cdot 10^{-2} \text{ m}^3 \cdot \text{kg}^{-1}$.

4.1.5 Results from SCK*CEN

Most calculations performed by SCK/CEN were done in 2D. Their only result in the 1D axial geometry is for linear K_d ($0.1 \text{ m}^3/\text{kg}$) and a constant Cs dissolution rate.

The total mass of Cs is 4.72 kg per waste form. This mass is released in 50,000 years following a constant dissolution rate. One simulation was also repeated for a variant case with 4% instantly released.

Figure 4.1.17 shows the total Cs concentration (sum of all isotopes) profiles in an inverted geometry (the bentonite plug is within -4m to -1m abscissas).

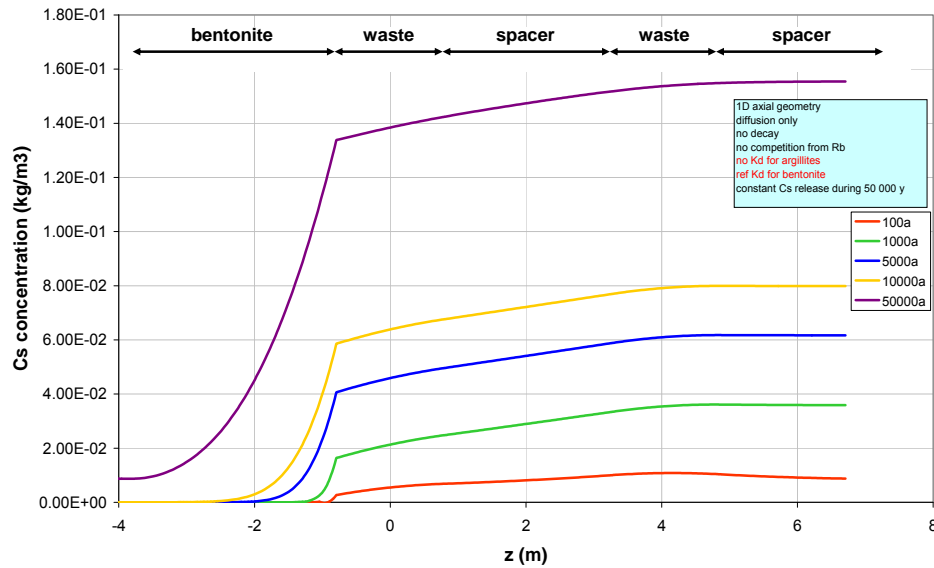


Figure 4.1.17: COMSOL axial concentration profile for the simple model with linear K_d (1D) and constant C_s dissolution rate.

4.1.6 General comments

We got both K_d /SL and thermodynamic results from 3 participants: Andra, CEA and IRSN (JRC and SCK only performed K_d /SL calculations in this geometry). All of them show a very good agreement between the two sorption models but there are some discrepancies between participants.

For instance, the C_s concentration at the contact with the waste after 10,000 years is about $2 \cdot 10^{-4}$ moles/L (Andra), $1 \cdot 10^{-5}$ moles/L (CEA) and 10^{-4} to 10^{-3} moles/L (IRSN). These differences can be explained by the different dissolution rates and the different flux ratio that cross the bentonite plug. However, the effect of mineral changes and the decrease of exchange sites concentration in the near field, modelled by Andra, seem to have rather low influence on C_s transfer.

All participants noticed that in a 1D axial simulation, the boundary is very quickly reached. However, the C_s plume would not reach the concrete plug with additional clay minerals (as large sorption sink) as it was observed in the 2D radial calculations (transport is then dominated by the radial direction).



4.2 Radial Cs transfer in claystones obtained with Kd/SL, Langmuir and thermodynamic models

The following results and comments were asked to all participants:

- Plots of Cs concentration profile as a function of radius at 100, 1,000, 5,000, 10,000 and 50,000 years after the release
- Plots of the evolution with time (from 0 to 50,000 years) of Cs concentration, at points located 0 and 1 m from the waste
- Discussions about the Cs sorption models and differences between the 3 models (constant isotherm, Langmuir and thermodynamic);
- If possible for interpretation, plots of Cs isotherms solid vs solution.

4.2.1 Results from Andra

The radial transfer of Cs in the Callovo-Oxfordian claystone was simulated by three different sorption models: Kd, Langmuir and thermodynamic models, corresponding respectively to the tasks 2, 5 and 6 of the benchmark.

4.2.1.1 Kd/SL Model

Two different Kd values are considered to represent the radial Cs transfer, one in the EDZ ($0.01 \text{ m}^3/\text{kg}$) and another one in the undisturbed claystone ($0.3 \text{ m}^3/\text{kg}$). Figure 4.2.1 shows the evolution of concentration profiles in Cox claystones and Figure 4.2.2 shows Cs concentration over time at two points: one is at the interface with the waste and the other one is located 1 m from the waste interface.

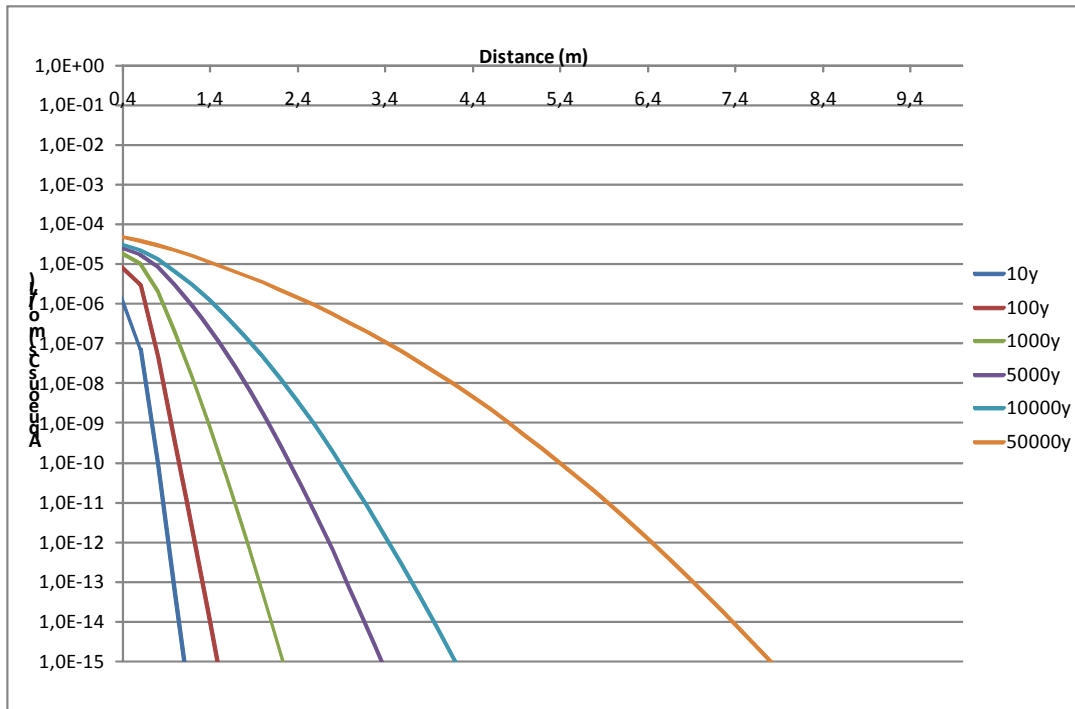


Figure 4.2.1: Evolution with time of Cs concentration profiles in claystones, Kd model

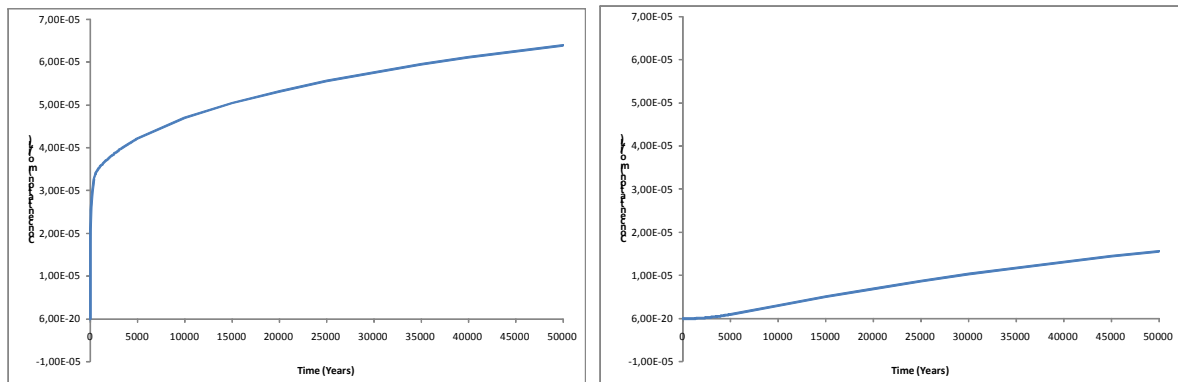


Figure 4.2.2: Temporal evolution of Cs concentration at 0 m (left) and 1 m (right) in claystones, Kd model

4.2.1.2 Langmuir model

In the view to represent Cs sorption following a Langmuir isotherm as defined in the benchmark (Figure 4.2.3 and Figure 4.2.4), two surface sites are defined in the Phreeqc input script. The first one allows taking in account Cs sorption for lower than 10^{-5} mol/L concentrations, whereas the second sorption site allows considering Cs sorption for higher concentrations.

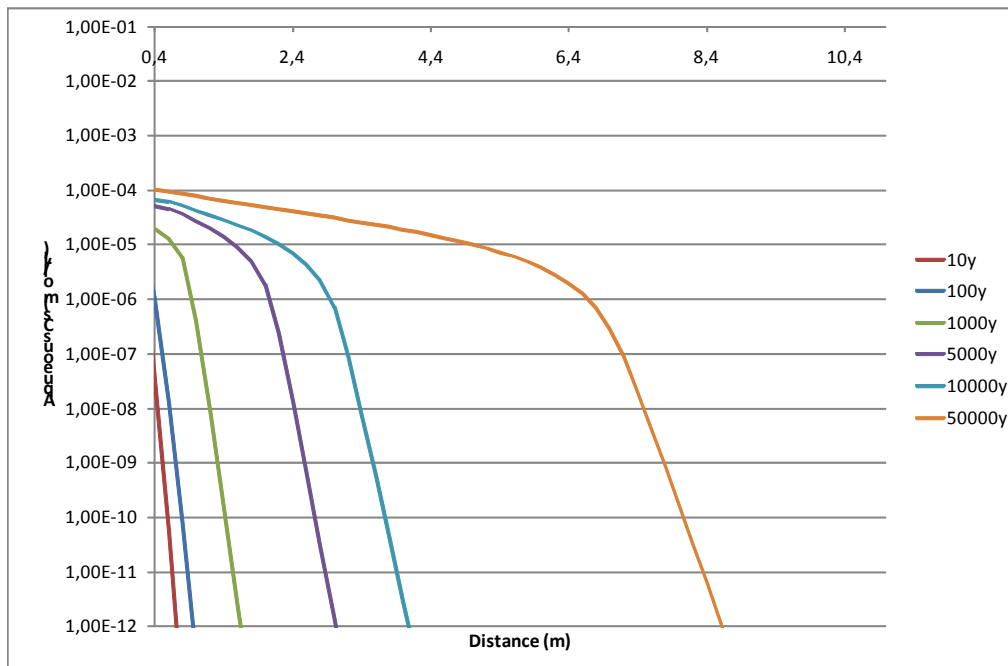


Figure 4.2.3: Evolution with time of Cs concentration profiles in claystones, Langmuir model

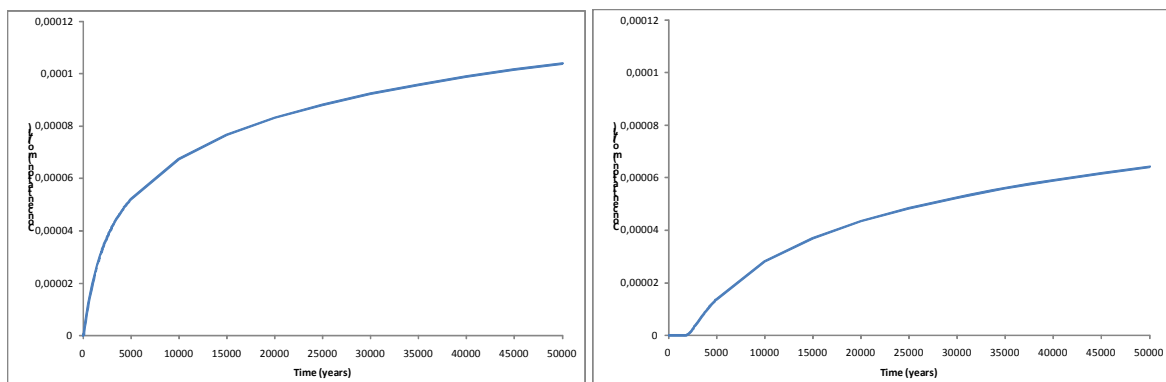


Figure 4.2.4: Temporal evolution of Cs concentration at 0 m (left) and 1 m (right) in claystones, Langmuir model

Cs sorption isotherm with the Langmuir model is drawn in Figure 4.2.5. The partition coefficient is strongly non linear. However, the linearity domain is limited to small Cs concentration ($< 10^{-6}$ mol/L), as it was the case for the Cs axial transfer simulated with the thermodynamic model (cf. § 4.1.1.3).

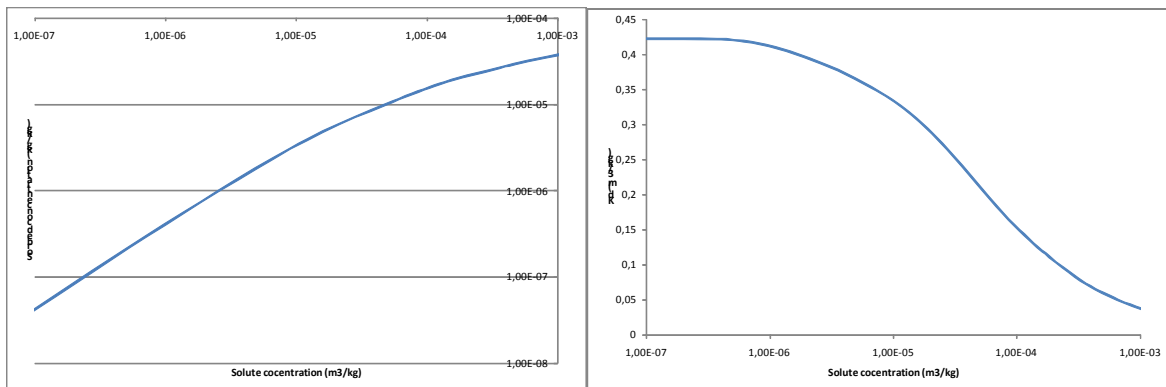


Figure 4.2.5: Cs Sorption isotherm in claystones, Langmuir model.

4.2.1.3 Thermodynamic model

The thermodynamic model used to represent the host rock formation is derived from the one used in bentonite, because of the absence of detailed chemical description of this formation in the benchmark. Surface sites being stuck to the smectitic phase, we suppose that the amount of available sorption sites can be directly estimated from the ratio of the smectite amount defined in the bentonite plug and in claystones. Thus, the bentonite plug presents 7 times more sorption sites than claystones. The competition between Cs and Rb is taken into account in the thermodynamic approach (Figure 4.2.6 and Figure 4.2.7).

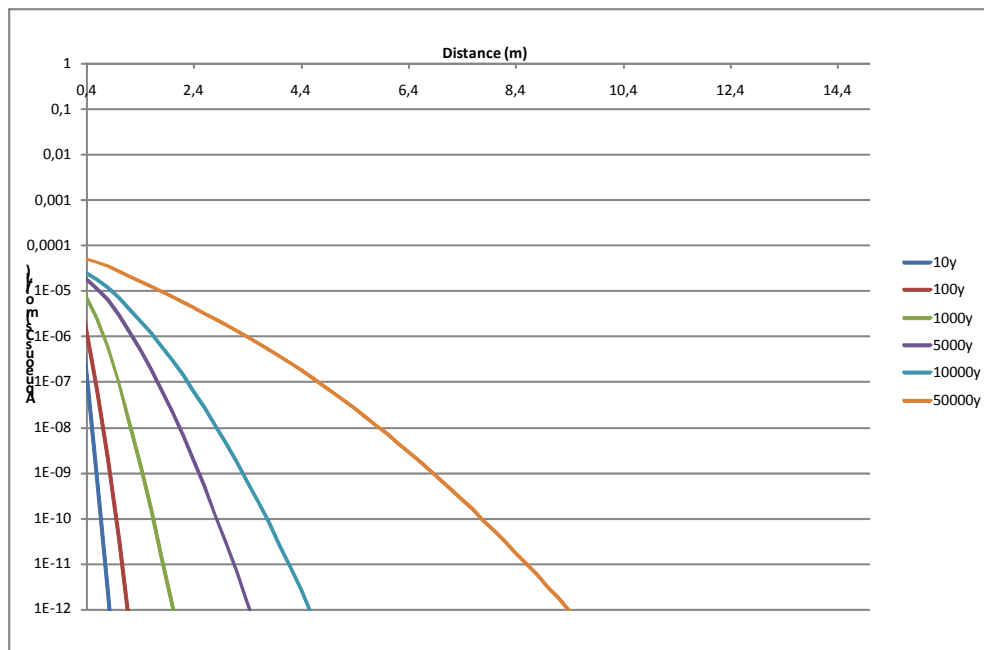


Figure 4.2.6: Evolution with time of Cs concentration profiles in claystones, thermodynamic model

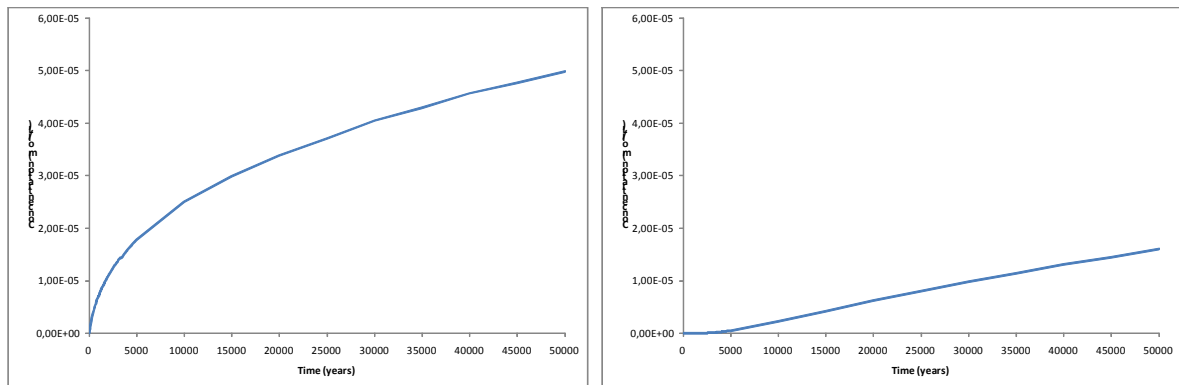


Figure 4.2.7: Temporal evolution of Cs concentration at 0m (left) and 1m (right) in claystones, thermodynamic model

The Cs exchange coefficient appears to be almost linear in the considered concentration range (Figure 4.2.8). This profile implies that the sorption sites are not saturated as they are in the bentonite plug (see section 4.1.1.2 and Figure 4.1.5), due to the claystone volume seen by caesium in 1D radial which counterbalances the exchange site concentration lower in claystones than in the bentonite plug. The thermodynamic model can thus be correctly simulated by a Kd model considering an equivalent Kd value.

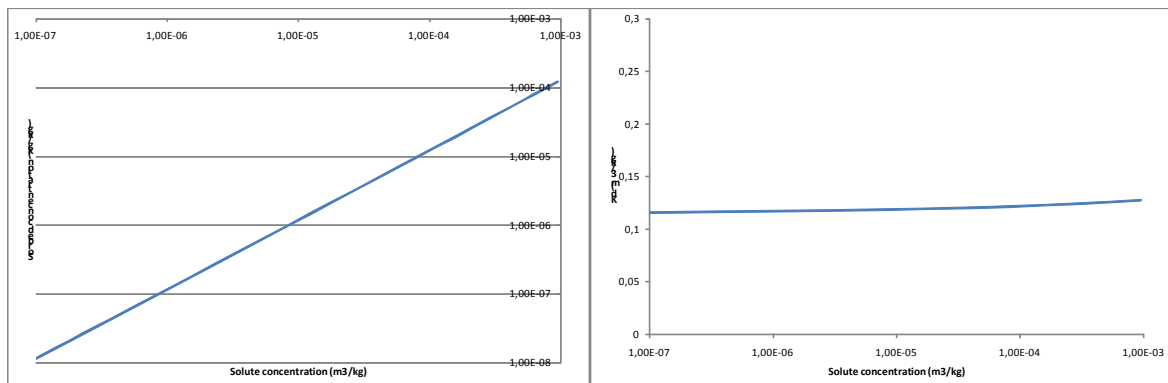


Figure 4.2.8: Cs Sorption isotherm (left) and exchange coefficient (right) in claystones, thermodynamic model

4.2.1.4 Comparison of results in Callovo-Oxfordian claystones

The three sorption models are presented in Figure 4.2.9. Comparing these models, the highest simulated Cs transfer lengths are obtained with the Langmuir model and the shortest with the Kd model. Thus, the Kd approach with the considered parameters is not conservative.

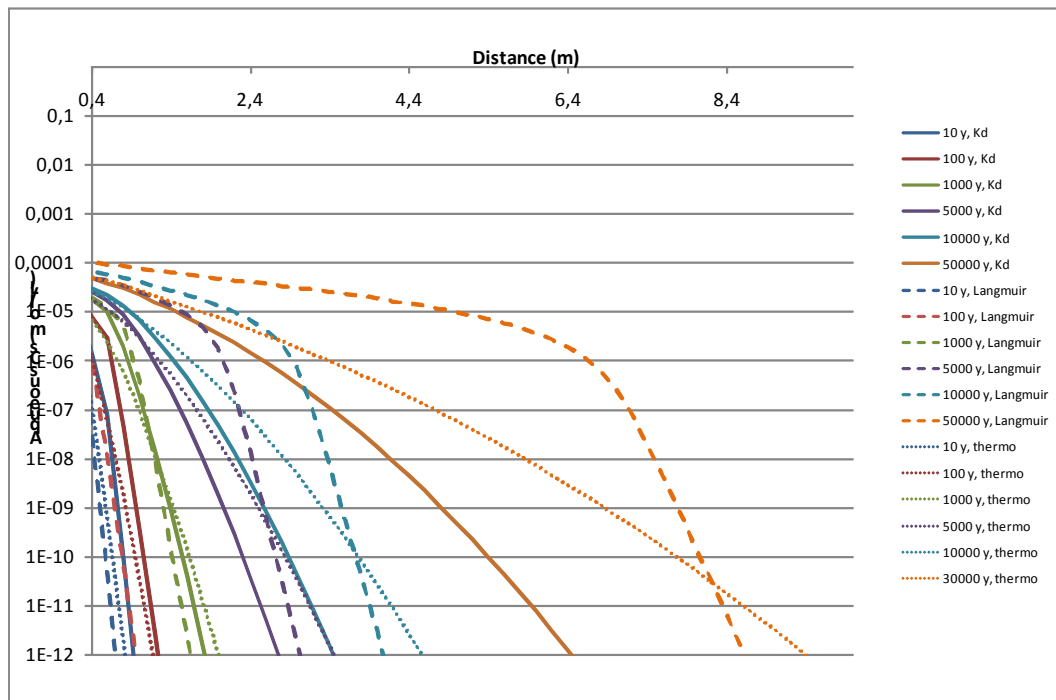


Figure 4.2.9: Comparison of concentration profiles in claystones with different models (Kd, Langmuir and thermodynamic)

Figure 4.2.10 shows the evolution of Cs concentration near the waste interface, according to the three models. The important amount of available claystone around the waste package in comparison to the amount of bentonite leads to a lower degradation of the claystone (see section 3.1.3.1). Thus, the dissolution of smectite at the interface with the glass does not lead to a significant reduction of the Cs sorption modelled by the thermodynamic model.

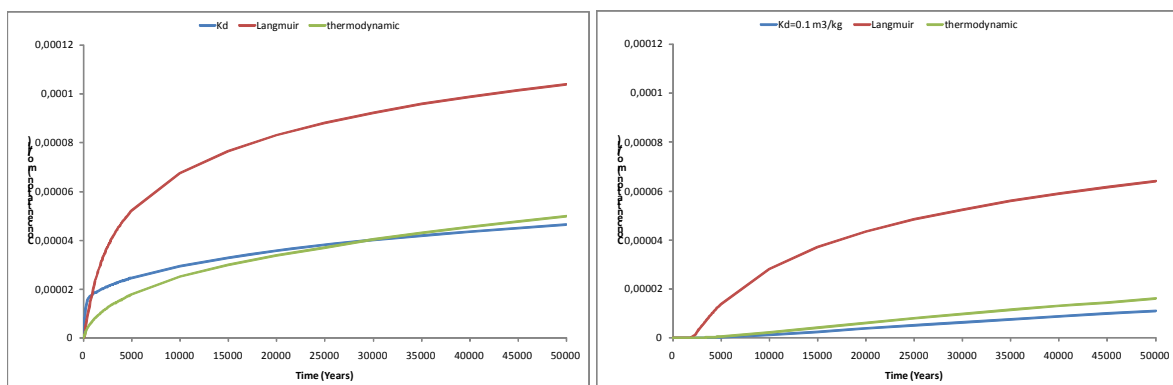


Figure 4.2.10: Comparison of Cs profiles at the waste interface (left) and 1m from the interface (right) in claystones with different sorption models (Kd, Langmuir and thermodynamic)

Figure 4.2.11 presents the comparison of Cs sorption isotherms in claystones with the three different models. With the thermodynamic model, the Cs partition coefficient appears to be almost linear in the considered concentration range. It appears that the Kd model in claystones leads to much higher Cs sorption rates and thus is not conservative in comparison

with the thermodynamic model. Actually, smaller sorption at high concentration with the Langmuir model leads to a greater capacity to make Cs diffuse in claystones, even if, for lower solute concentration (below 10^{-6} mol/L), the sorbed concentration becomes the highest with the Langmuir model.

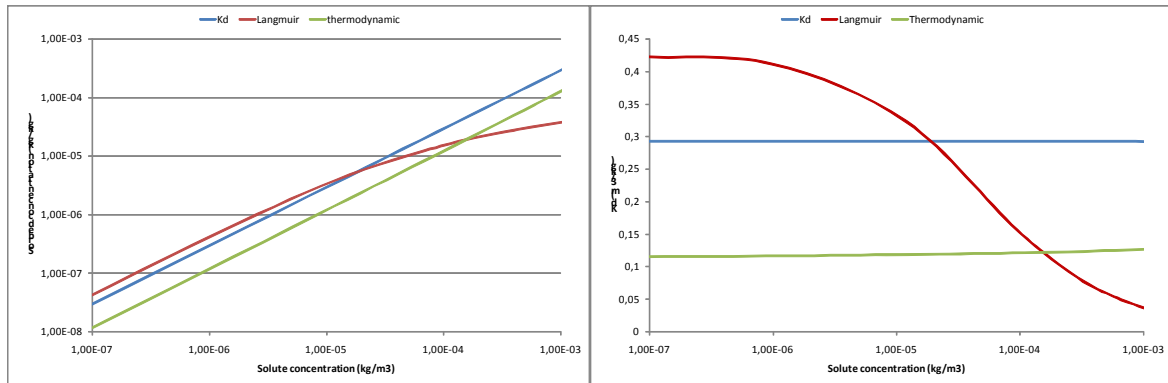


Figure 4.2.11: Comparison of Cs sorption isotherms (left) and partition coefficient (right) in claystones with different models (Kd, Langmuir and thermodynamic)

4.2.2 Results from CEA

In this radial case, the three models (Kd, Langmuir and thermodynamic) have a different behaviour. First, the Kd approach (Figure 4.2.12) seems to slow too much the diffusion. Then, the values taken for the Kd don't give an upper bound result of the thermodynamic model (as defined here). At the opposite, with the Langmuir approach (Figure 4.2.13 - with the limitations due to the code, see section 3.2.2.1) the aqueous front penetrates the most in the claystone. As a result, the front of Cs is in advance of time compared to the other approaches. This model is upper bound. At least, the results of the thermodynamic model (Figure 4.2.14) show a similar evolution than the Langmuir approach with a more important sorption.

The concentration history shows that for the Langmuir approach, the aqueous concentration is higher in the first time and stay one order over the other approach.

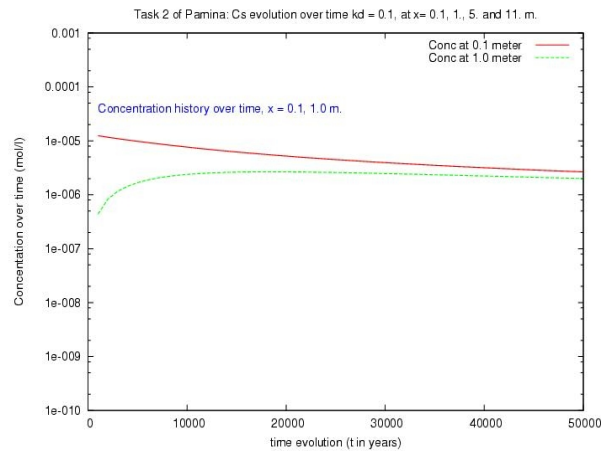
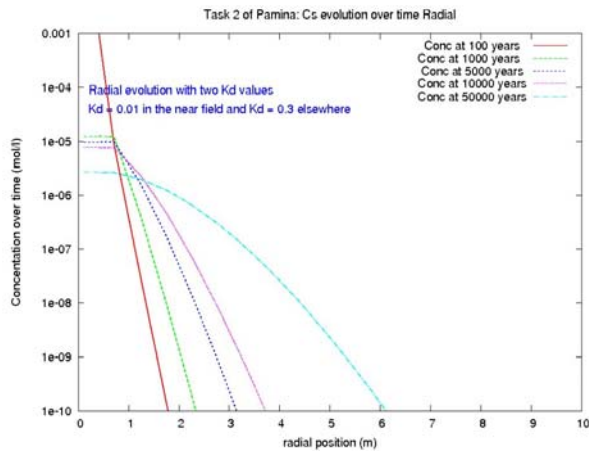


Figure 4.2.12: *Kd sorption model. Left: Cs evolution over time; right Cs concentration over time at x = 0.1 and 1.0 m*

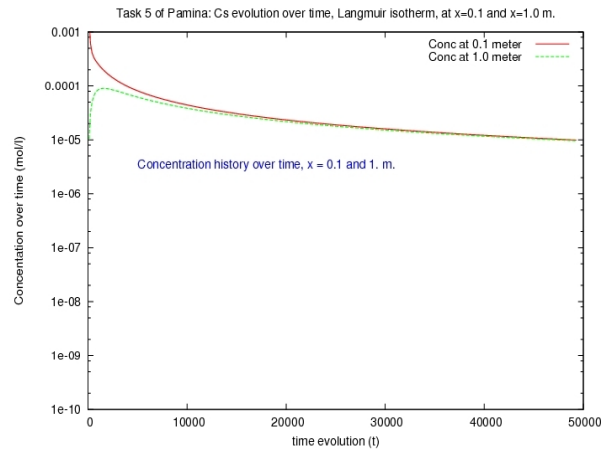
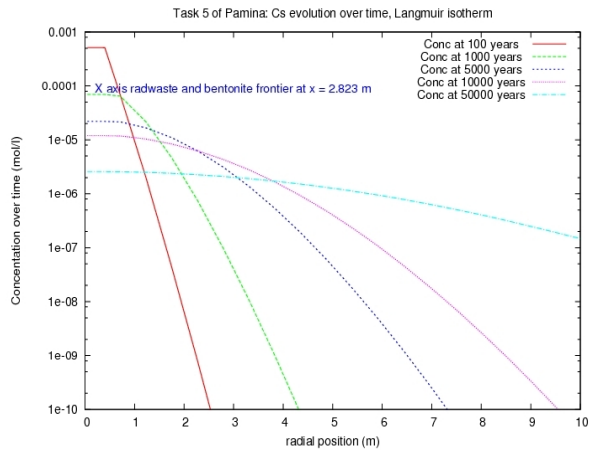


Figure 4.2.13: *Langmuir isotherm. Left: Cs evolution over time; right Cs concentration over time at x = 0.1 and 1.0 m*

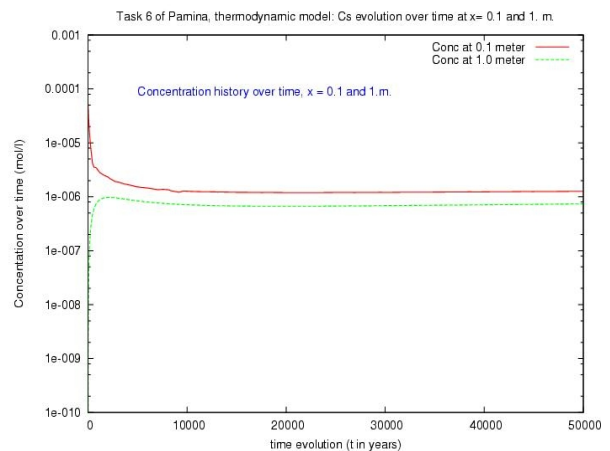
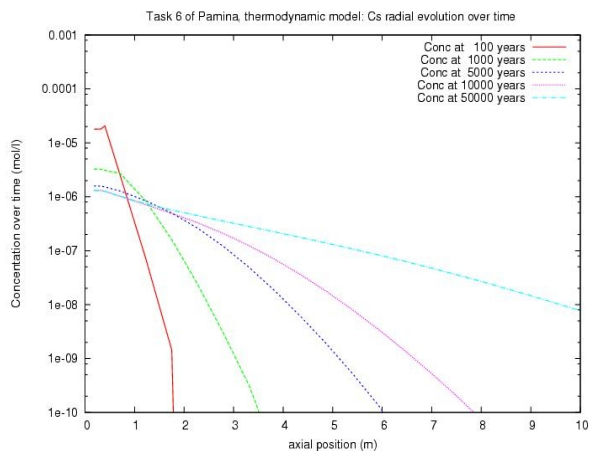


Figure 4.2.14: *Thermodynamic model. Left: Cs evolution over time; right Cs concentration over time at x = 0.1 and 1.0 m*

4.2.3 Results from IRSN

4.2.3.1 Linear K_D

Cs migration with constant K_D simulations in the Callovo-Oxfordian claystones are in very good agreement in both HYTEC modelling methods. Cs migrates over 6 m into the claystone with HYTEC method B and 5 m with HYTEC method A (Figure 4.2.15).

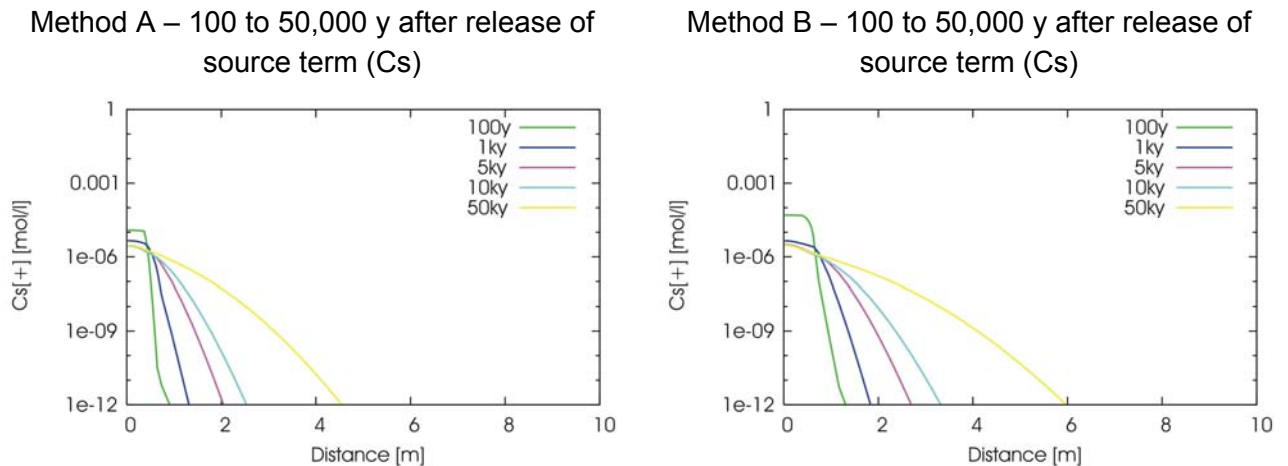


Figure 4.2.15: Task 2: 1D-radial with constant K_D/SL . Cs evolution over 50,000 years

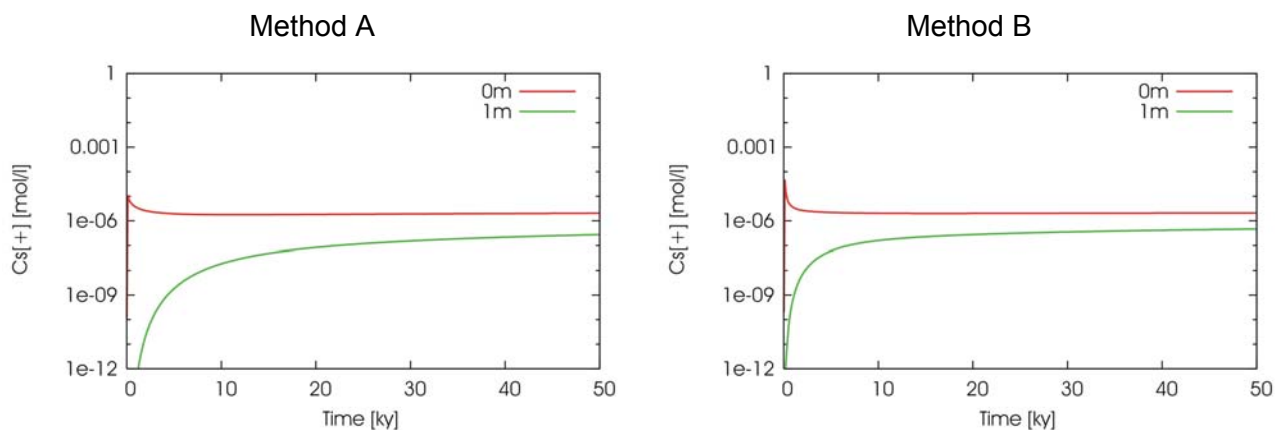


Figure 4.2.16: Task 2: 1D-radial with constant K_D/SL . Cs concentration over time at $x = 0m$ and $x = 0.1 m$

4.2.3.2 Langmuir isotherm

The Cs migration with Langmuir isotherm also occurs over 6 m into the Callovo-Oxfordian claystone (Figure 4.2.17). A slight competition effect occurs in the presence of Rb (with same sorption characteristics than Cs) involving the migration of Cs a little further. Equivalent $\rho_d \cdot R_D$ has been calculated around 4,000 for low Cs concentrations (under 10^{-5} mol/L). When Cs concentration is above 10^{-5} mol/L, the sorption on strong sorption site is predominant inducing

a slow migration of Cs. However, the strong sorption sites are almost fully saturated and a small part of weak sorption sites starts to be occupied when Cs concentration comes close to 10^{-5} mol/L (close to the waste package). This induces a decrease of R_D and thus an increase of Cs mobility close to the waste package.

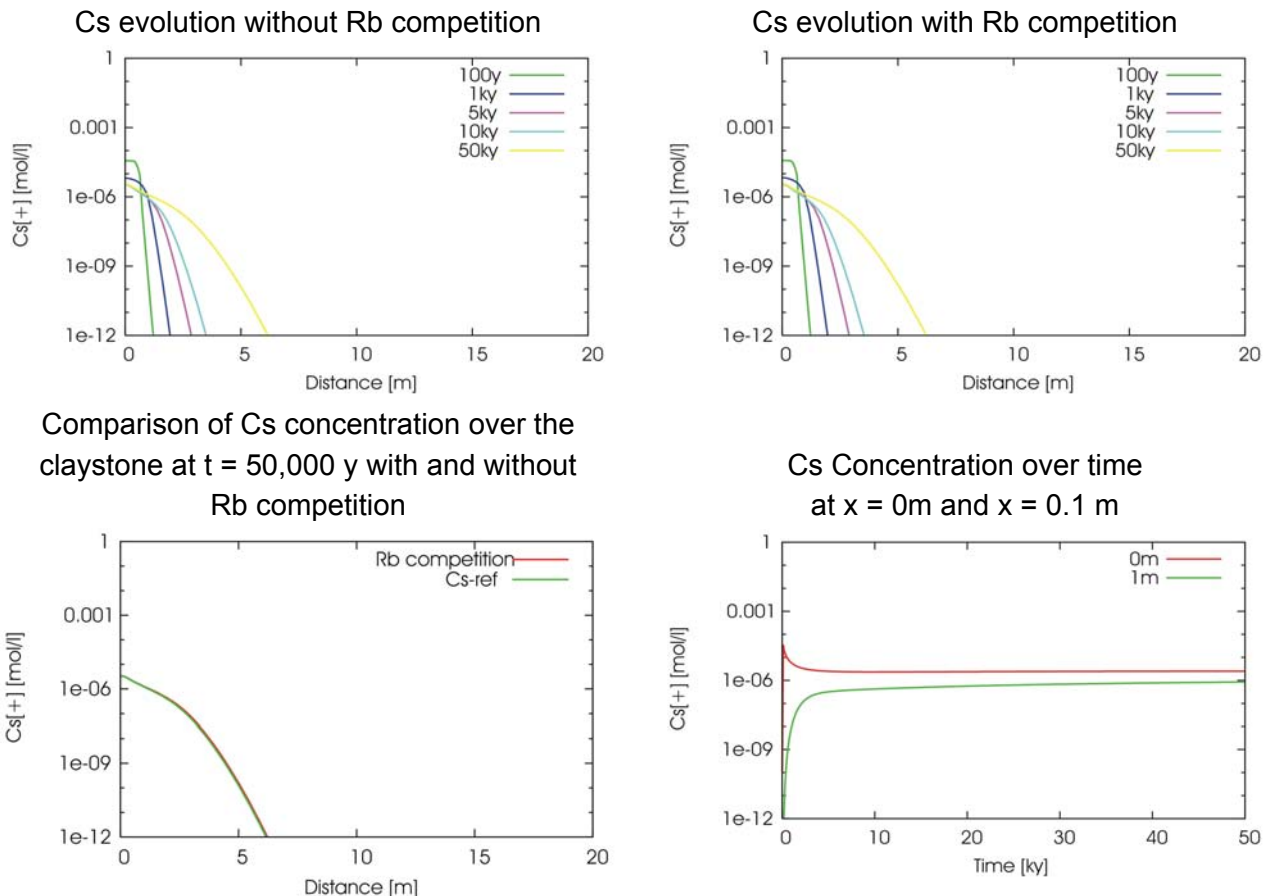


Figure 4.2.17: Task 5: 1D-radial with Langmuir isotherm sorption model

4.2.3.3 Thermodynamic model

Cs migrates over 11 m in the claystone and no competitive effect of Rb is noticed (Figure 4.2.18).

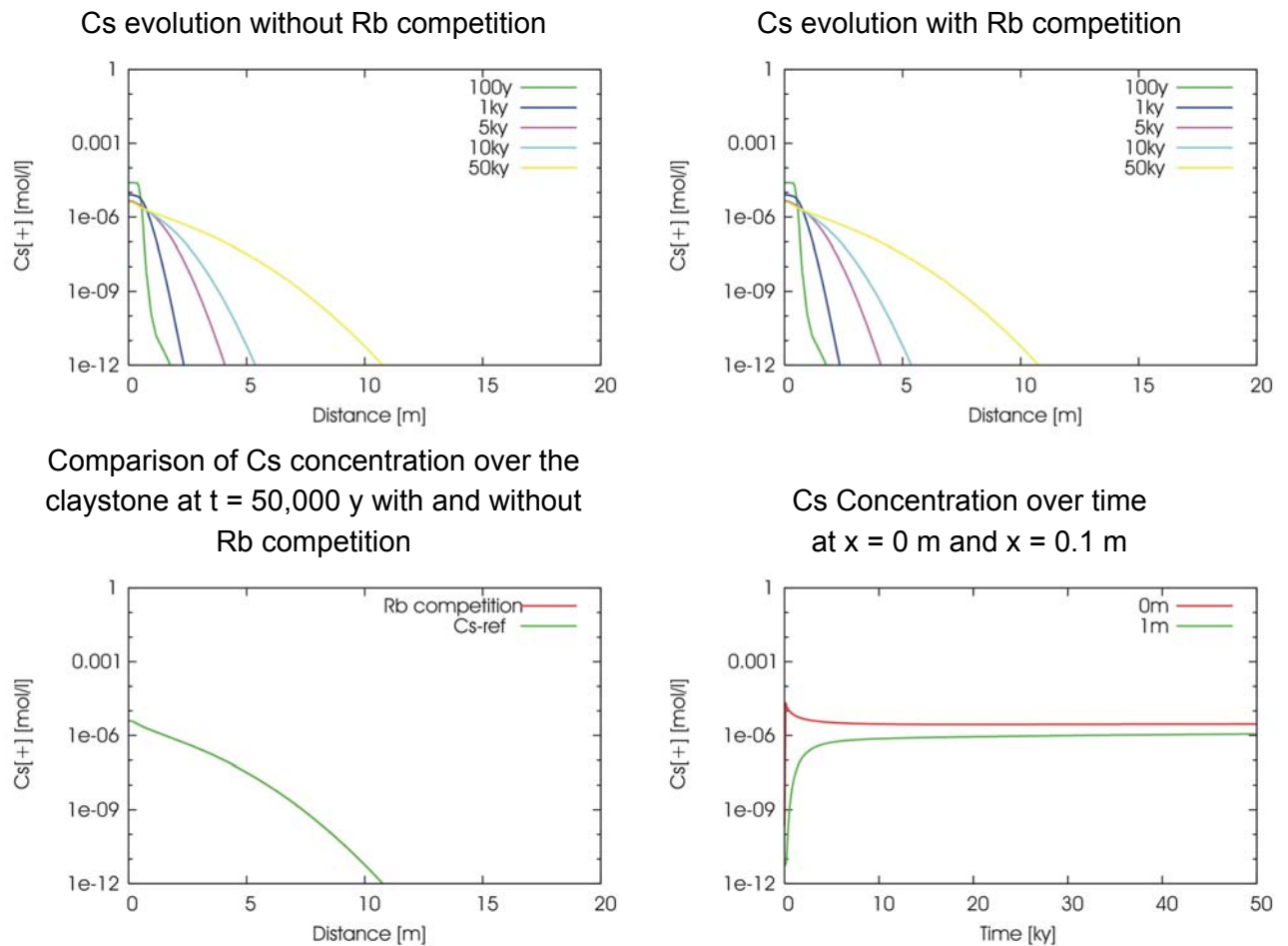


Figure 4.2.18: Task 6: 1D-radial with thermodynamic sorption model

4.2.4 Results from JRC

Results from 1D radial model (Kd/SL sorption model) are presented in Figure 4.2.19. The radial direction does not involve the bentonite barrier so the results are not affected by the different distribution coefficients in bentonite. No calculation was performed with thermodynamic model.

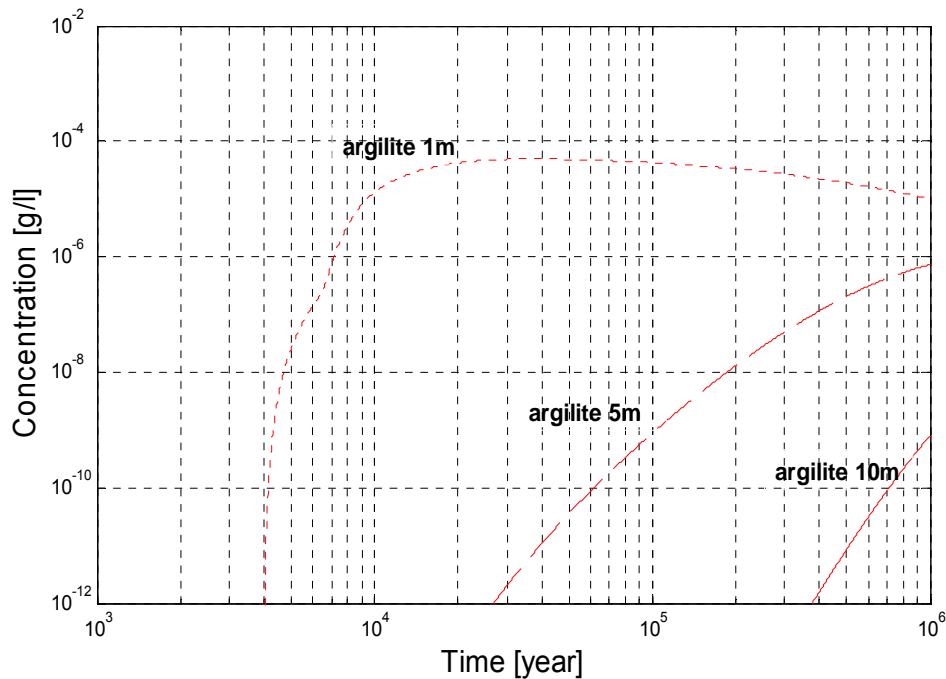


Figure 4.2.19: Concentration of ^{135}Cs in 1D radial direction, at 1 m, 5 m and 10 m through claystones

4.2.5 Results from SCK•CEN

4.2.5.1 Linear K_d

The predicted Cs concentration profiles for a 1D case with constant dissolution rate (lasting 50,000 years) are very different to those resulting for a case which considers an initial higher dissolution rate (4% in the first 3 years) and a very low dissolution rate thereafter (Figure 4.2.20). The former logically results in higher concentrations after longer times. The quasi immediate dissolution of 4% of the waste in the latter case resembles a pulse type source term. The remaining 96% of the waste dissolves so slowly (in $\approx 300,000$ years) that concentrations keep decreasing (after 1,000, 5,000, 10,000 and 50,000 years).

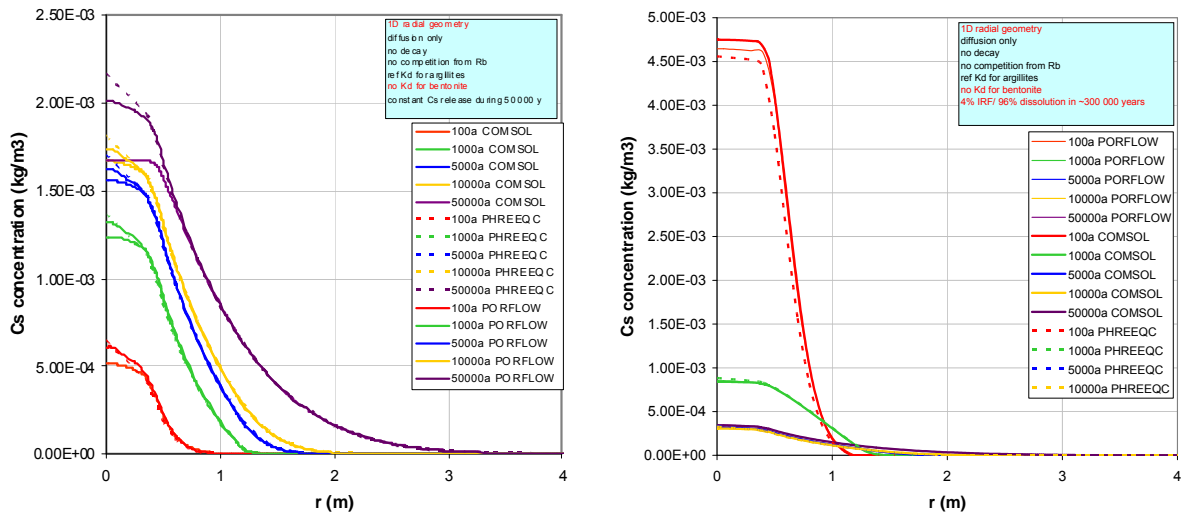


Figure 4.2.20: Radial concentration profiles for the simple model with linear K_d and constant C_s dissolution rate (left) and higher C_s dissolution rate at the start (right)

All C_s concentration plots shown hereafter represent C_s total concentration (all isotopes, in kg/m³) and stand for a constant dissolution rate (all the glass is dissolved in 50,000 years).

4.2.5.2 Langmuir sorption

The concentration profiles at $t = 100, 1,000$ and $5,000$ years show lower C_s concentrations in solution than for linear K_d (Figure 4.2.20). For $t = 10,000$ and $50,000$ years the opposite is true. This is consistent with the plot of the isotherms (Figure 3.5.3), which shows a crossing of the linear K_d and Langmuir isotherms at higher concentrations.

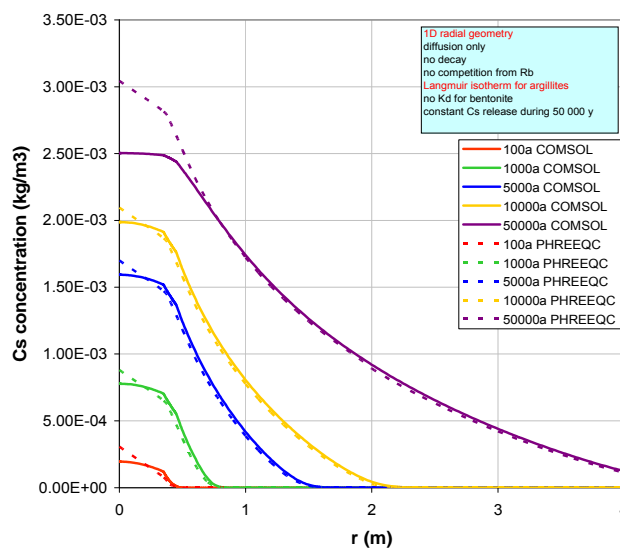


Figure 4.2.21: Radial concentration profiles for the simple model with Langmuir sorption

4.2.5.3 Thermodynamic model

For the thermodynamic models, Figure 4.2.22 shows that case 3a gives lower concentrations than case 3b and 3c. This is in line with our expectations based on the isotherms (Figure 3.5.3): case 3a gives a higher sorbed concentration for the same solute concentration. This means that a better representation of the pore water has an effect on the sorption behaviour, *i.e.* there clearly is a competition effect between the cations Na^+ , K^+ , Mg^{2+} , Ca^{2+} , Sr^{2+} , Fe^{2+} and Cs^+ .

A second observation is that case 3b and 3c give the same results. This was also already clear from the isotherms which coincide. This means that the additional release of Na and Ca from the waste (in case 3c) has no influence on the Cs sorption.

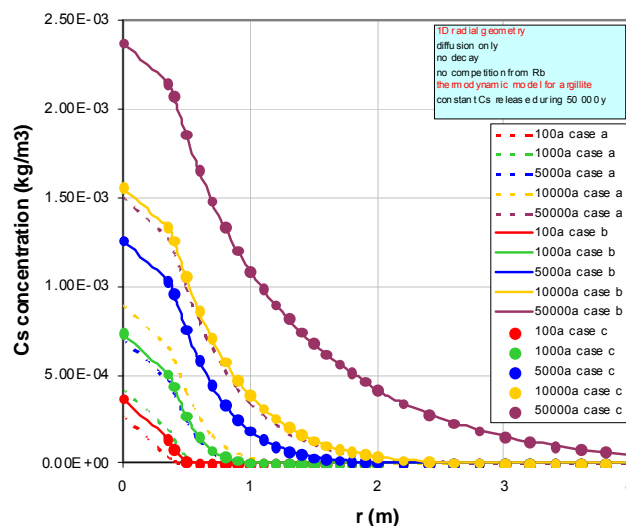


Figure 4.2.22: Radial concentration profiles for the complex models

4.2.5.4 Comparison of results in Callovo-Oxfordian claystones

Figure 4.2.23 compares the radial concentration profiles for Case 1 (linear K_d) and Case 3b/c (thermodynamic model). Concentration profiles for the first four output times (100, 1,000, 5,000 and 10,000 years) of the thermodynamic model are lower than those of the linear K_d approach, whereas the reverse is true after 50,000 years. This is related to the different sorption properties in the EDZ and the undisturbed claystone. In Case 1, the K_d in the EDZ is taken to be $0.01 \text{ m}^3/\text{kg}$ and $0.3 \text{ m}^3/\text{kg}$ for the Callovo-Oxfordian claystone (see Table 4.2.1 and isotherms in Figure 4.2.24). In case of the thermodynamic model, a K_d of about $0.08 \text{ m}^3/\text{kg}$ is calculated for the claystone, while the K_d of the EDZ for the thermodynamic model is only slightly smaller due to a small porosity change. In the beginning, the Cs front will mainly reach the EDZ, and concentrations calculated with the thermodynamic model (Case 3b) will be lower. Later on, sorption on the Callovo-Oxfordian claystone is more dominant and concentrations will be higher for the thermodynamic model compared to the linear K_d

approach. As such, the linear K_d model is not conservative for the defined thermodynamic model in the undisturbed COX claystone.

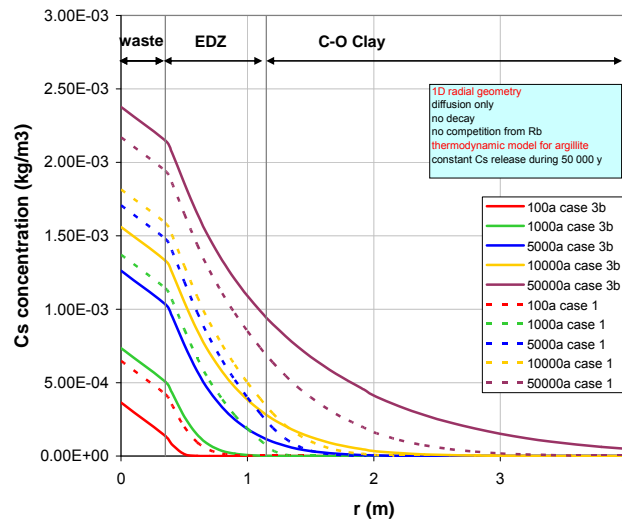


Figure 4.2.23: Comparison between the 1D radial concentration profiles for case 1 (linear K_d) and case 3b (thermodynamic model)

Table 4.2.1: Comparison of applied K_d values for case 1 and calculated K_d values for case 3 b/c

Sorption model		EDZ	Undisturbed Callovo-Oxfordian claystone
Case 1 (linear K_d model)	applied K_d value (m^3/kg)	0.01	0.3
Case 3 b/c (thermodynamic model)	calculated " K_d " value (m^3/kg)	0.063	0.08

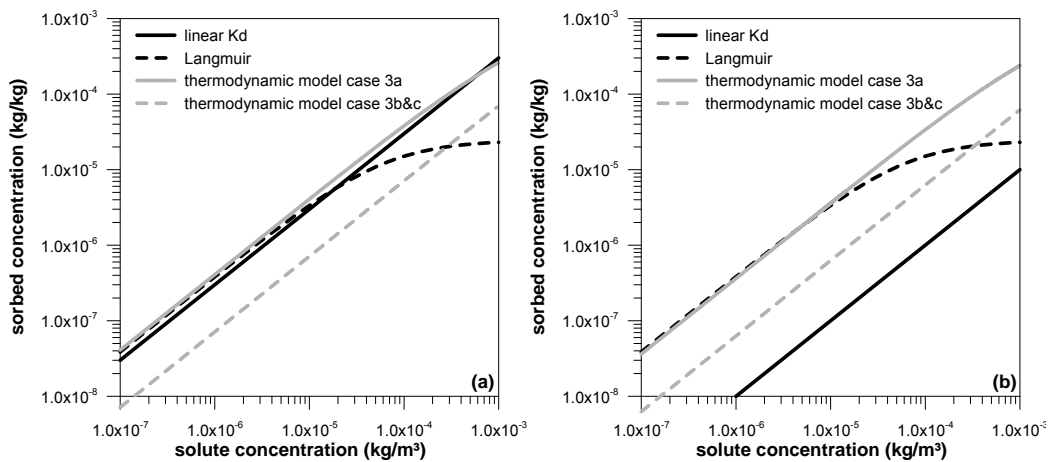


Figure 4.2.24: Comparison between isotherms (sorbed concentration vs. solute concentration) for linear K_d , Langmuir and thermodynamic cases in Callovo-Oxfordian claystone

The plots of the observation nodes (Figure 4.2.25) again show a good agreement between COMSOL, PORFLOW and PHREEQC for the reference Kd's (case 1). The agreement is a little less good for the Langmuir isotherm (case 2). COMSOL suffered from some instability problems (red curves), but this could be overcome by applying smaller time steps.

The same discussion applies for the observation nodes at 1 m in the radial direction.

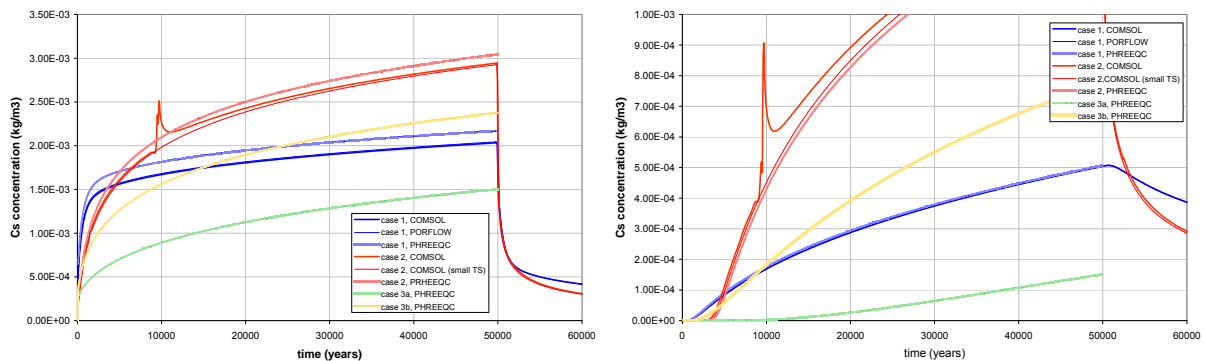


Figure 4.2.25: Observation nodes: concentration in the waste zone (left) and at $r = 1\text{ m}$ (right) for the different cases (1D).

4.2.6 General comments

All participants agree to say that the Kd model is not conservative for radial Cs transfer. However, all models (Kd/SL, Langmuir and Thermodynamic) give quite similar results.

According to Andra, Cs transfer with Kd model is the slowest and Langmuir is the fastest. At the waste interface Cs concentration is about $3 \cdot 10^{-5}$ Moles/L after 10,000 years but it is higher ($6 \cdot 10^{-5}$ moles/L) with the Langmuir model.

CEA's results give the same trends: Kd model is the slowest. After 10,000 years Cs concentration is about $1 \cdot 10^{-5}$ moles/L for Kd and Langmuir models but it is lower ($1 \cdot 10^{-6}$ moles/L) with the Langmuir model, at the waste interface.

IRSN results show that Cs transfer is faster using thermodynamic sorption model than using Kd/SL or Langmuir models. The concentration at the interface is $5 \cdot 10^{-6}$ moles/L in all cases.

Finally, results from SCK*CEN show no hierarchy between models. After conversion from kg/m^3 to moles/L (and considering the higher glass dissolution rate), surface Cs concentration ranges between $1.5 \cdot 10^{-6}$ and $3 \cdot 10^{-6}$ moles/L after 10,000 years.

Note that participants had to overcome some lacking definitions in the benchmark (sorption sites density). This explains the discrepancies between their results.



4.3 2D cylindrical Cs transfer at the head of the disposal cell (i.e. claystones and bentonite)

The following results and comments were asked to all participants:

- Plots of Cs iso-concentration maps 10,000 years after the release (2 cases: Kd and thermodynamic, not Langmuir)
- Plots of Cs concentration profiles along the same axes as those defined for axial and radial calculation
- Plots of the evolution with time (from 0 to 50,000 years) of Cs concentration, at the same points as those defined for axial and radial calculations (radially along an axis perpendicular to the waste axis, 1 m from the plug)
- Cs release rate and remaining Cs mass in the glass
- Discussions about the Cs sorption models and differences between the Kd and thermodynamic models
- If possible for interpretation, plots of Cs isotherms solid vs. solution

4.3.1 Results from Andra

Andra has performed no simulation in 2D.

4.3.2 Results from CEA

For the 2D model, Cs concentration profile is drawn along the canister symmetry plane (perpendicular to the canister axis) and Cs concentration histories are drawn in 2 point in the same plane and 2 points along the canister axis (2 additional points for thermodynamic results). Results from the 1D radial model are confirmed: the Kd approach is not upper bound. Then the results issued from the thermodynamic model show that the Cs plume goes further: more than 10 m at 50,000 y against 5 m in the 1D radial model (Figure 4.3.1 to Figure 4.3.3). Note that diffusion lengths are shorter than in 1D radial. This might be due to presence of intercalation blocks and to the fact that bentonite has a very high sorption capacity that limits Cs transfer across claystones.

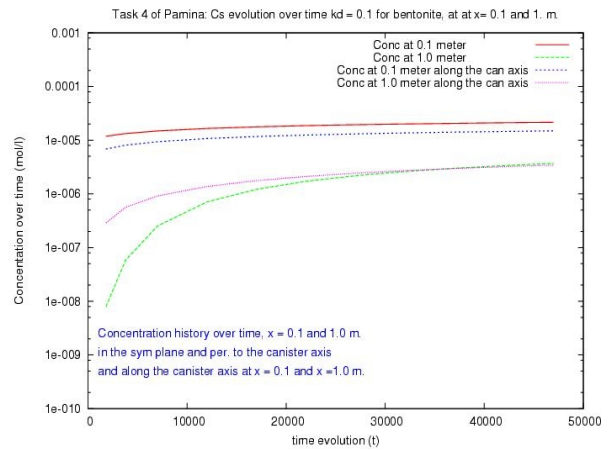
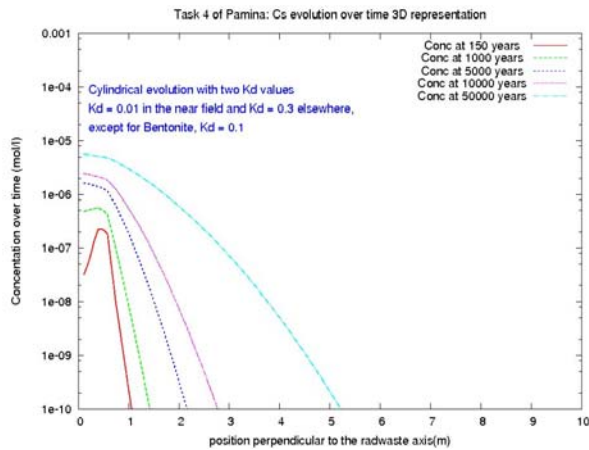


Figure 4.3.1: 2D model, $K_d = 0.1$, Cs concentration over time in the radial direction (left) and Cs history at different points (right)

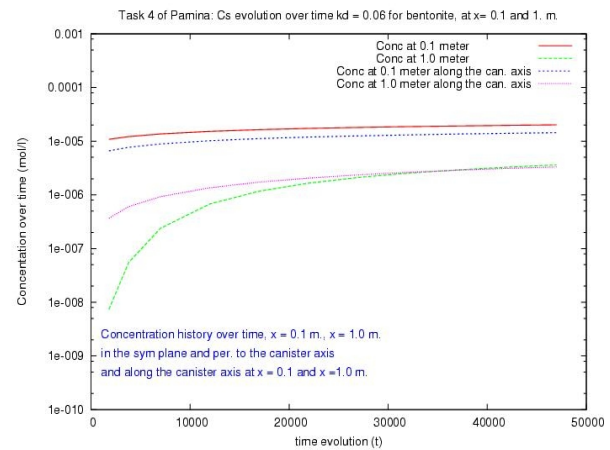
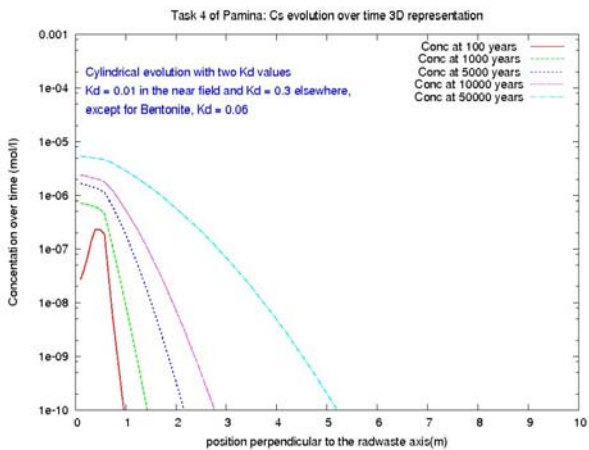


Figure 4.3.2: 2D model, $K_d = 0.06$, Cs concentration over time in the radial direction (left) and Cs history at different points (right)

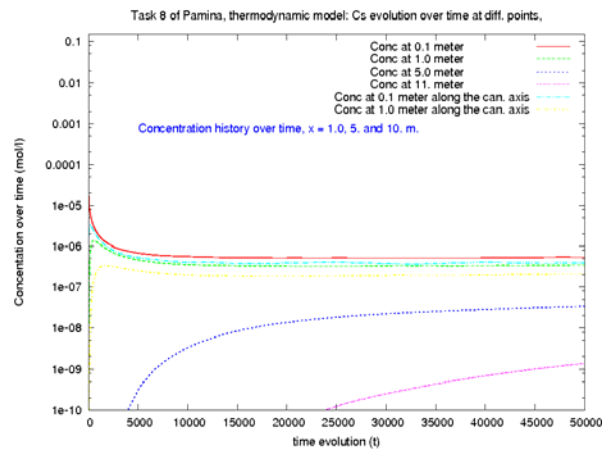
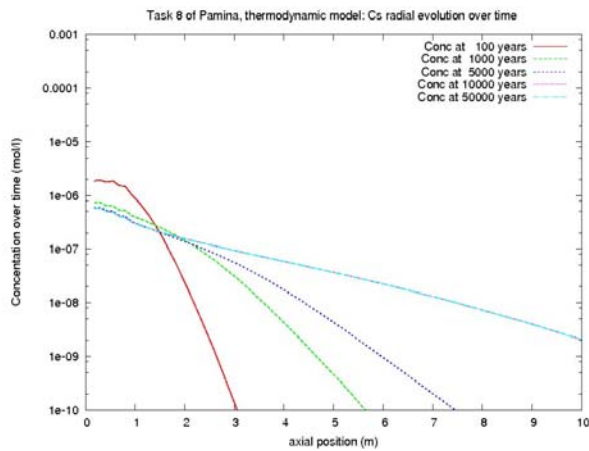
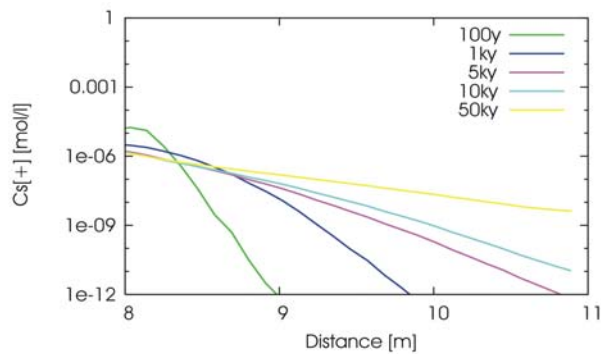


Figure 4.3.3: 2D radial thermodynamic simulation, Cs evolution over time in the radial direction (left) and concentration over time at $x = 0.1, 1., 5.$ and $11. m.$

4.3.3 Results from IRSN

4.3.3.1 Constant K_D/SL

Method B - 50,000 y after release of source term (Cs) ($\rho_d \cdot K_D = 291$)



Method B - 50,000 y after release of source term (Cs) ($\rho_d \cdot K_D = 486$)

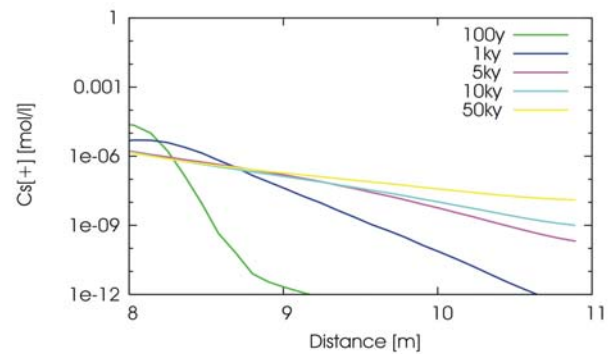


Figure 4.3.4: 2D-cylindrical with constant K_D/SL . Plots along the canister axis (bentonite). Cs evolution over 50,000 y

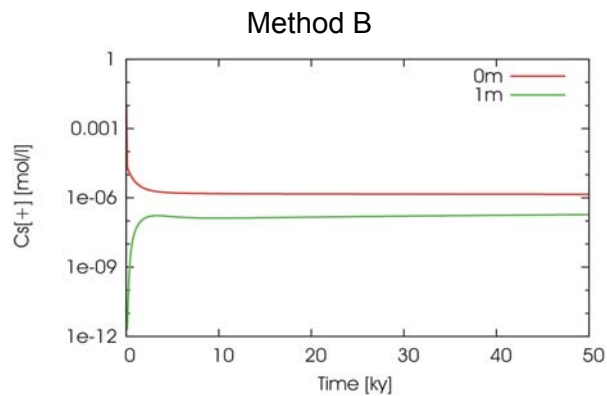


Figure 4.3.5: 2D-cylindrical with constant K_D/SL . Cs Concentration over time at points on the canister axis (bentonite): $x = 0$ m and $x = 0.1$ m

Method B - 50,000 y after release
of source term (Cs)

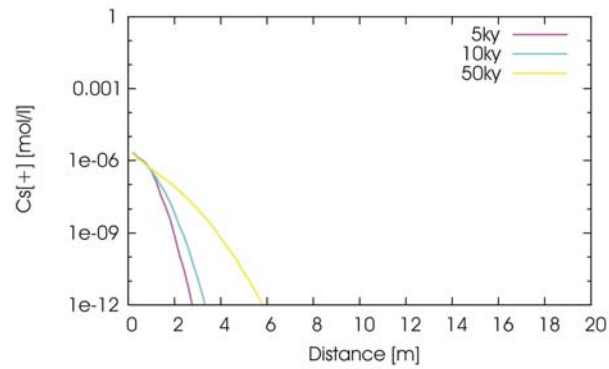


Figure 4.3.6: 2D-cylindrical with constant K_D/SL . Plots perpendicular to the canister axis (bentonite). Cs evolution over 50,000 y

Method B

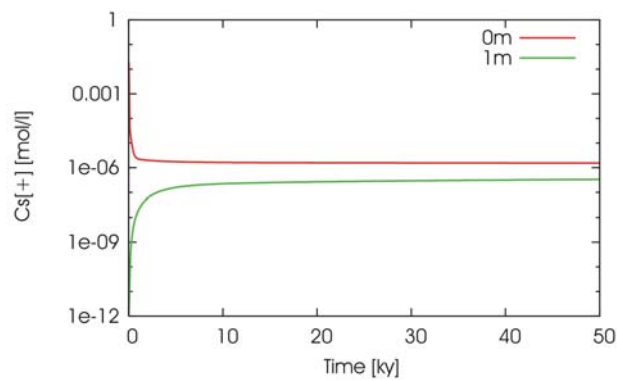


Figure 4.3.7: 2D-cylindrical with constant K_D/SL . Cs Concentration over time at points on the perpendicular axis (claystones): $x = 0$ m and $x = 0.1$ m

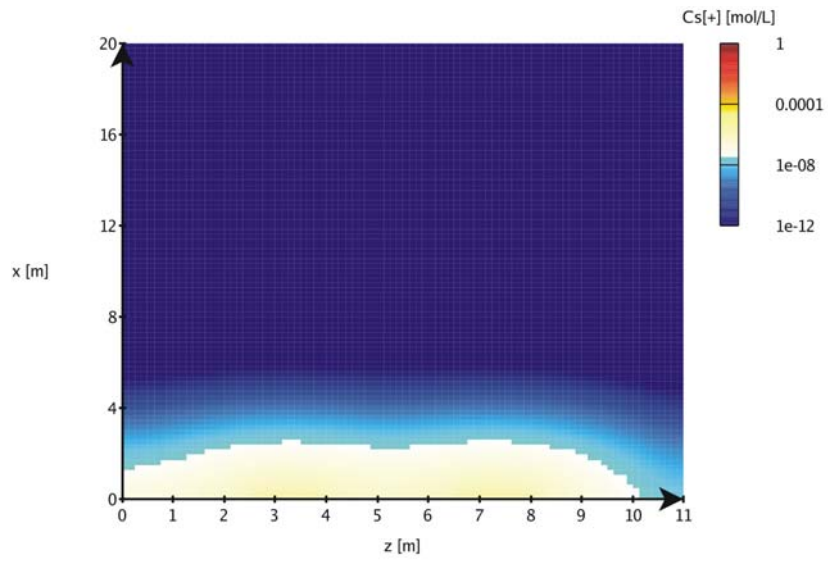


Figure 4.3.8: 2D-cylindrical with constant K_D/SL . Cs iso-concentration curves

4.3.3.2 Thermodynamic model

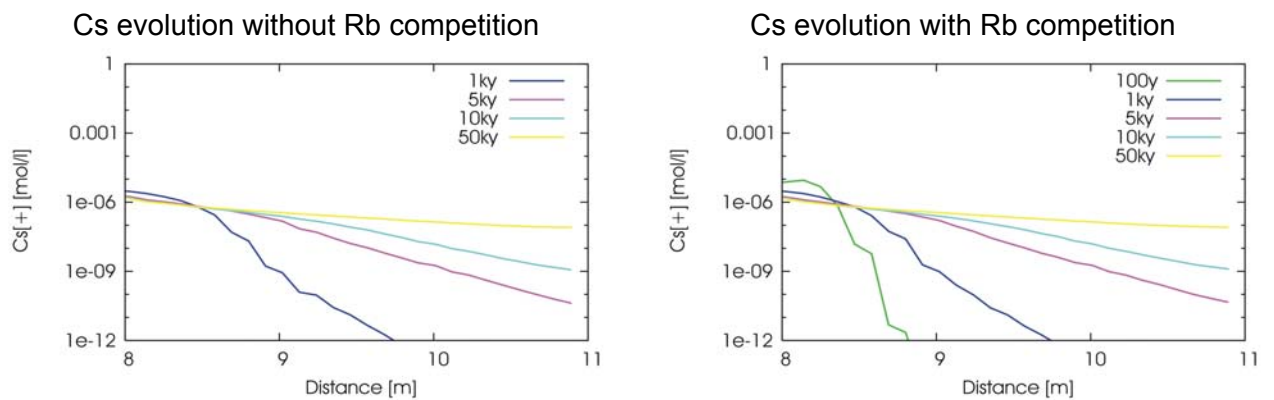


Figure 4.3.9: 2D-cylindrical with thermodynamic model. Plots along the canister axis (bentonite). Cs evolution over 50,000 y

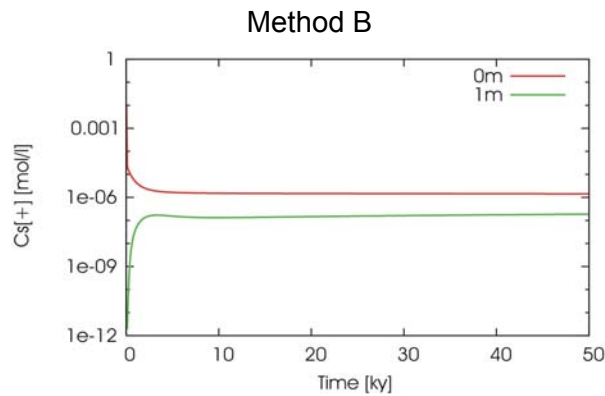


Figure 4.3.10: 2D-cylindrical with thermodynamic model. Cs Concentration over time at points on the canister axis (bentonite): $x = 0\text{ m}$ and $x = 0.1\text{ m}$

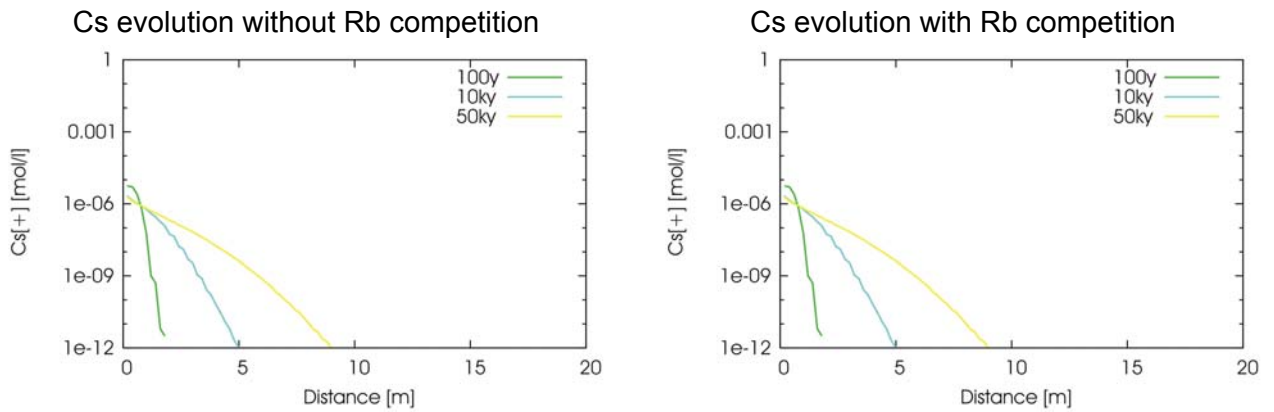


Figure 4.3.11: 2D-cylindrical with thermodynamic model. Plots perpendicular to the canister axis (claystones). Cs evolution over 50,000 y

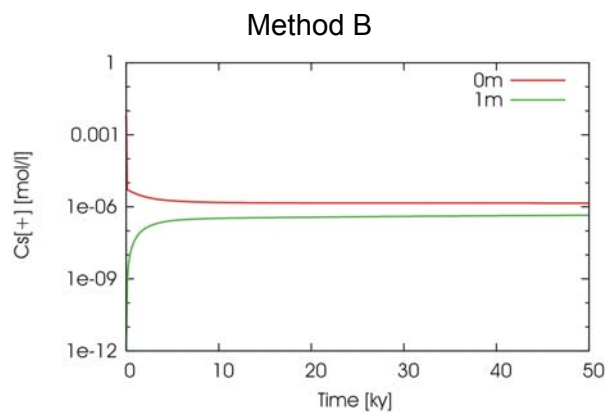


Figure 4.3.12: 2D-cylindrical with thermodynamic model. Cs Concentration over time at points on the perpendicular axis (claystones): $x = 0\text{ m}$ and $x = 0.1\text{ m}$

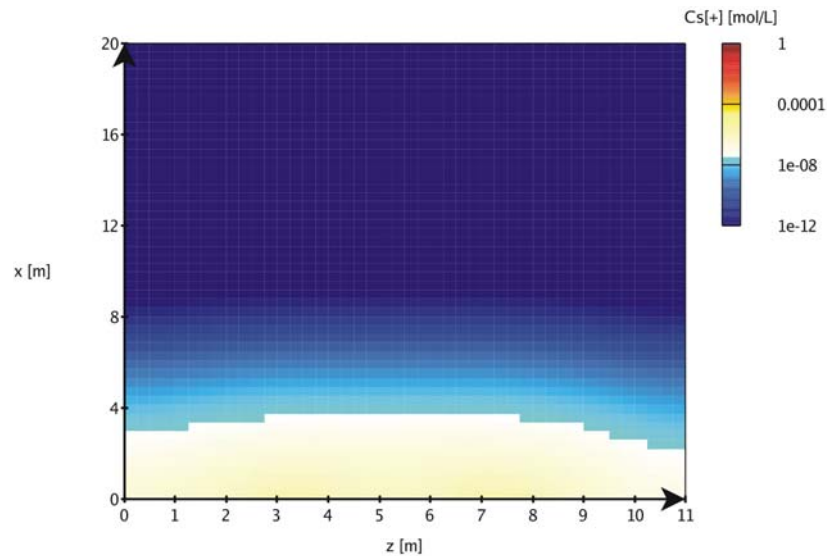


Figure 4.3.13: 2D-cylindrical with thermodynamic model. Cs iso-concentration curves

4.3.3.3 Comparison of Cs transfer models with 1D and 2D geometry

The migration of Cs has been modelled with three different approaches (constant K_D approach, Langmuir isotherm and full thermodynamic calculations). Globally, the results obtained with these different methods are quite similar: Cs migrates all over the bentonite plug and over a few meters into the argillaceous host rock (Figure 4.3.14).

Equivalent $\rho_d \cdot R_D$ value in 2D-cylindrical geometry is found out to vary between 200 for the higher Cs concentrations to 800 for the lower ones, which is in good agreement with constant $\rho_d \cdot K_D$ values proposed in this benchmark (291 and 486). Thus, considering that simulations performed with 2D-cylindrical geometry are more representative than those performed with 1D-axial symmetry, the equivalent R_D calculated have the same order of magnitude than known Cs K_D values in the bentonite:

$$K_D \sim R_D \text{ (thermo).}$$

Finally, even if thermodynamic calculations performed in this work appear to be more conservative than those with constant K_D , the description of Cs migration with these three methods is quite equivalent. However, it is worth mentioning that the results obtained are strongly dependent of the input parameters chosen and it is not possible to conclude whether K_D or thermodynamic parameters taken into account in this study are the most suitable to model accurately Cs migration.

Cs concentration profiles along the canister axis
(bentonite)

Cs concentration profiles perpendicular to the
canister axis (claystones)

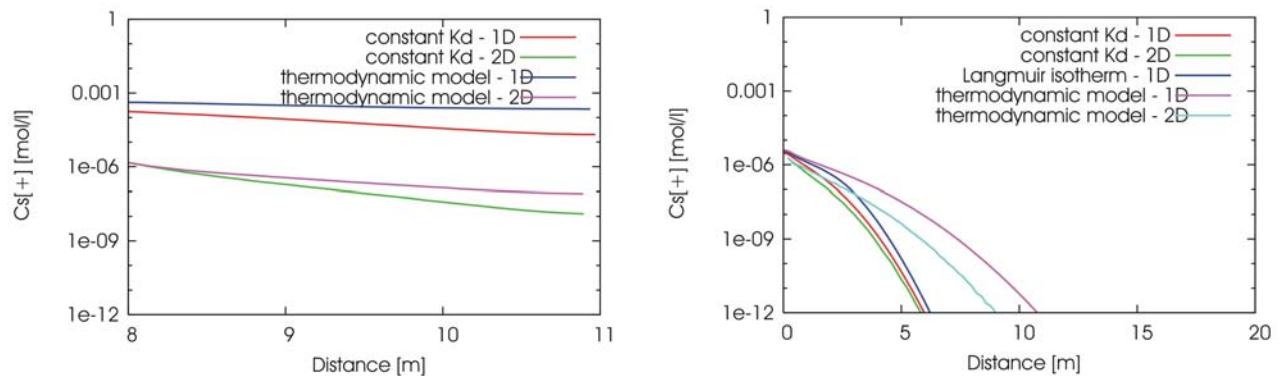


Figure 4.3.14. Cs transfer modelling cross-comparison. Comparison of Cs concentration profiles at 50,000 y with different sorption models

As in 1D-axial calculations, Cs still migrates over the whole bentonite plug with 2D-cylindrical symmetry. A strong channelization effect is observed in the bentonite when comparing 1D-axial and 2D-cylindrical calculations in both constant K_D /SL and thermodynamic modelling, which leads to a strong overestimation of Cs concentration of 2 to 3 orders of magnitude in the bentonite in 1D-axial simulations (Figure 4.3.14). Because of this and as detailed in § 4.1.3, equivalent R_D value calculated in 1D-axial symmetry (125) is probably underestimated and thus the Cs migration overestimated.

Regarding the migration of Cs in the claystone (Figure 4.3.14), 1D-radial and 2D-cylindrical calculations are also in very good accordance.

Regarding to the calculation times, 1D calculations are clearly shorter than those in 2D. However, if 1D-radial calculations are in good agreement with those performed with 2D-cylindrical geometry for the claystone, 2D-cylindrical symmetry is necessary to model accurately sorption process in the bentonite instead of 1D-axial geometry in order to account efficiently for the dilution effect.

4.3.4 Results from JRC

2D cylindrical calculations for concentrations obtained with Kd/SL model are presented in the form of two 1D plots in axial (Figure 4.3.15) and radial directions (Figure 4.3.16). The distribution coefficient of bentonite has again no influence on the results in radial direction. No calculation was performed with thermodynamic model.

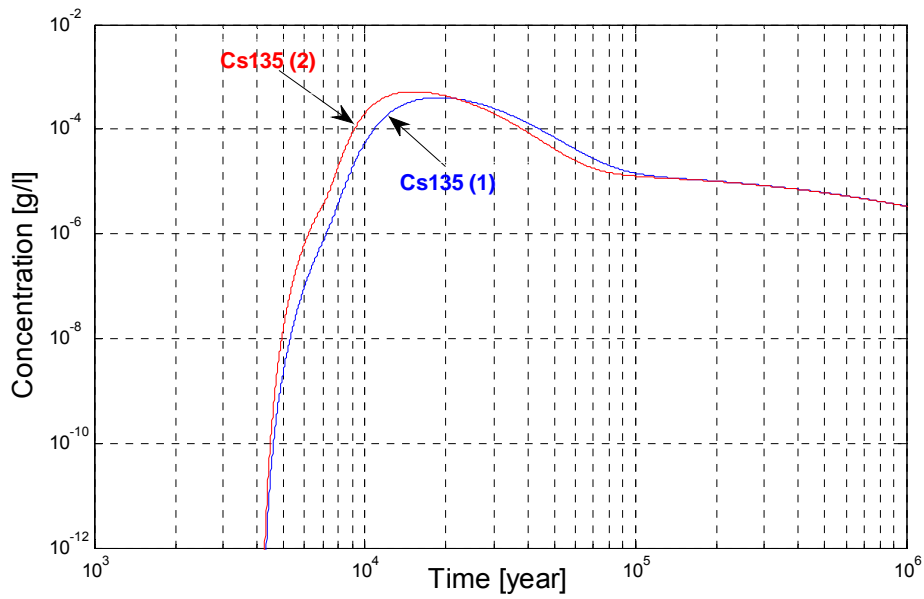


Figure 4.3.15: Concentration of ^{135}Cs in 2D axial direction, in the bentonite plug 1 m from the waste package:
 (1) reference distribution coefficient for bentonite $K_d = 0.1 \text{ m}^3 \cdot \text{kg}^{-1}$,
 (2) conservative distribution coefficient $K_d = 6 \cdot 10^{-2} \text{ m}^3 \cdot \text{kg}^{-1}$

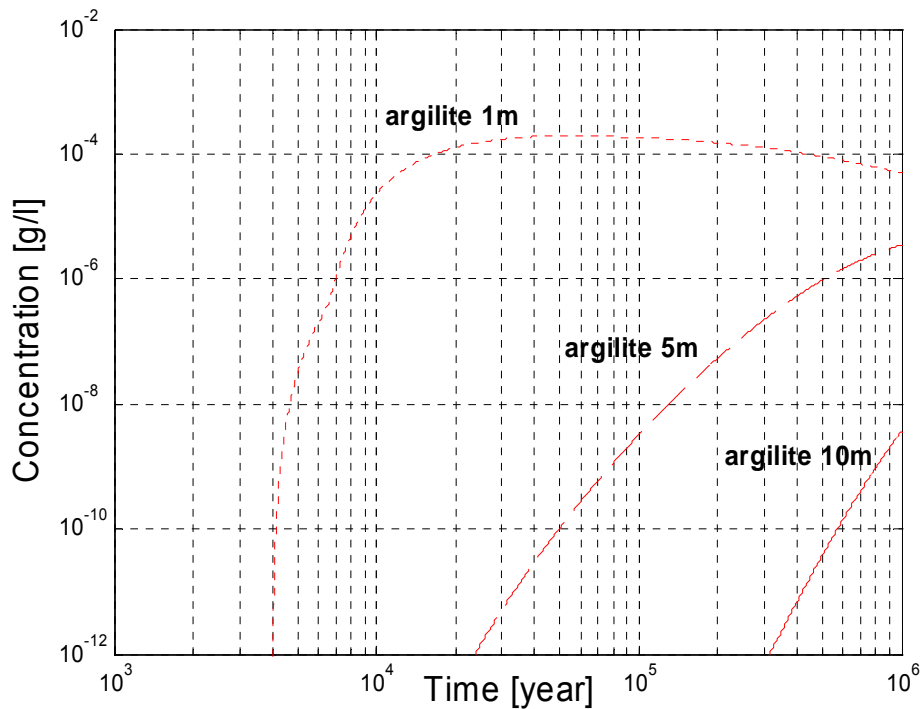


Figure 4.3.16: Concentration of ^{135}Cs in 2D radial direction, at 1m, 5m and 10m through claystones

4.3.5 Results from SCK*CEN

4.3.5.1 Linear Kd

The 2D simulations give lower Cs concentrations than 1D radial simulations (see section 4.2.5.1), which can be partially explained by the presence of additional sorption sites (*i.e.* on bentonite) (Figure 4.3.17). A second reason is the dilution effect: because of the presence of spacers and bentonite in the axial direction, the average Cs concentration per meter is not the same as in the 1D model.

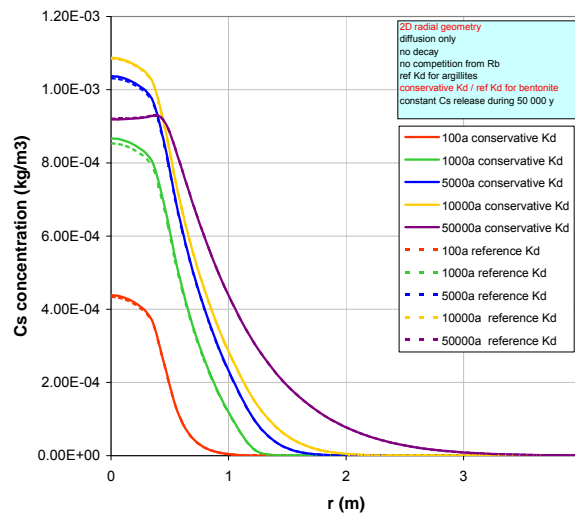


Figure 4.3.17: Radial concentration profiles for the linear Kd (2D) and constant Cs dissolution rate (COMSOL); comparison between a simulation using the conservative Kd and reference Kd for bentonite

In Figure 4.3.18 the influence of using a conservative Kd (0.06 m³/kg) instead of the reference Kd (0.1 m³/kg) for bentonite is examined and is found to be negligible.

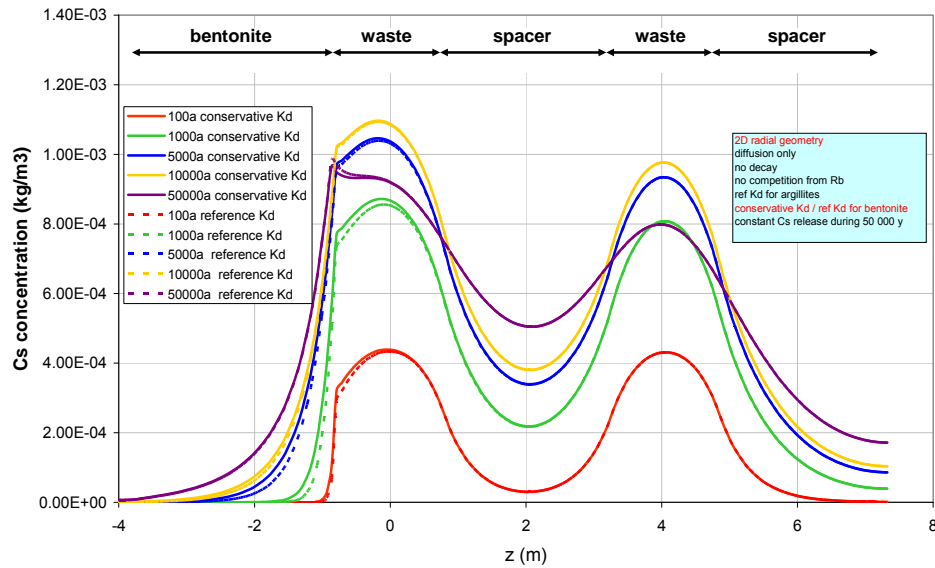


Figure 4.3.18: Axial concentration profiles for the simple model with linear K_d (2D) and constant C_s dissolution rate (COMSOL); comparison between a simulation using the conservative K_d and reference K_d for bentonite.

The effect of sorption in the bentonite is clearly visible in Figure 4.3.18 (steeper gradient at the bentonite/waste interface than at the spacer/waste interface). The differences in the height of the peaks are again due to the grid size limitation in PHREEQC. Note also that the C_s concentration in the waste cell next to the bentonite plug is higher than in the waste cell enclosed by two spacers. This is due to the fact that the porosity (0.36) and diffusion coefficient ($1.315 \times 10^{-2} \text{ m}^2/\text{y}$) of the bentonite plug are smaller than those of the spacer (0.40 and $1.578 \times 10^{-1} \text{ m}^2/\text{y}$, respectively). Note that the concentrations for the COMSOL model after 50,000 years (when all the vitrified waste has been dissolved) already started to decrease because of its interpolation procedure.

Figure 4.3.19 shows the C_s concentration field and iso-concentration lines after 10,000 and 30,000 years for the 2D radial model in case of linear sorption isotherms (K_d approach).

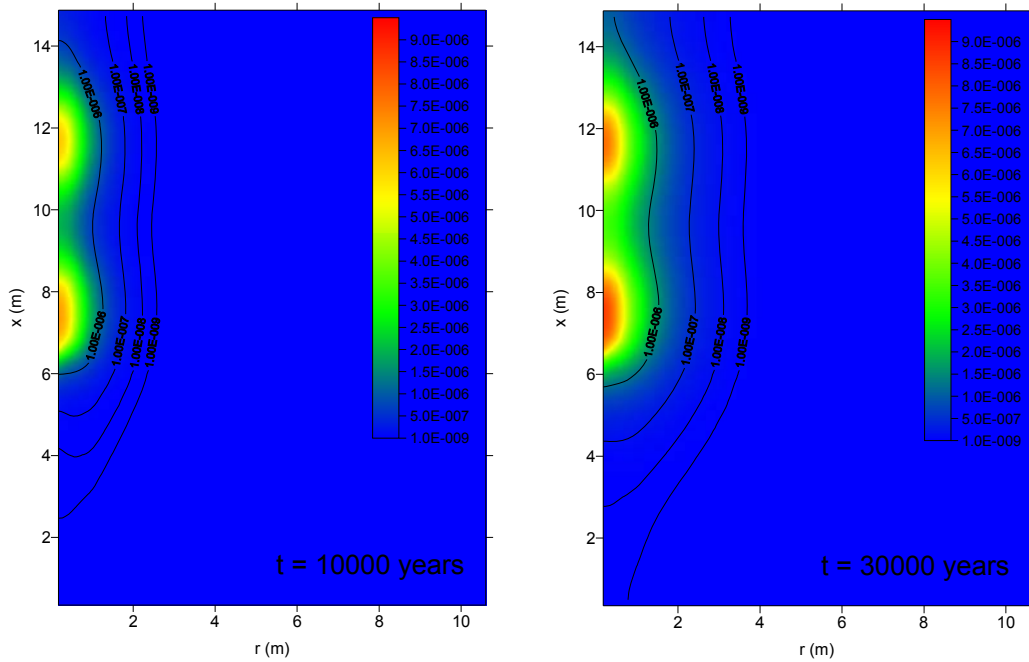


Figure 4.3.19: Iso-concentration maps for Kd/SL model at $t = 10,000$ and $30,000$ years after the release of Cs. Concentrations are in mol/l

4.3.5.2 Thermodynamic model

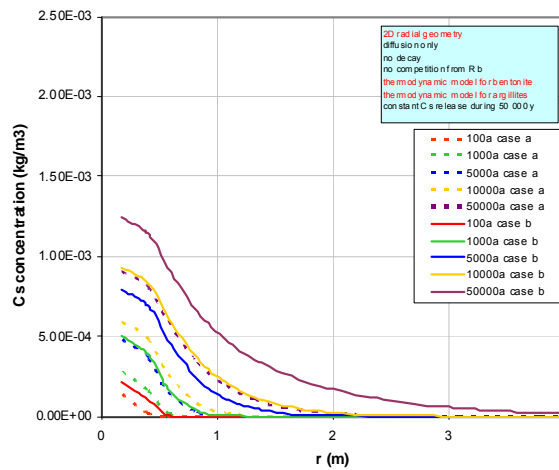


Figure 4.3.20: Radial concentration profiles for the complex models

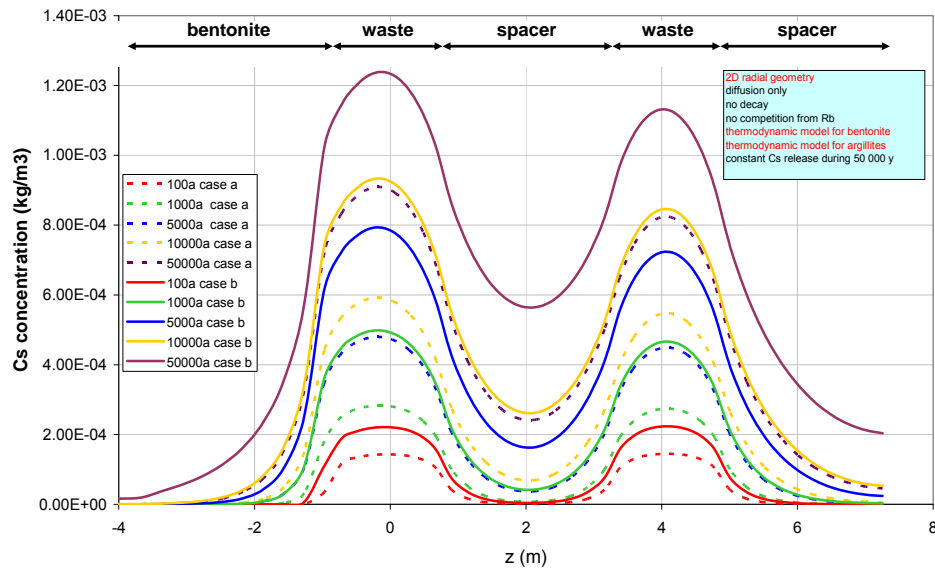


Figure 4.3.21: Axial concentration profiles for the complex models (2D)

Conclusions in radial 1D remain true (see section 4.2.5.3).

Figure 4.3.22 shows similar concentration maps and isolines in case of the thermodynamic sorption model (case 3 b/c). At 10,000 years, Cs is more confined within and in the direct environment of the waste packages than in case 1. Indeed, the ' K_d ' for the EDZ in case 3b/c is higher than in case 1, resulting in lower concentrations.

After 30,000 years, the concentration maps and isolines for case 1 and case 3b/c are very similar and higher concentrations for case 3b/c are expected at later times (not shown) since the calculated ' K_d ' for the host formation in case 3b/c is lower compared to case 1 (see Table 4.2.1 in section 4.2.5.4).

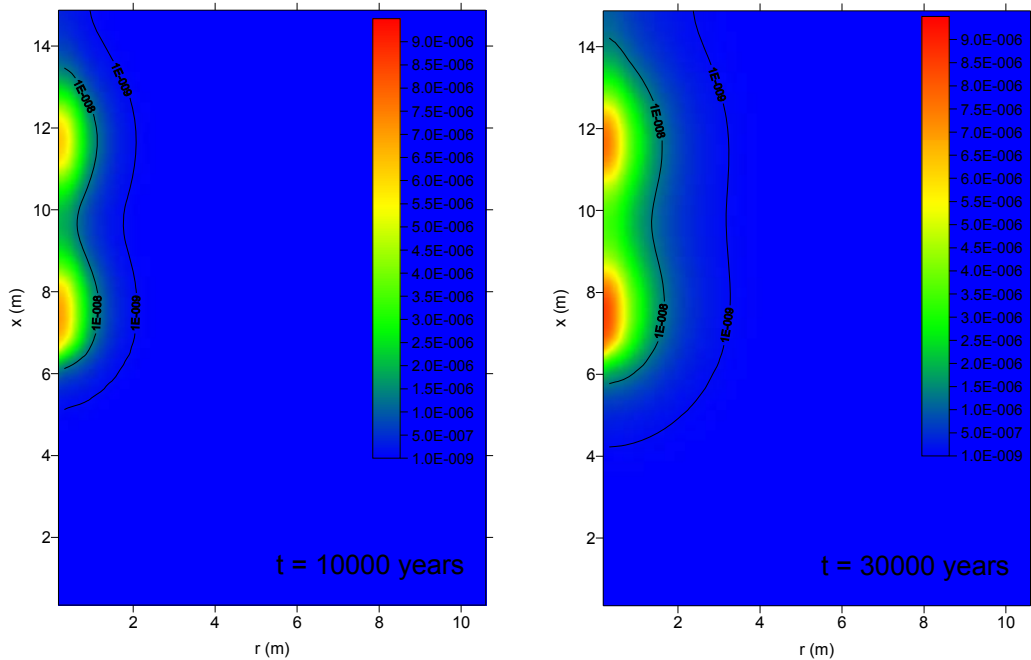


Figure 4.3.22: Iso-concentration maps for case 3c (thermodynamic sorption model) at $t = 10,000$ and $30,000$ years after the release of Cs. Concentrations are in mol/l

4.3.5.3 Comparison between models

As mentioned before, the concentrations for the 2D simulations are lower than for the 1D simulations because of the presence of a bentonite plug in the 2D model. 1D is thus not a good representation of a system that is *in se* 2D radial.

The same discussion applies for the observation nodes at 1 m in the radial direction (Figure 4.3.23).

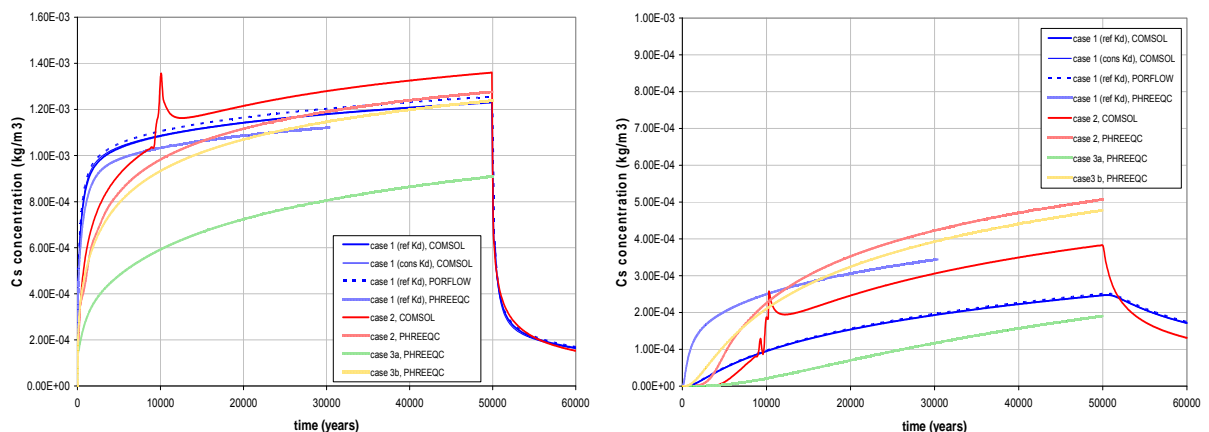


Figure 4.3.23: Observation nodes: concentration in the waste zone (left) and at $r=1$ m (right) for the different cases (2D)



4.3.5.4 Conclusions for exercise 1

Overall conclusions of this exercise:

Comparison of thermodynamic models with simple models for reduced geometry (near field) and relatively short timescales (compared to traditional PA spatial and timescales) provides supporting information for how to choose adequate (*i.e.* conservative) K_d values for the expected concentration range. In this benchmark, not all the proposed K_d 's are conservative (cf. Figure 3.5.2 and Figure 3.5.3).

For the cases studied in this benchmark, a linear model is sufficient to represent sorption, but a proper choice of the K_d 's is very important. Of course it is acknowledged that K_d values should be selected on the basis of experimental studies and (static) thermodynamic modelling but an "upscaling" to repository scale (and hence the concentration range expected around a real disposal system) including radionuclide transport could provide additional information to support the assessment basis.

Implementation of full thermodynamic models for full PA (large domain and very large timescales ($> 1M$ years)) remains practically not feasible in PHREEQC because of excessive computational times.

4.3.6 General comments

3 participants have solved 2D cylindrical simulations for constant K_d and thermodynamic sorption models: CEA, IRSN and SCK*CEN. They all have noticed a significant discrepancy of 2D results with 1D axial and radial simulations. First, the bentonite plug has high sorption properties that decrease the amount of Cs in claystones. Second, the Cs flow rate is not uniform around the canister wastes.

It is difficult to give an accurate and argued interpretation starting from CEA graphs. However there are some differences between linear K_d and thermodynamic models. The former leads to $1 \cdot 10^{-5}$ moles/L Cs concentrations near the canister interface whereas the later leads to concentrations lower than 10^{-6} moles/L. These values are similar to those obtained with radial 1D simulations.

Cs concentration at the interfaces ranges from 1 to $2 \cdot 10^{-6}$ moles/L in IRSN results. This confirms the analogy between sorption models already observed with 1D radial simulations, but these concentrations are a bit lower, maybe because the high sorption properties of the bentonite plug and the intercalation blocks are not accounted for in 1D radial simulations.

SCK*CEN also got similar results with linear K_d and thermodynamic sorption models. They got a 10^{-3} kg/m³ Cs concentration at the interface and slightly lower values with the thermodynamic model, equivalent to 1 to $2 \cdot 10^{-6}$ moles/L with a corrected glass dissolution rate. Again, these values are lower than those obtained with 1D radial simulation (by a factor of 2).



At this stage it is possible to affirm that despite huge differences between the ways the problem was handled by participants, they went to analogue results and to the same conclusion: it is possible to solve transfer problems with the full thermodynamic resolution. However some data were missing so some assumptions were necessary in the scope of the benchmark. Results from thermodynamic calculations are quite similar to those obtained with constant K_d values. There are also large differences between radial 1D and 2D calculations, due to the intercalation blocks and the bentonite plug.

5 Congruent release and competitive / additive effects between radionuclides

Chemical and radiological inventory of C1 (HA) wastes is defined with a few elements/radionuclides. Among this list, several chemical elements have similar behaviour with regard to sorption processes. Inventory (in mass) is given in the benchmark, for trivalent and tetravalent elements. Two comments can be developed:

- For zirconium, the mass ratio between stable and radio-isotope is around 20. Moreover, if we consider as a first estimation a chemical analogy between trivalent lanthanides and trivalent actinides, the mass ratio between stable isotopes and Am243f is around 80.
- All of these elements/radionuclides will compete together for surface sites of clay minerals (especially for 'strong edge' sites).

The aqueous concentration of all of these elements/radionuclides is limited by precipitation processes. Solubility limitation can be described by three models defined in the benchmark.

The actual state of knowledge limits the application of such an exercise to the bentonite plug. Sorption data are recalled in section 2.2.4.1 and solubility limits are given in Table 5.1.

Table 5.1: *Calculated solubility limits for elements of interest*

Element	Solid phase	Solubility limit (mol.L ⁻¹)
Zr(IV)	ZrO ₂	2.10 ⁻⁸
Tc(IV)	TcO ₂ .nH ₂ O	4.10 ⁻⁹
U(IV)	UO ₂	7.10 ⁻⁷
Ln(III)	LnOHCO ₃	10 ⁻⁷
Am(III)	AmOHCO ₃	4.10 ⁻⁷

The exercise can be defined as:

- Comparison between Kd/SL approach and thermodynamic sorption model, with regard to several levels of analogy/competition.
- Solubility limits (SL) analysis, with regard to several levels of chemical analogy and with respect to co-precipitation process. Comparison with constant SL approach.

Table 5.2: Benchmark tasks for Zr and Am transfer

		Sorption model	N° Task in the benchmark
1D axial: Section 5.1	Zr93, transfer modelling in the bentonite plug	constant Kd/SL	part of task 3
		thermodynamic sorption model and SL for a pure Zr solid phase	9
	Am243, transfer modelling in the bentonite plug	constant Kd/SL	part of task 3
		thermodynamic sorption model and SL for a pure Am solid phase	10
		thermodynamic sorption model and SL for a mixed Ln(III) solid phase	11
1D radial and 2D cylindrical: Section 5.2	Am243 transfer at the head of the disposal cell (i.e. claystone and bentonite)	constant Kd/SL	4
		Tentative of an overall modelling on Am243 transfer	12

5.1 Axial Zr and Am transfer in the bentonite plug obtained with Kd/SL and thermo dynamic models

The following results and comments were asked to all participants:

- Plots of Zr and Am concentration profiles along the axis through the bentonite plug, 100, 1,000, 5,000, 10,000 and 50,000 years after the release
- Plots of the evolution with time (from 0 to 50,000 years) of Zr and Am concentrations, at points located 0 and 0.1 m from the waste
- Discussions about Zr/Am differences; difference between Kd/SL and thermodynamic models for both species; competitive effects of Ln(III)
- If necessary for interpretation, plots of Zr and Am isotherms

5.1.1 Results from Andra

5.1.1.1 Zr and Am transfer with Kd/SL model

The axial Zr and Am transfer was simulated with two models: Kd (100 m³/kg) and thermodynamic, corresponding respectively to tasks 3 and 9 of the benchmark.

For simulations with the Kd model, Zr and Am concentrations are limited by their solubility limit (2 10⁻⁸ mol/L for Zr and 4 10⁻⁷ mol/L for Am, respectively), imposed by means of a fictive mineral. It can be noticed on Figure 5.1.1 and Figure 5.1.3 that these solubility limits are not respected anymore after 10,000 years. From this date, the smectite of the bentonite plug progressively dissolves; this dissolution is total at 0 m after 40,000 years (see Figure 3.1.2). It leads locally to a great modification of the mineral composition and the water composition

(increase of the ionic strength and pe), in parallel with the local lost of sorption sites. These modifications of water composition spread over the whole bentonite plug prevent from reaching the solubility limit.

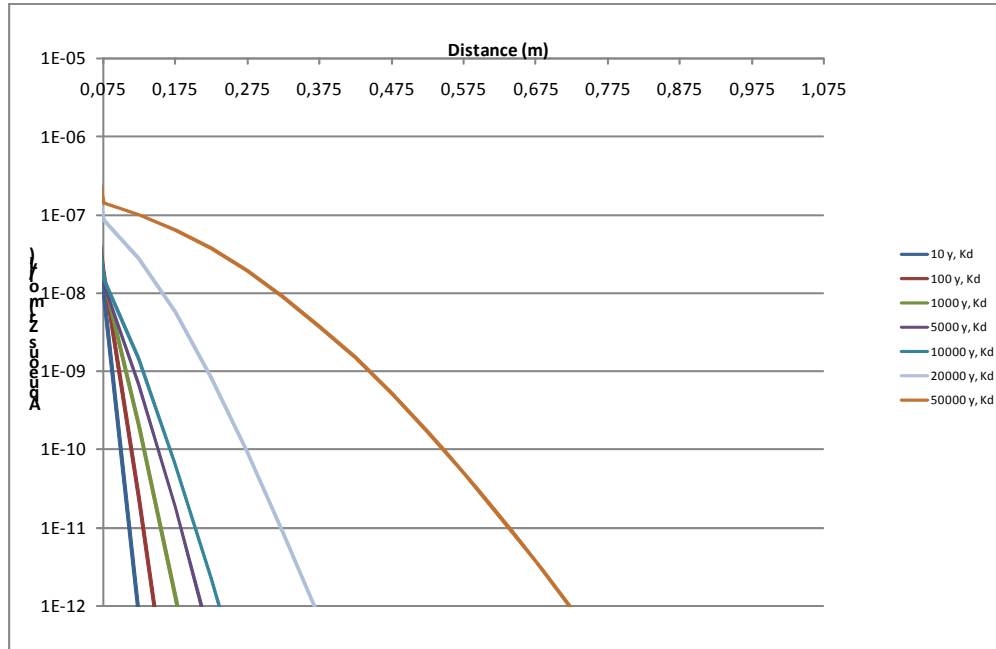


Figure 5.1.1: Evolution with time of Zr concentration profiles in the bentonite plug, Kd model ($K_d=100 \text{ m}^3/\text{kg}$)

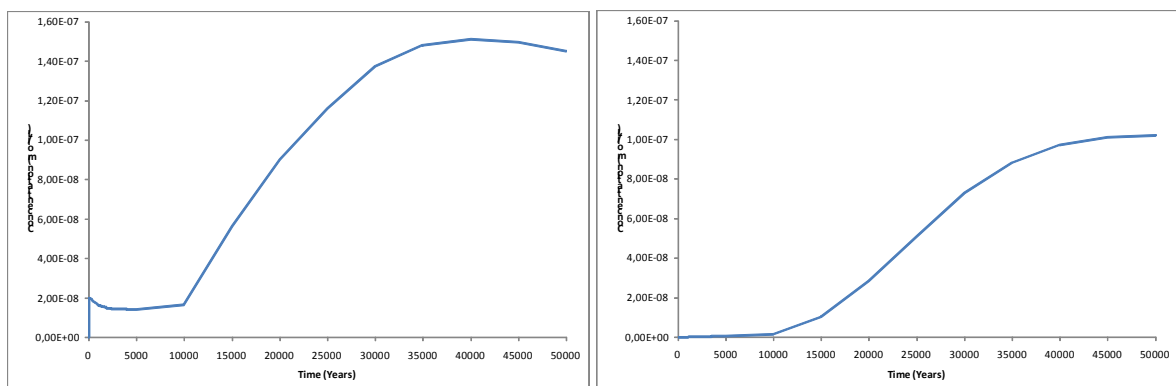


Figure 5.1.2: Temporal evolution of Zr concentration at 0 m (left) and 0.1 m (right) in the bentonite plug, Kd model ($K_d=100 \text{ m}^3/\text{kg}$)

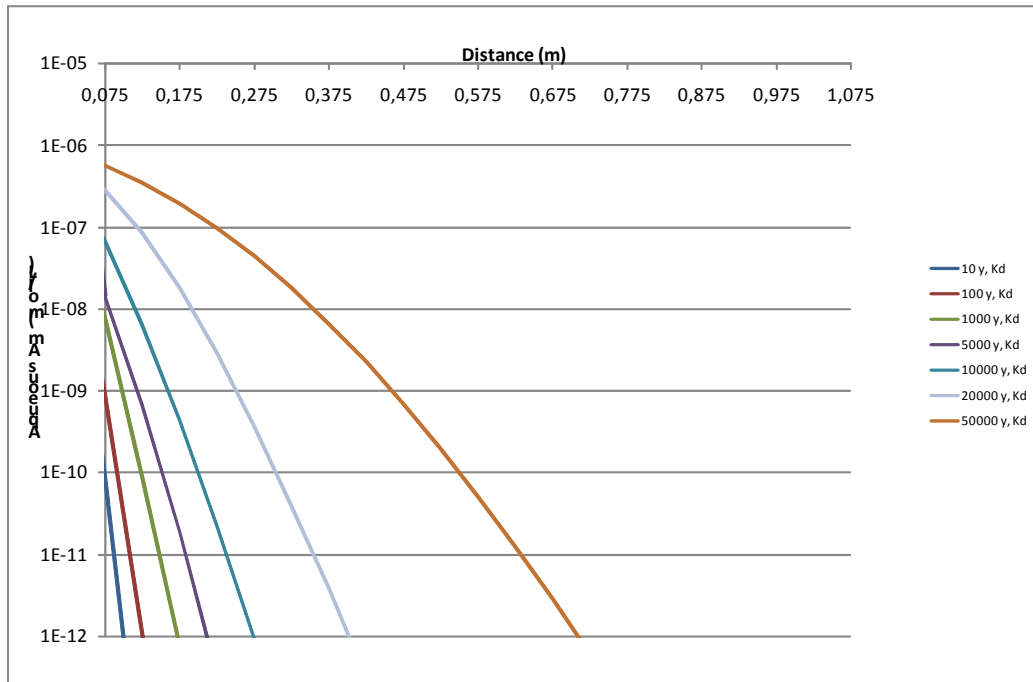


Figure 5.1.3: Evolution with time of Am concentration profiles in the bentonite plug, Kd model ($K_d=50.12 \text{ m}^3/\text{kg}$)

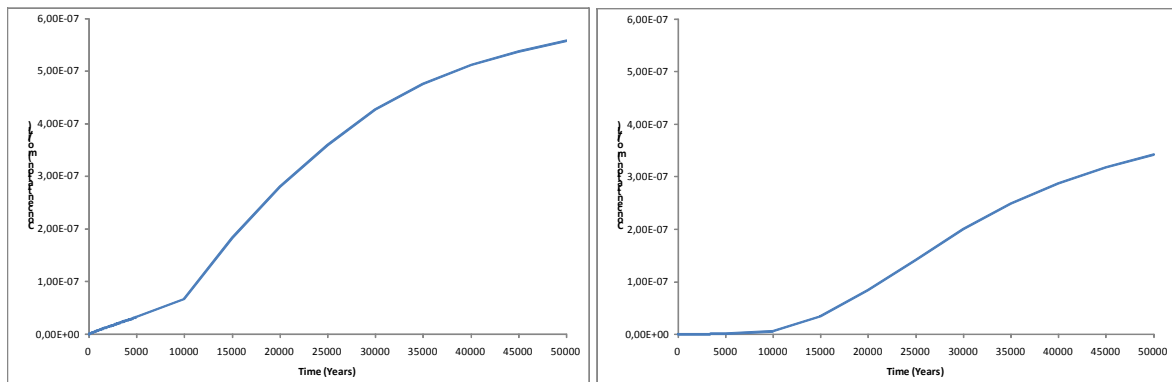


Figure 5.1.4: Temporal evolution of Am concentration at 0m (left) and 0.1m (right) in the bentonite plug, Kd model ($K_d=50.12 \text{ m}^3/\text{kg}$)

5.1.1.2 Zr and Am transfer with thermodynamic sorption model

Simulation results show the strong precipitation of $\text{Ca}_2\text{ZrSi}_3\text{O}_{12}(\text{cr})$ mineral in the first mesh of the bentonite plug (minerals authorized to precipitate are listed in Appendix 4 of the benchmark). The solubility of this mineral is so low that Zr solution concentration is almost equal to zero in the first mesh of the bentonite plug. As a consequence of this set of minerals authorized to precipitate, no diffusion of Zr is observed.

Am transfer is plotted in Figure 5.1.5. It must be noticed that the brutal increase of Am concentration observed on Figure 5.1.6 after 20,000 years must result of a punctual failure in convergence which has later recovered.

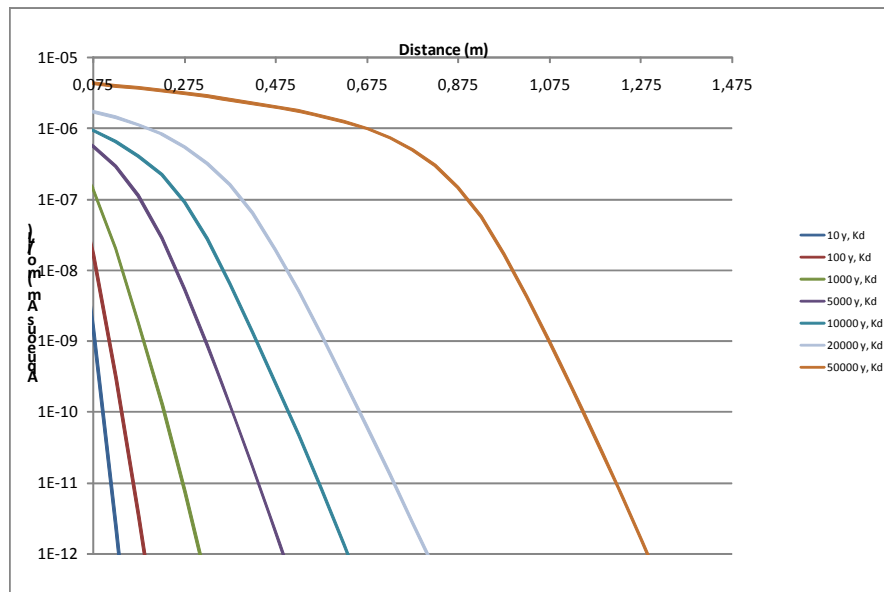


Figure 5.1.5: Evolution with time of Am concentration profiles in bentonite, thermodynamic model.

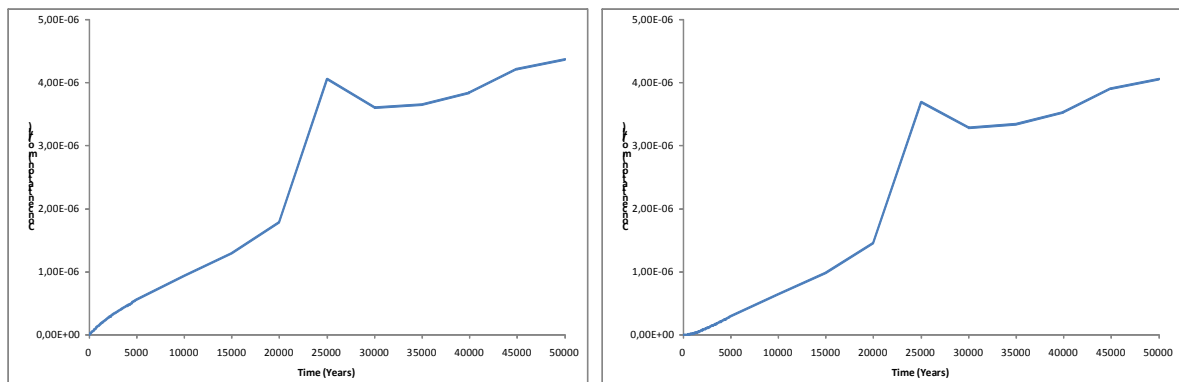


Figure 5.1.6: Temporal evolution of Am concentration at 0m (left) and 0.1 m (right) in bentonite, thermodynamic model.

5.1.1.3 Comparison of results in the bentonite plug

The axial Am transfer was simulated with two models: Kd/Csat and thermodynamic, corresponding respectively to the task 3 and to the tasks 10 and 11 of the benchmark.

Figure 5.1.7 shows that Am transfer length is higher with the thermodynamic model. Thus the Kd value ($K_d=50.12 \text{ m}^3/\text{kg}$) used in the Kd model is not conservative.

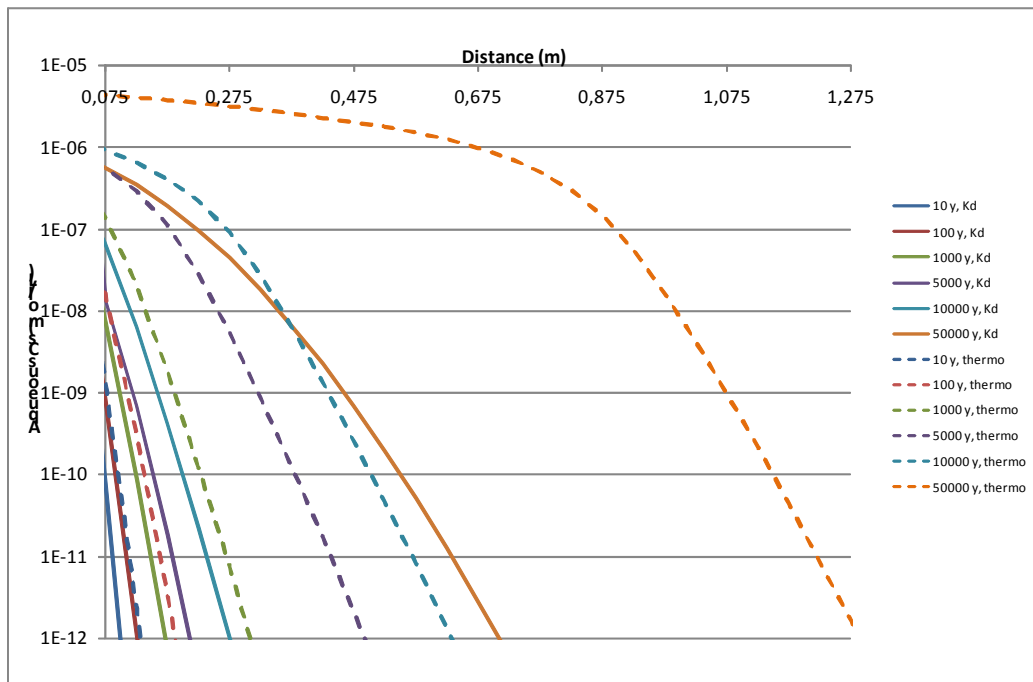


Figure 5.1.7: Comparison of Am concentration profiles in the bentonite plug with different models ($K_d=50.12 \text{ m}^3/\text{kg}$ and thermodynamic)

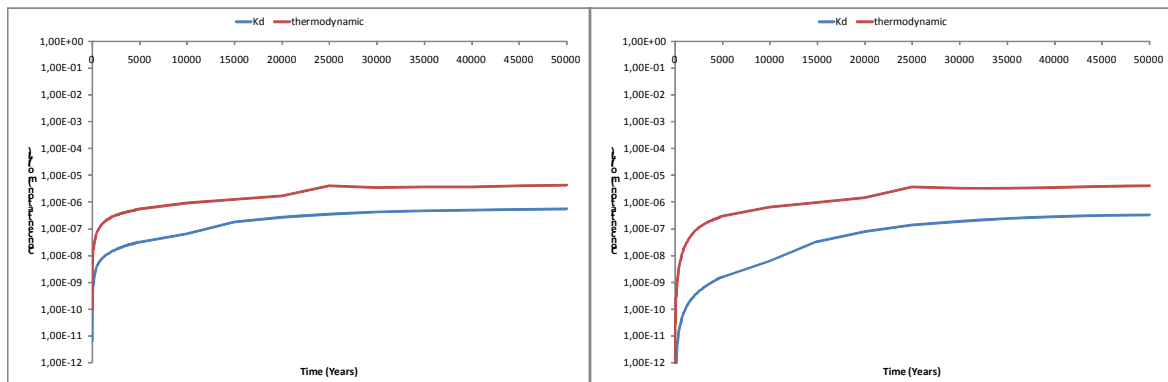


Figure 5.1.8: Comparison of Am profiles at 0 m (left) and 0.1 m (right) in bentonite with different models)

Figure 5.1.7 and Figure 5.1.8 show that the K_d/C_{sat} model for Am diffusion in bentonite can be considered as conservative in comparison with the thermodynamic model.

5.1.2 Results from CEA

The first results obtained with the thermodynamic model show a very different behaviour from the K_d model for Zr. The Zr seems to diffuse with low sorption (see Figure 5.1.9 and Figure 5.1.10). The sorption sites introduced in this model are not efficient on Zr, probably due to other competition and pH values.

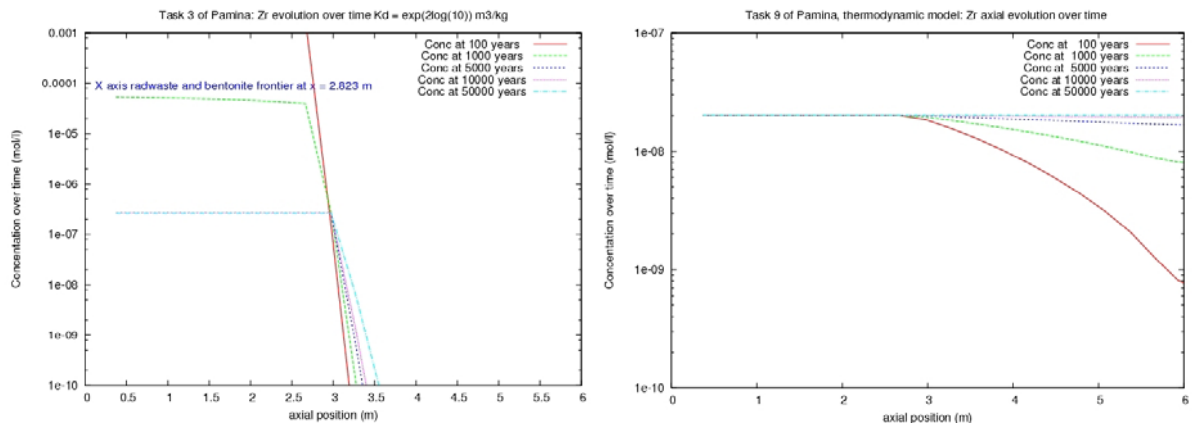


Figure 5.1.9: Zr concentration profiles in the bentonite plug with Kd (left) and thermodynamic (right) models

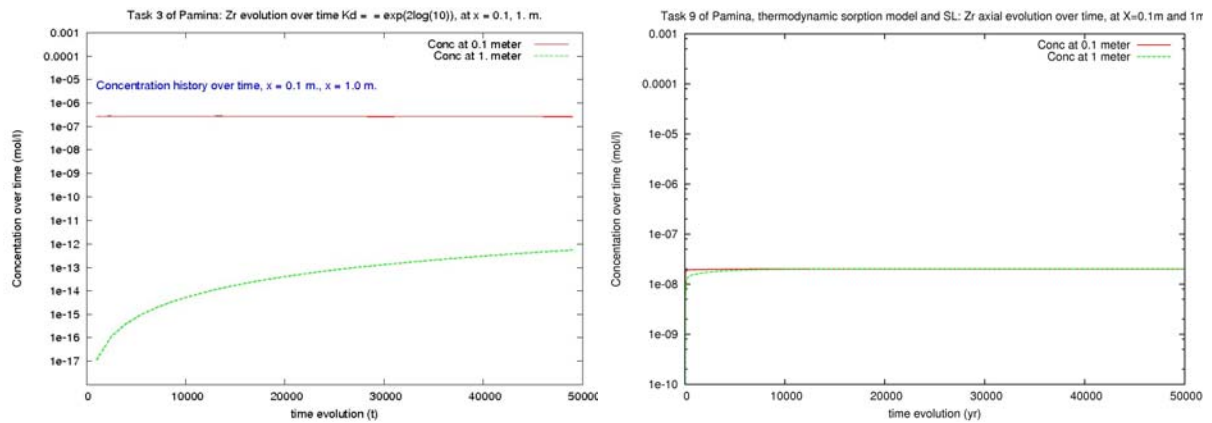


Figure 5.1.10: Zr concentration at $x=0.1$ and 1.0 m in the bentonite plug with Kd/SL model (left) and thermodynamic model (right)

For Am, the thermodynamic and the Kd models give very close results; and the Kd approach can be considered as conservative in comparison with the thermodynamic model (see Figure 5.1.11 and Figure 5.1.12).

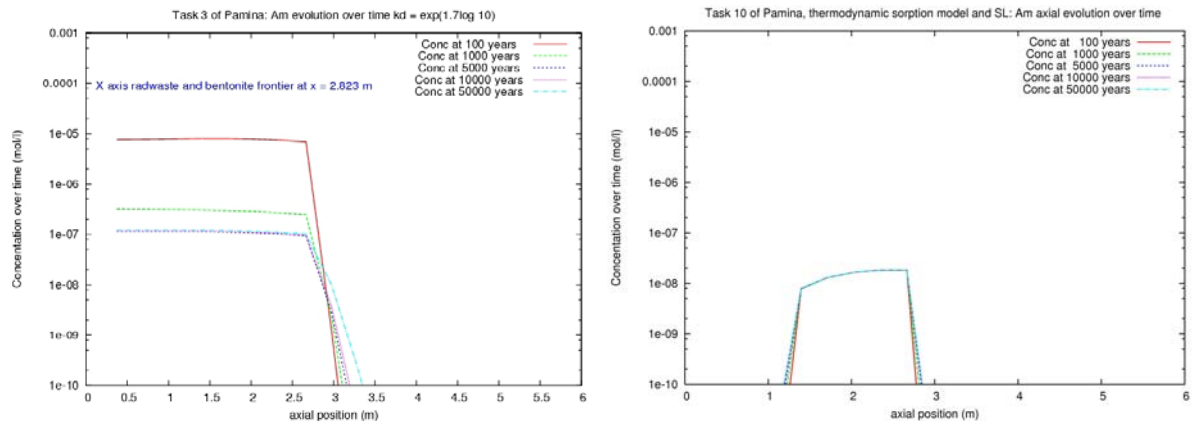


Figure 5.1.11: Am concentration profiles in the bentonite plug with Kd (left) and thermodynamic (right) models

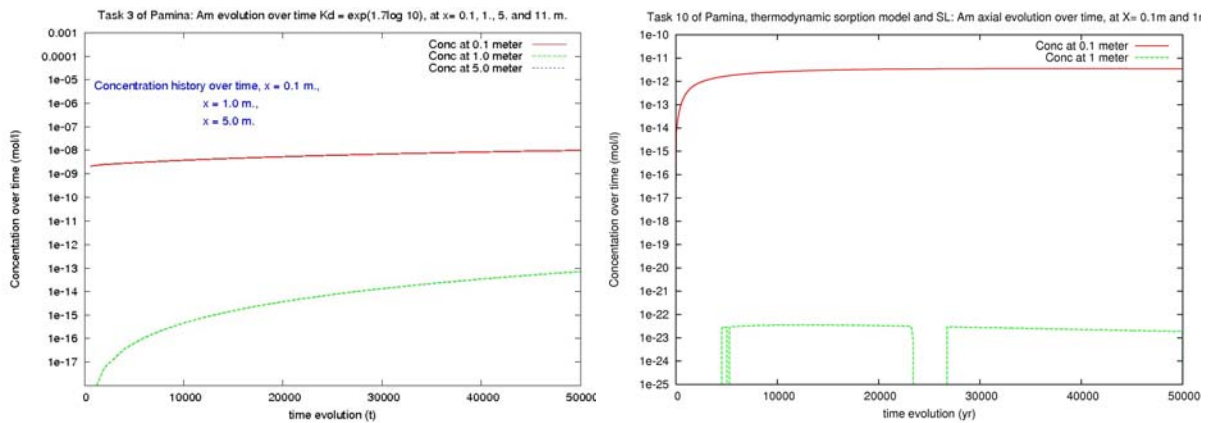


Figure 5.1.12: Am concentration at fixed points in the bentonite plug: $x = 0.1., 1.$ and 5.0 m with K_d/SL model (left) and $x = 0.1$ and 1.0 m with thermodynamic model (right)

5.1.3 Results from IRSN

5.1.3.1 Linear K_D

In 1D-axial geometry (Task 3), Am and Zr migration is localized close to the waste package (Figure 5.1.13 and Figure 5.1.14):

- Zr migration occurs over 1.2 m out the waste package
- Am migrates over 1 m through the bentonite

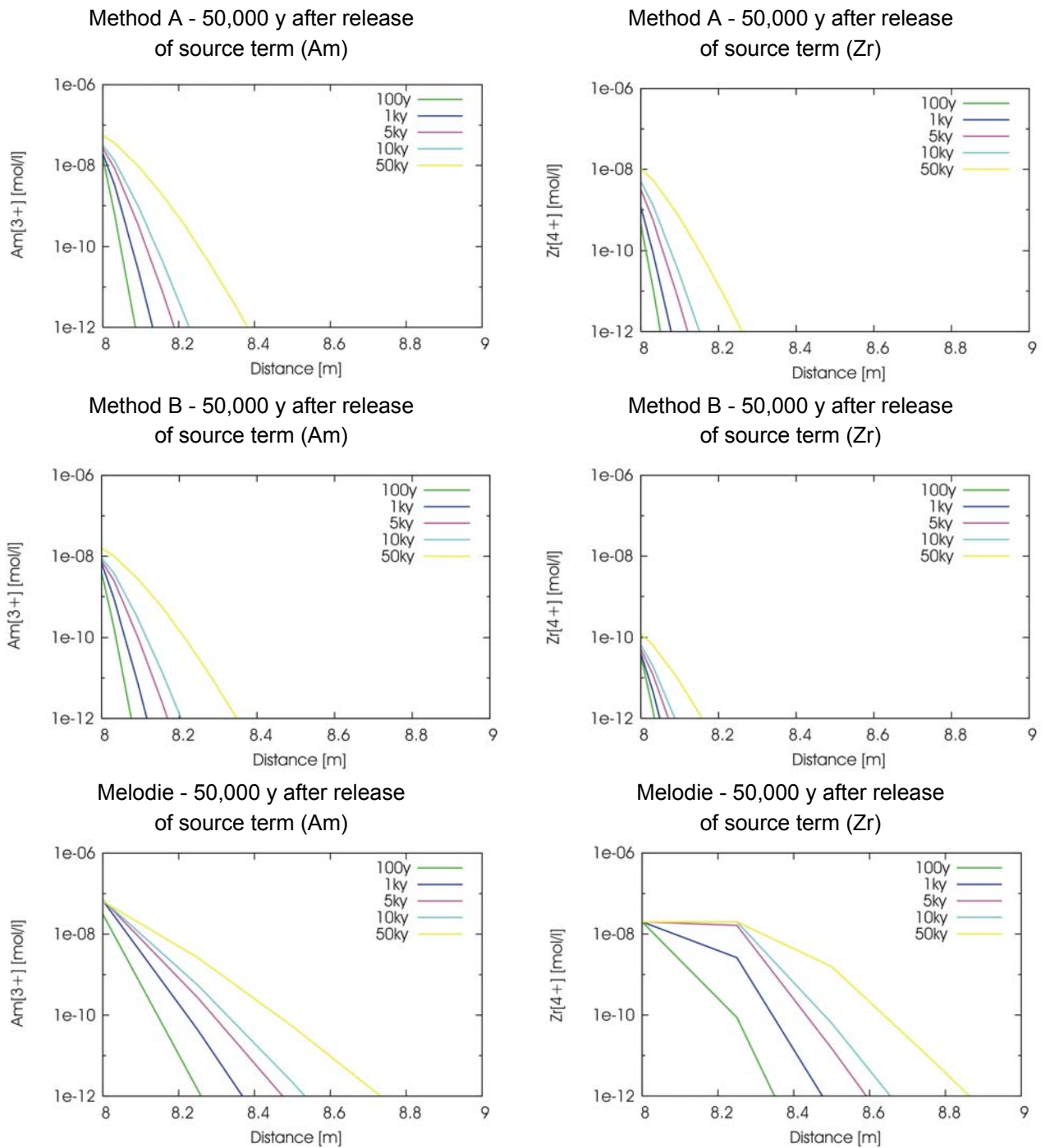


Figure 5.1.13: Zr and Am concentration profiles in 1D-axial with constant K_D/SL

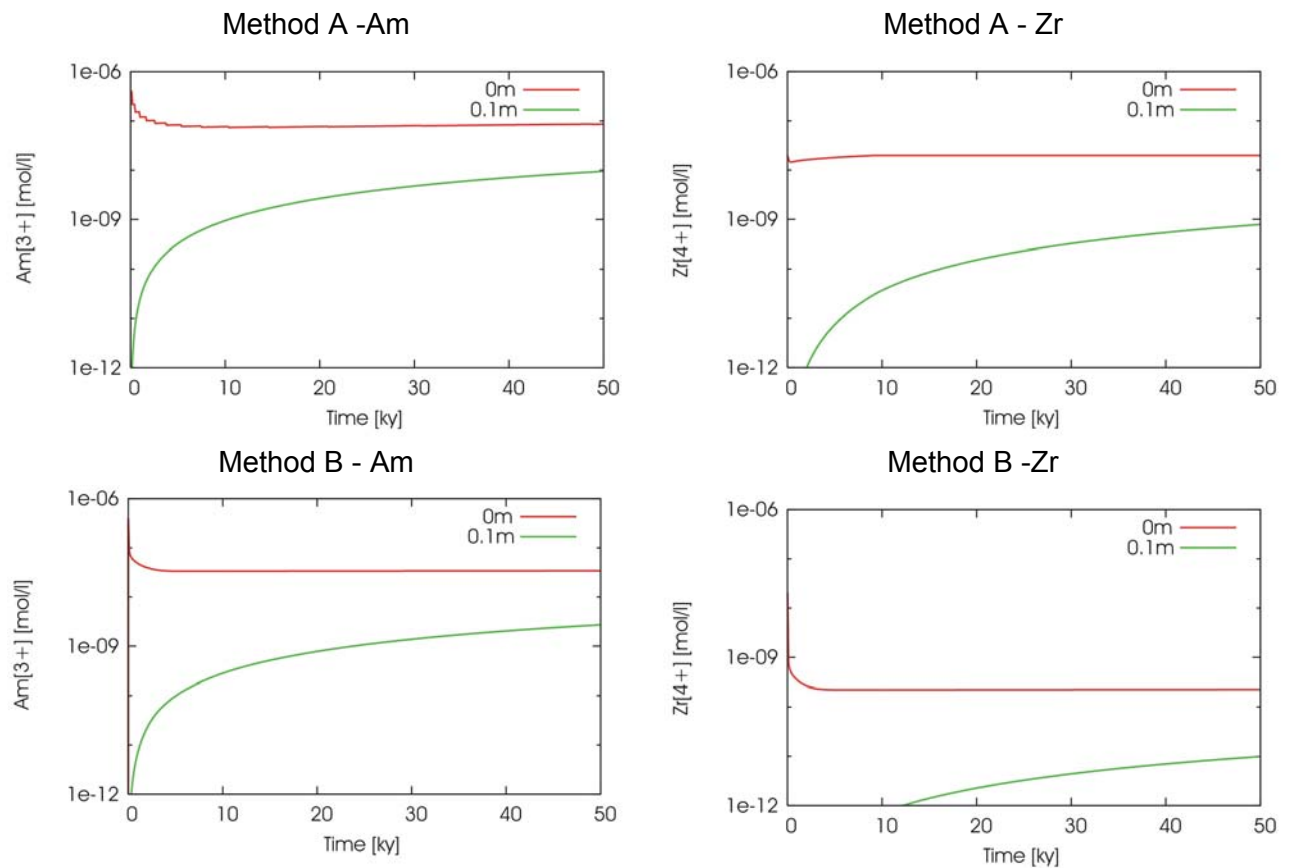


Figure 5.1.14: *Am and Zr transfer in 1D-axial with constant K_D/SL . Concentration over time at $x = 0$ m and $x = 0.1$ m.*

5.1.3.2 Thermodynamic model

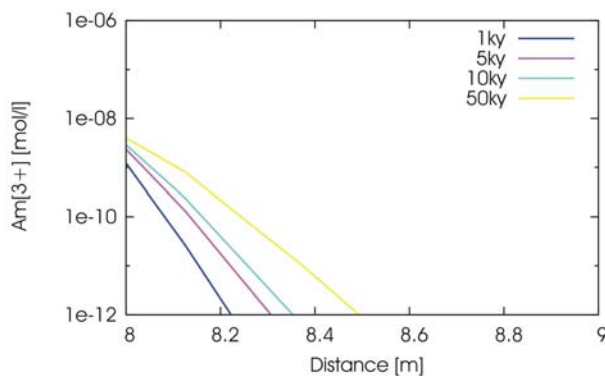
Calculations taking into account all the ThermoChimie database species have been performed and led to the massive formation of phases unlikely to precipitate, which limit aqueous concentration of radionuclides to very low values with no significant physical meaning (concentrations under 10^{-16} mol/l). Thus, pure phases are selected to control the solubility of radionuclides, which are LnOHCO_3 or $\text{Ln}(\text{OH})_3$ for Ln, $\text{TcO}_2 \cdot \text{H}_2\text{O}$ for Tc and UO_2 for U. Zr solubility is supposed to be controlled either by ZrO_2 or by ZrSiO_4 while three different species are tested to limit Am solubility: $\text{Am}(\text{OH})_3$, amorphous $\text{Am}(\text{OH})_3$, and AmOHCO_3 . As recommended in the benchmark definition, a supplementary case is performed considering the co-precipitation of Am with Ln ($\text{Am}_{0.05}\text{Ln}_{0.95}\text{OHCO}_3$). Am and Zr migration are simulated with HYTEC in 1D-axial symmetry in about 10 hours (44 cells, 2 GHz), first without any competition (Figure 5.1.15) and then with the whole set of radionuclides (Figure 5.1.16).

The sorption of tetravalent radionuclides occurs exclusively by surface complexation reactions. This sorption process appears to be insufficient for them to be efficiently retarded: Tc is the most retained tetravalent radionuclide but still migrates over the whole bentonite plug in 50,000 y, whereas the migration of U and Zr are barely retained by sorption on montmorillonite over 50,000 y. As specified above, aqueous concentration of Zr is controlled by the precipitation of either ZrO_2 or ZrSiO_4 , and is fixed in the whole bentonite to 2.5×10^{-8} mol/l in

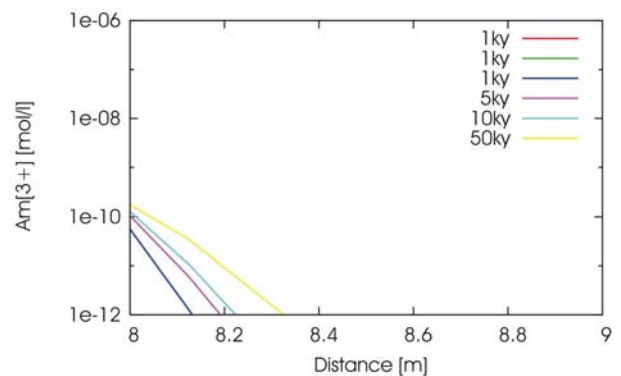
the case of ZrO_2 , and to 10^{-13} mol/l in the case of $ZrSiO_4$. The presence or not of tetravalent competitors U and Tc does not influence the sorption of Zr.

Regarding the trivalent radioelements, ion exchange is the main sorption process that takes place. Am migration is still limited close to the waste package if its concentration is controlled either by $Am(OH)_3$, amorphous $Am(OH)_3$ or $AmOHCO_3$. The Ln competition does not influence Am migration if Ln aqueous concentration is controlled by $Ln(OH)_3$. However, the migration of Am has a particular behaviour when the Ln pure phase is $LnOHCO_3$: this mineral precipitates massively in the host rock, consuming high quantity of aqueous carbonates and Ln, limiting its migration in a first step, and letting Am being sorbed on the clayey minerals. Once the equilibrium between aqueous carbonate and $LnOHCO_3$ is reached, aqueous Ln is then allowed to reach its solubility limit, leading to its intense sorption on montmorillonite and pushing subsequently the Am further in the bentonite until the repetition of this process, which clearly increases the propagation of Am in the bentonite. In this case Am migrates over about 2 m of bentonite in 50,000 y. A Ln and Am co-precipitated phase is also taken into account in a complementary calculation, but does not induce any change in terms of Am migration. Globally, the equivalent $\rho_d \cdot R_D$ value was found out to be close to 10^6 without any competition and when Ln concentration is controlled by $Ln(OH)_3$, but clearly decreases to values below 100 when Ln concentration is controlled by $LnOHCO_3$.

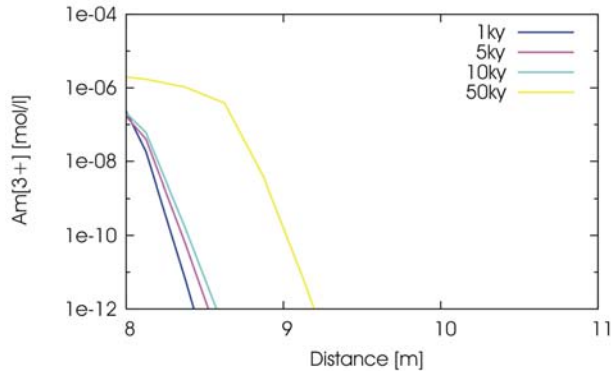
a) Evolution of Am concentration in the bentonite over 50,000 y – $Am(OH)_3$ as pure phase



b) Evolution of Am concentration in the bentonite over 50,000 y – amorphous $Am(OH)_3$ as pure phase



c) Evolution of Am concentration in the bentonite over 50,000 y – AmOHCO₃ as pure phase



d) Evolution of Am concentration in the bentonite over 50,000 y – AmOHCO₃ as Am pure phase with competition of Ln

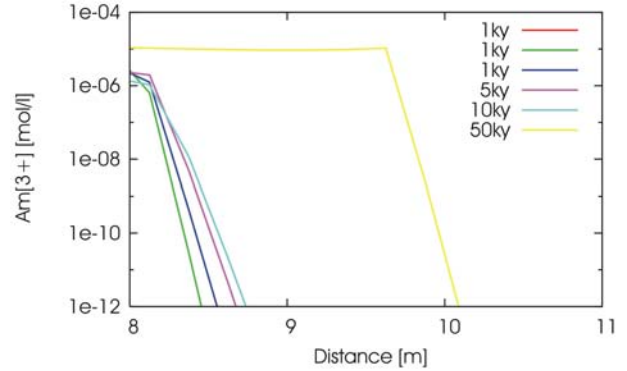


Figure 5.1.15: Am concentration profiles in 1D-axial with thermodynamic sorption models.

Zr, U and Tc concentration in the bentonite after 50,000 y depending on the pure phase

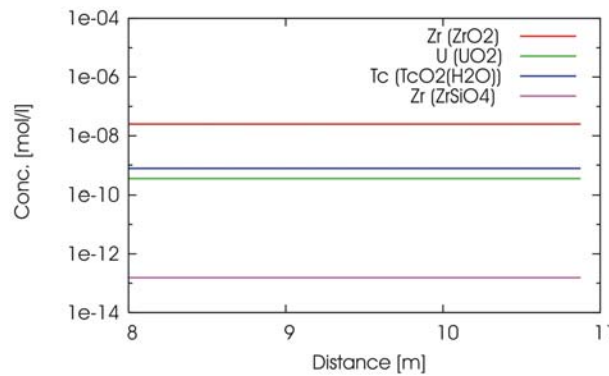


Figure 5.1.16: Task 3: 1D-axial. Migration of Am and Zr in the bentonite 50,000 y after the release of radionuclides from the waste package.

5.1.4 Results from JRC

The Exercise 2 considers the migration of radionuclides Zr (stable), ⁹³Zr, ⁹⁹Tc, ²³⁵U, ²³⁶U, ²³⁸U and ²⁴³Am. The nuclides were treated as cations with Kd/SL model (no calculation with thermodynamic model). Results from 1D axial model are presented in Figure 5.1.17.

Because of the very low concentration values in the last 10 m layer of claystones, the scale of concentration has been extended down to the lower limit 10⁻²⁰ g/l.

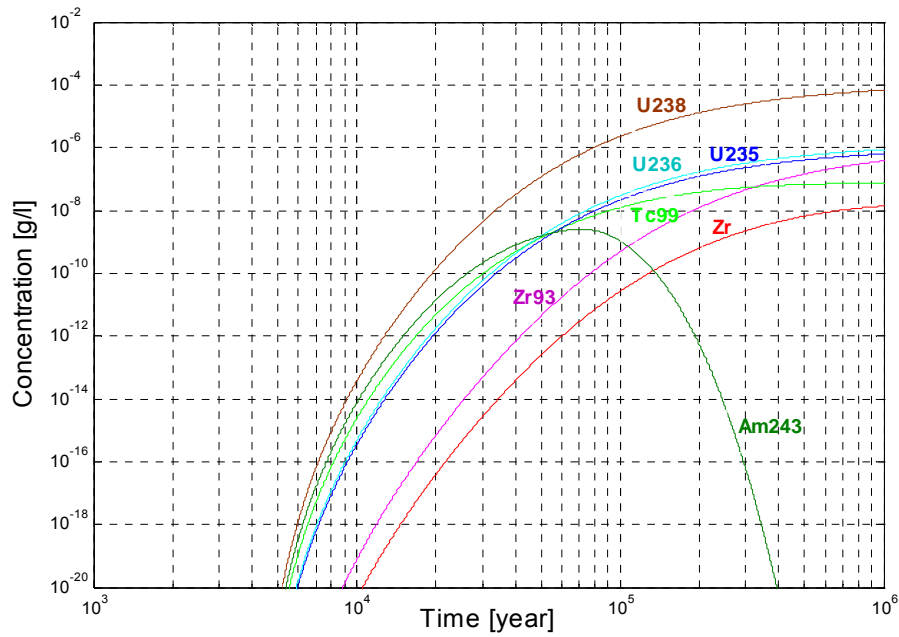


Figure 5.1.17: Concentrations in 1D axial direction, in the bentonite plug 1 m from the waste package.

5.1.5 Results from SCK*CEN

No calculation was performed in axial 1D (in the bentonite plug) except for Kd/SL model applied to Am and Zr transfer. Zr concentration profile is displayed in Figure 5.1.18.

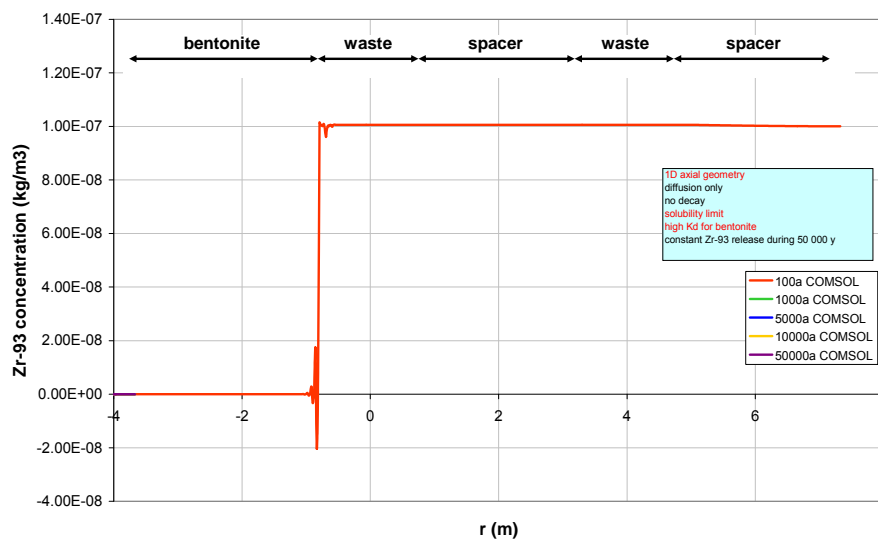


Figure 5.1.18: Zr-93 axial concentration profiles for the simple model with linear sorption and solubility limit (1D).

The 1D axial concentration profile (Figure 5.1.18) illustrates the high sorption capacity of the bentonite plug. In order to stabilize the steep concentration gradient at the bentonite/waste interface, COMSOL even calculates negative concentrations.

In the spacer, which has no sorption capacity, the concentration limit is achieved after 100 years already (Figure 5.1.18) due to the fact that diffusion into the claystone is not possible (1D axial model).

Axial Am-243 concentration profiles for the 1D case are shown in Figure 5.1.19. It is clear that the Am-243 concentration in the spacers rises so quickly that within 100 years time the concentration limit is reached.

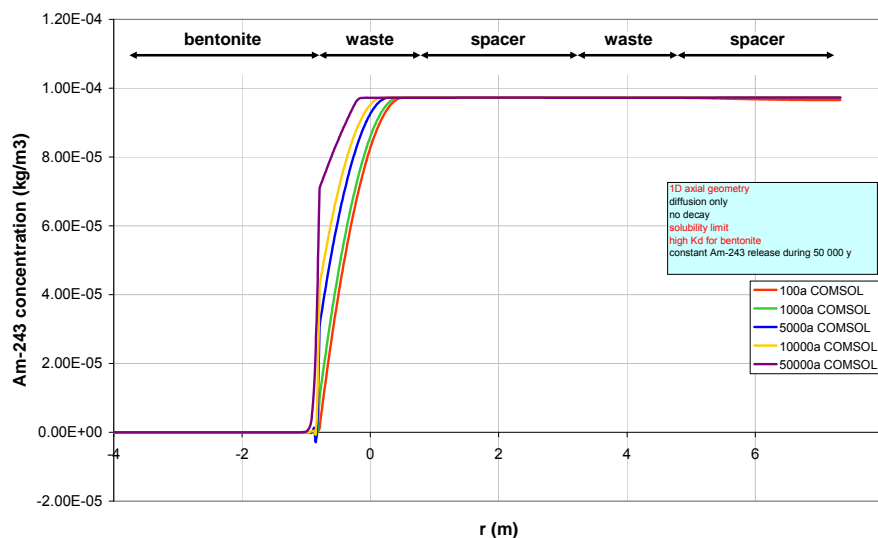


Figure 5.1.19: Am-243 axial concentration profiles for the K_d/SL model with linear sorption and solubility limit (1D).

5.1.6 General comments

3 participants gave a complete set of results for axial transfer of Am and Zr in the bentonite plug: Andra, CEA and IRSN. They got very different results, it is then impossible to give any general comment about them. Nevertheless we can examine the origin of these discrepancies: the definition of precipitating minerals. A full geochemical modelling then seems to be necessary.

5.2 1D or 2D radial Am transfer at the head of the disposal cell (i.e. claystone and bentonite)

The following section is an attempt to perform calculations with somewhat arbitrary models and parameters, knowing that geochemical and thermodynamic data are not available in claystones. Participants then assumed that the montmorillonite content in claystones is 33.4%. The following results and comments were asked to all participants:

- Plot of Am iso-concentration maps 10,000 years after the release for the 2 approaches (Kd and thermodynamic)
- Plots of Am concentration profiles along the same axes as those defined for axial and radial calculations for Cs transport
- Plot of the evolution with time (from 0 to 50,000 years if possible) of Am concentration, at 4 points located on the same lines as those defined for Cs, 0 and 0.1 m from the waste
- Am release rate and remaining Am mass in the glass
- Discussions about the differences between the Kd and thermodynamic models

5.2.1 Results from Andra

As mentioned in the conceptual section, Zr and Am transfer through claystones have been modelled in radial geometry instead of 2D cylindrical. The radial Zr and Am transfer were simulated with two models: Kd/SL (Kd= 2 and 100 m³/kg for Zr and Am respectively) and thermodynamic, corresponding respectively to tasks 2, 3 and 12 of the benchmark.

5.2.1.1 Zr and Am transfer with Kd/SL model

The claystones are less degraded with time than the bentonite plug and the solubility limit is maintained (Figure 5.2.1 to Figure 5.2.4).

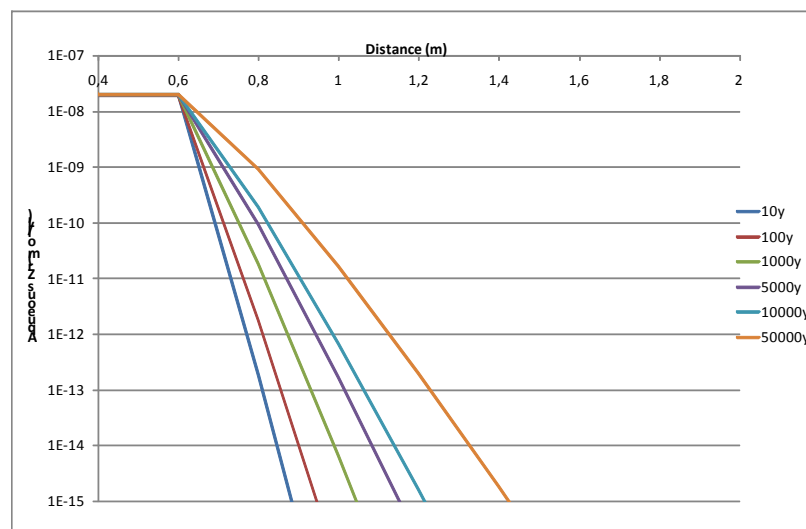


Figure 5.2.1: Evolution with time of Zr concentration profiles in claystones, Kd model (Kd=2 m³/kg)

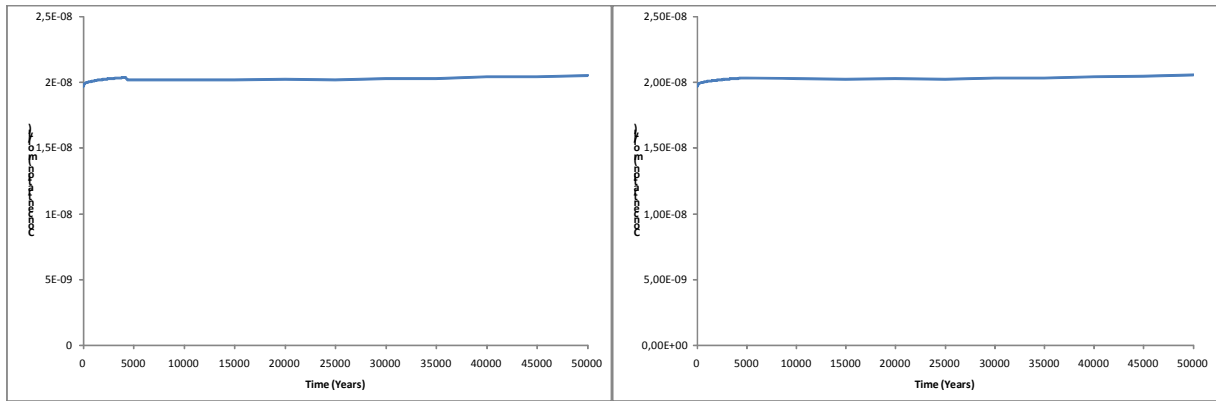


Figure 5.2.2: Temporal evolution of Zr concentration at 0 m (left) and 0.2 m (right) in claystones, Kd model ($K_d=2 \text{ m}^3/\text{kg}$)

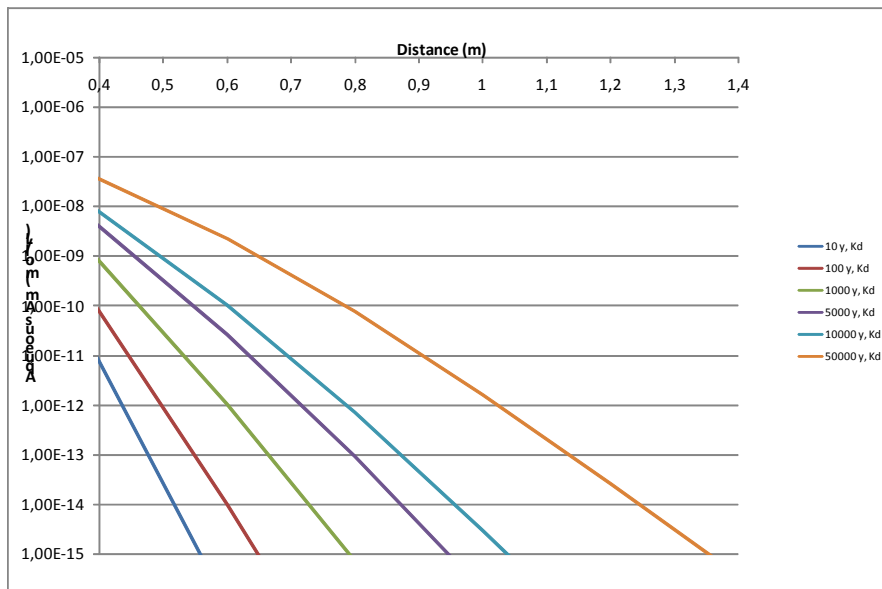


Figure 5.2.3: Evolution with time of Am concentration profiles in claystones, Kd model ($K_d=100 \text{ m}^3/\text{kg}$)

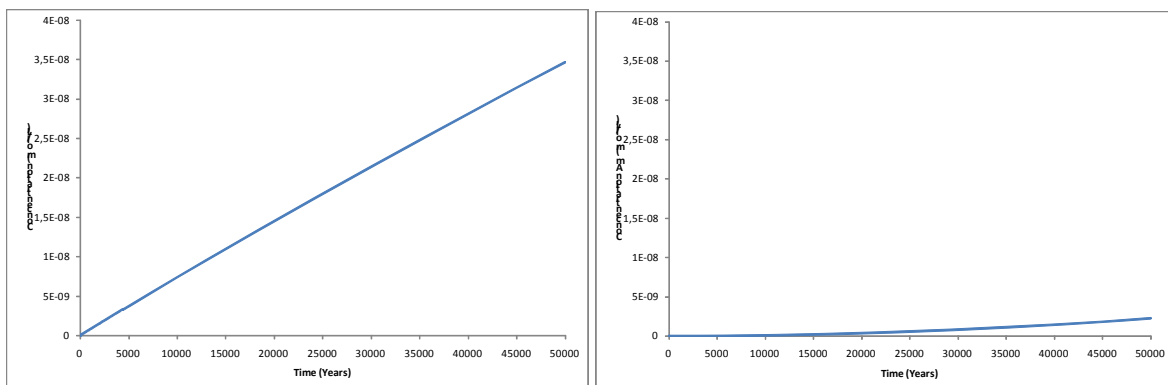


Figure 5.2.4: Temporal evolution of Am concentration at 0 m (left) and 20 cm (right) in claystones, Kd model ($K_d=100 \text{ m}^3/\text{kg}$)

5.2.1.2 Zr and Am transfer with thermodynamic model

As presented for the diffusion simulation in bentonite, the $\text{Ca}_2\text{ZrSi}_3\text{O}_{12}(\text{cr})$ mineral phase strongly precipitates in the first mesh outside of the source term. This mineral imposing an almost null concentration of Zr in solution, no diffusion of Zr is observed in the simulation with the thermodynamic model in claystones.

Am transfer is plotted in Figure 5.2.6 and Figure 5.2.7 where we can observe the reach of solubility limit of $\text{Am}_2(\text{CO}_3)_3\text{cr}$.

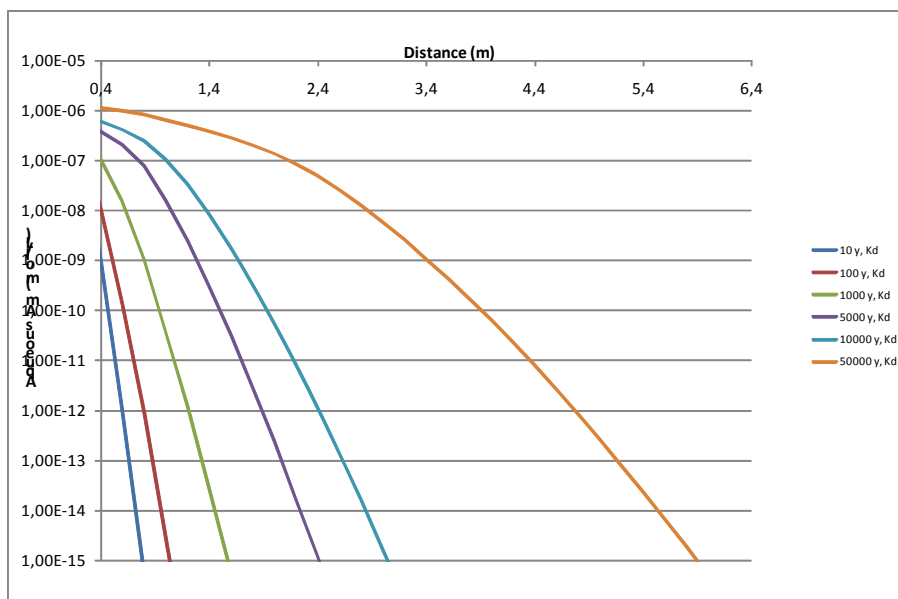


Figure 5.2.5: Evolution with time of Am concentration profiles in claystones, thermodynamic model

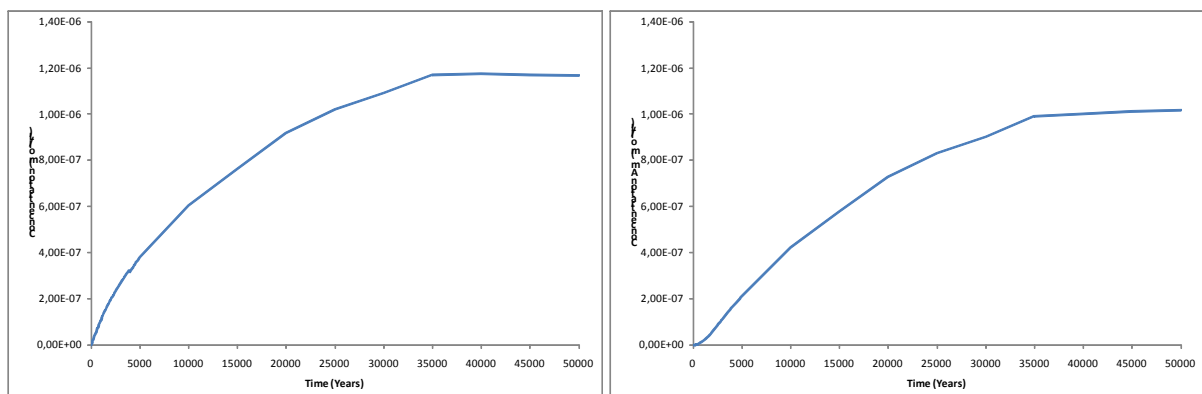


Figure 5.2.6: Temporal evolution of Am concentration at 0m (left) and 0.2m (right) in claystones, thermodynamic model.

5.2.1.3 Comparison of Kd/SL and thermodynamic results

Figure 5.2.7 shows that the Kd/SL model for Am diffusion in claystones is not conservative in comparison with the thermodynamic model since the extent of Am transfer are significantly less extended.

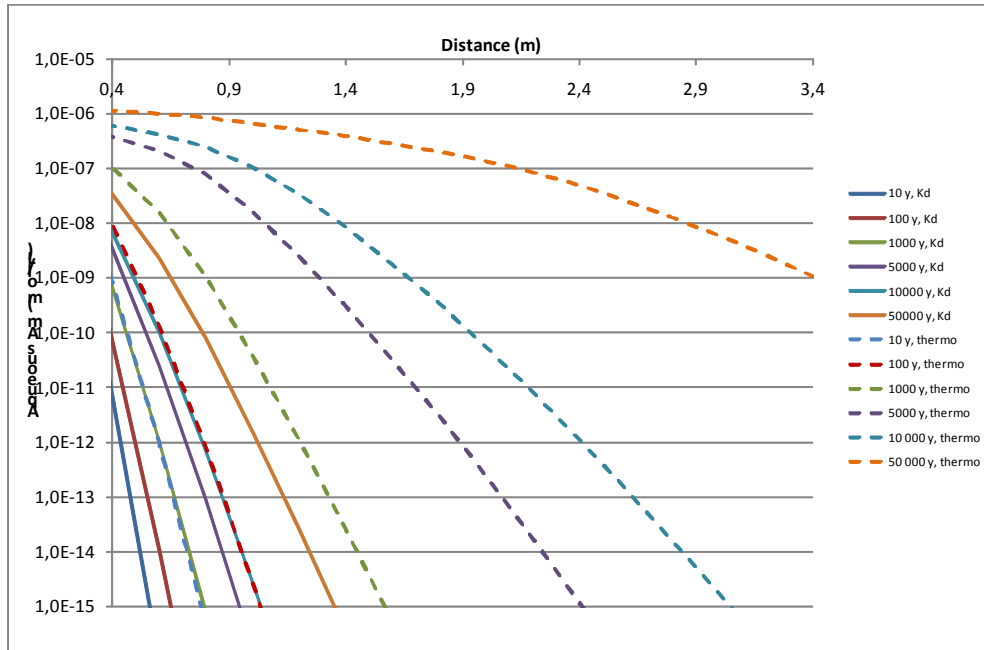


Figure 5.2.7: Comparison of Am concentration profiles in claystones with different models ($K_d=1.7 \text{ m}^3/\text{kg}$ and thermodynamic)

Figure 5.2.8 shows that the difference between Kd/SL and thermodynamic models in Am concentration at the interface with the waste package is about two orders of magnitude and more than three orders of magnitude at 0.2m over the simulation time (50,000 years).

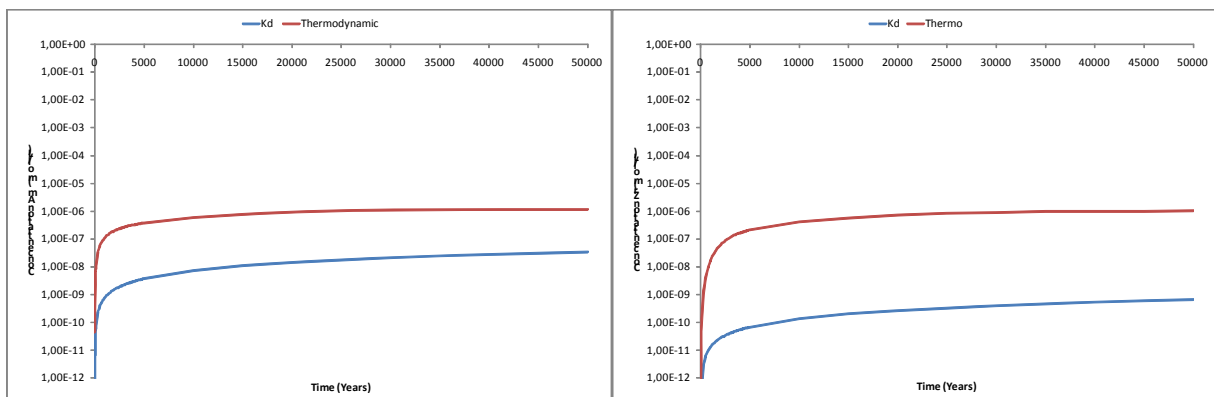


Figure 5.2.8: Comparison of Am profiles at 0 m (left) and 0.2 m (right) in claystones with different models ($K_d=1.7 \text{ m}^3/\text{kg}$ and thermodynamic)

5.2.2 Results from CEA

For the radial case, the results obtained with the K_d approach are upper bound (Figure 5.2.9 and Figure 5.2.10). The thermodynamic model shows a higher retention.

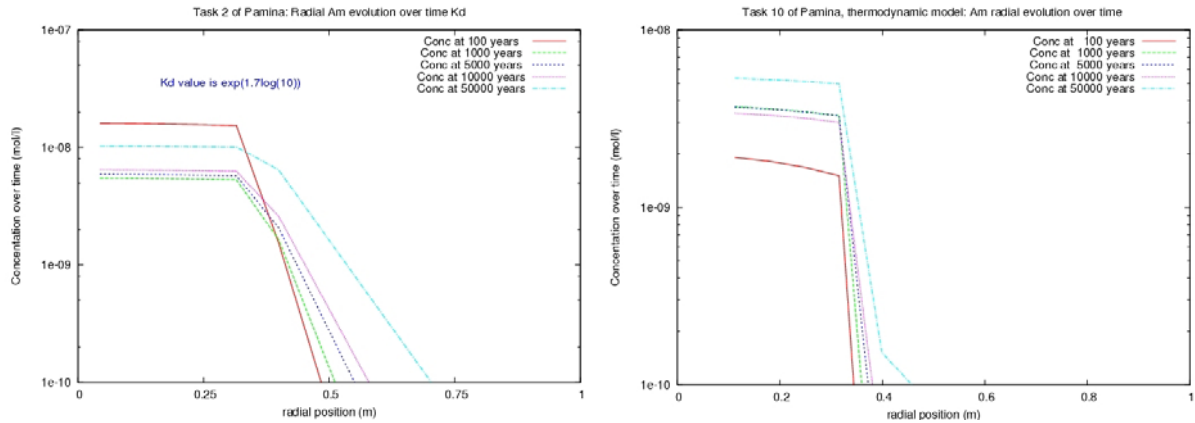


Figure 5.2.9: Am concentration profiles in claystone with K_d/SL (left) and thermodynamic (right) models

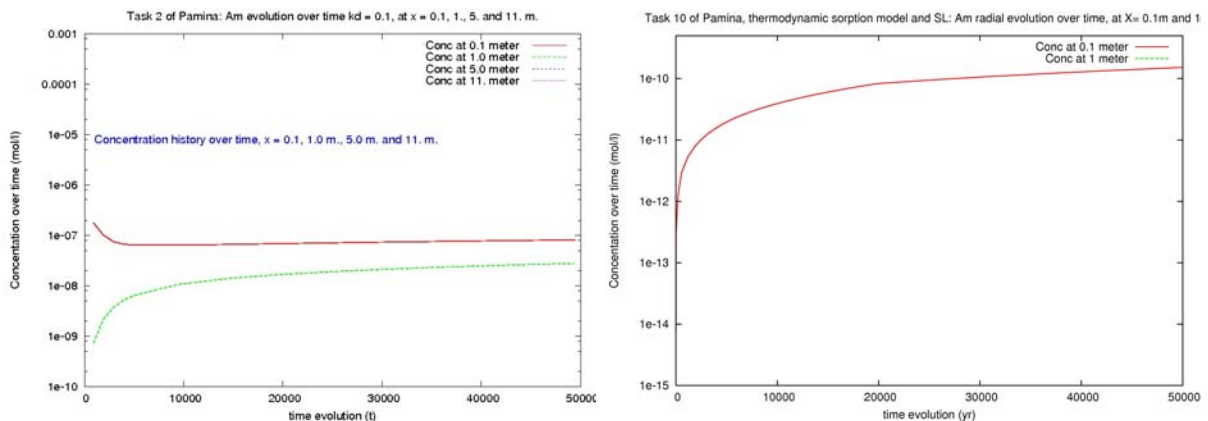


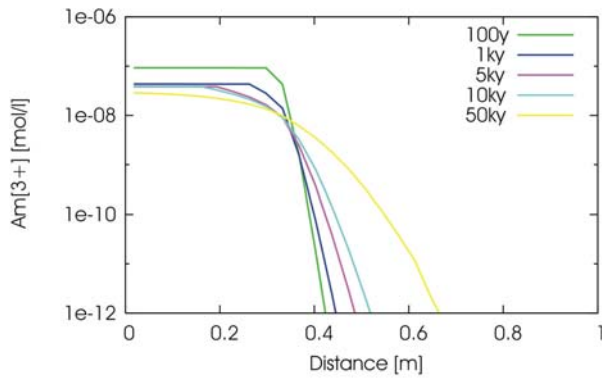
Figure 5.2.10: Am concentration at fixed points in the bentonite plug: $x = 0.1, 1, 5.0$ and 11 m with K_d/SL model (left) and $x = 0.1$ and 1.0 m with thermodynamic model (right)

5.2.3 Results from IRSN

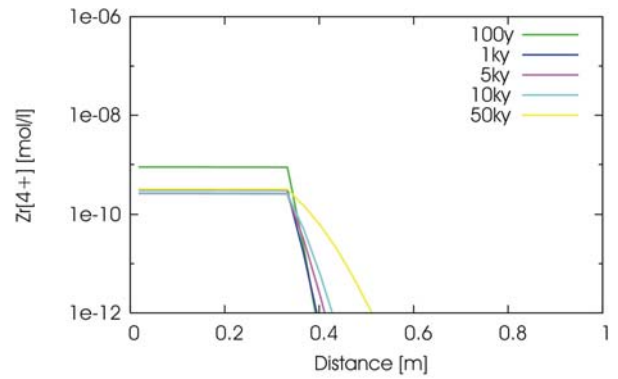
5.2.3.1 Linear K_D

A calculation with 2D-cylindrical symmetry has been attempted with an adapted grid and a simplified model. Am and Zr migration in the claystone is modelled in 1D-radial symmetry with constant K_D/SL , leading to similar results to those observed in the bentonite: Am and Zr are localized close to the waste package over 50,000 y (Figure 5.2.11 and Figure 5.2.12).

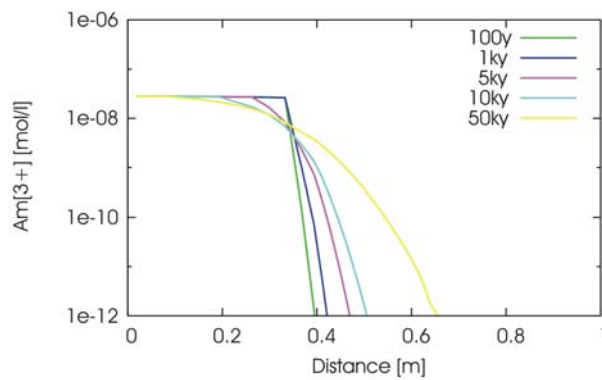
Method A - 50,000 y after release
of source term (Am)



Method A - 50,000 y after release
of source term (Zr)



Method B - 50,000 y after release
of source term (Am)



Method B - 50,000 y after release
of source term (Zr)

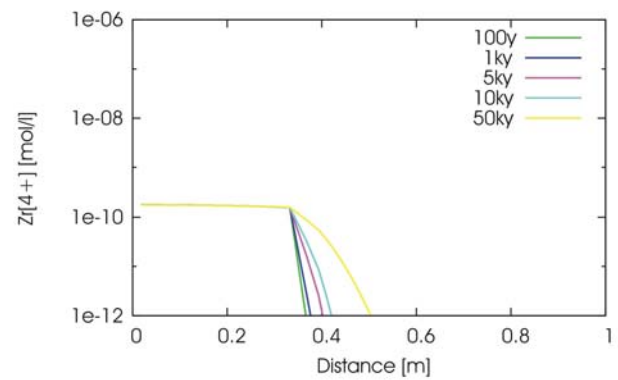


Figure 5.2.11: Task 2: 1D-radial. Migration of Am and Zr

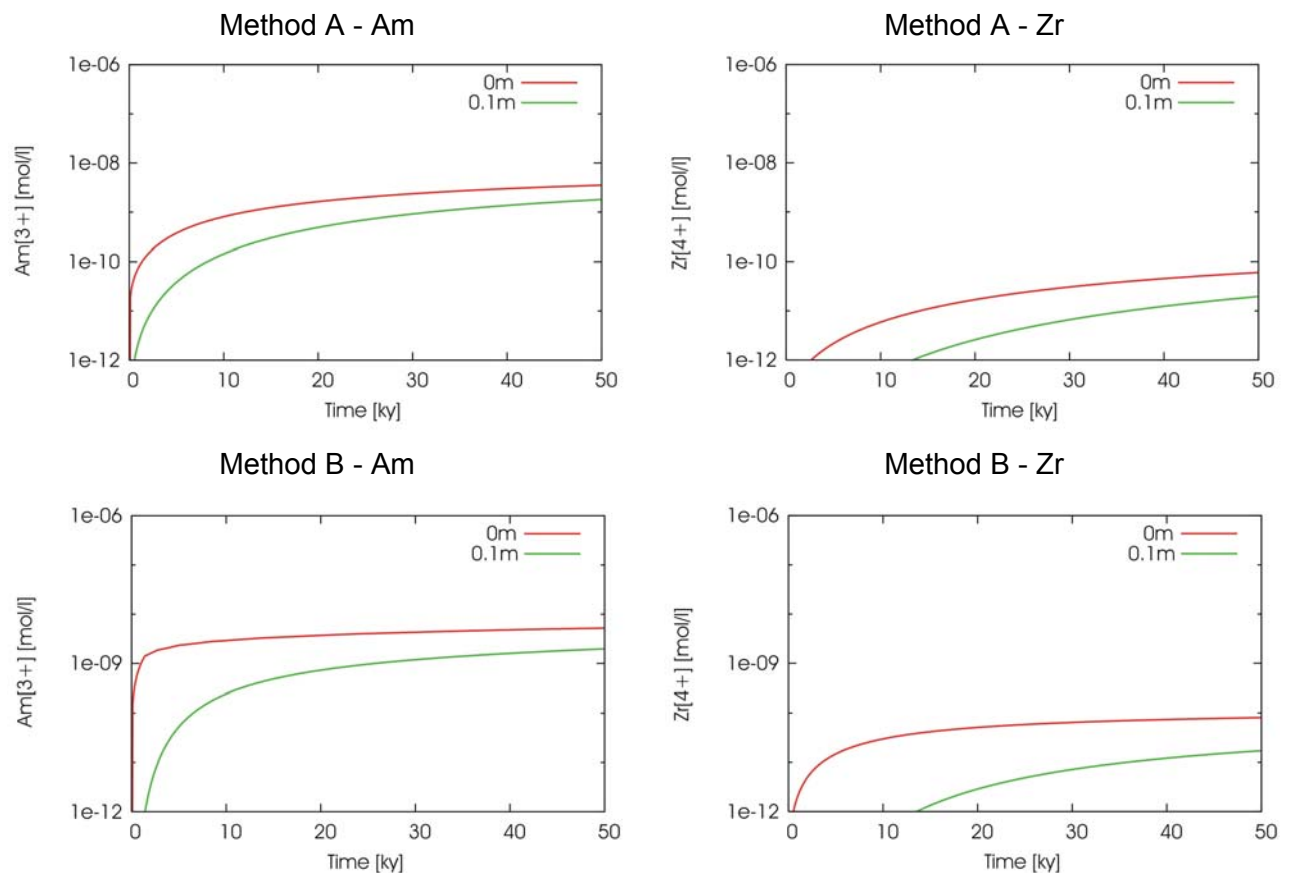


Figure 5.2.12: Task 2: 1D-radial. Migration of Am and Zr in the claystone 50,000 y after the release of radionuclides from the waste package at $x = 0$ m and $x = 0.1$ m.

5.2.3.2 Comparison of Am and Zr exercise results

The transfer of Am and Zr has been simulated with constant K_D/SL and with a full thermodynamic model. Globally, constant K_D/SL simulations resulted in a migration of Am and Zr localized close to the waste package (< 1 m in both bentonite and claystones). The migration of Am simulated with thermodynamic showed some different behaviours: Am is either localized close to the waste package or allowed to migrate further depending on the implemented conditions. Zr is barely retained in simulations with thermodynamic modelling and thus migrates over the whole domain.

As mentioned above, the transfer of Am is localized close to the waste package with constant K_D/SL (35 to 80 cm in the bentonite and 30 to 70 cm in the claystone depending on the method, see section 3.2.4 in M4.1.19 report (IRSN, 2009) for further details) and in some thermodynamic modelling (30 to 50 cm in the bentonite when Am concentration is controlled by $Am(OH)_3$ and amorphous $Am(OH)_3$). However, Am can migrate further in bentonite if its concentration is controlled by $AmOHCO_3$ (migration over 1.2 m) or if the concentration of its competitor (Ln) is controlled by $LnOHCO_3$ (migration over 2 m). This highlights that in thermodynamic modelling calculations, the choice of the pure phase controlling the studied radionuclide concentration is not the only fundamental, the choice of its competitive species is

important too, especially if their sorption affinity is high. This observation tends to confirm that constant K_D/SL modelling is not conservative in such specific conditions.

Discrepancies between constant K_D/SL and thermodynamic modelling are even more pronounced in the case of Zr: if its huge K_D values in both bentonite and claystones restrict its migration close to the waste package (15 to 85 cm in the bentonite and 15 to 50 cm in the claystone), the choice of particularly small sorption data in the benchmark definition causes its fast migration over the whole bentonite in 1D-axial simulations and in the whole domain in 2D-cylindrical simulations in full-thermodynamic model.

Constant K_D/SL modelling has not been found to be conservative comparatively to thermodynamic modelling in this study. Moreover, the discrepancies between K_D/SL and thermodynamic modelling are more pronounced for Am and Zr than for Cs. This statement highlights that the complexity of a radionuclide speciation induces a discrepancy in the comparison of K_D/SL and thermodynamic modelling.

Finally an overall modelling of Zr and Am is attempted in 2D-cylindrical geometry with an adapted grid (lower refinement and only 10 m of claystone) and scenario: only the Ln and Am co-precipitated phase is taken into account for Am and Ln migration without other competition effect and Zr aqueous concentration is controlled by $ZrSiO_4$ (Figure 5.2.13). Since no data about sorption on the claystones of Am and Zr is given in the benchmark definition, montmorillonite sorption data are used for claystones, with the application of a correction factor on the CEC. Despite the grid simplification, calculation time exceeds 6 days. Am migrates into the claystones and the bentonite over 1 m, whereas Zr reaches its solubility limit after 1,000 y in the whole domain.

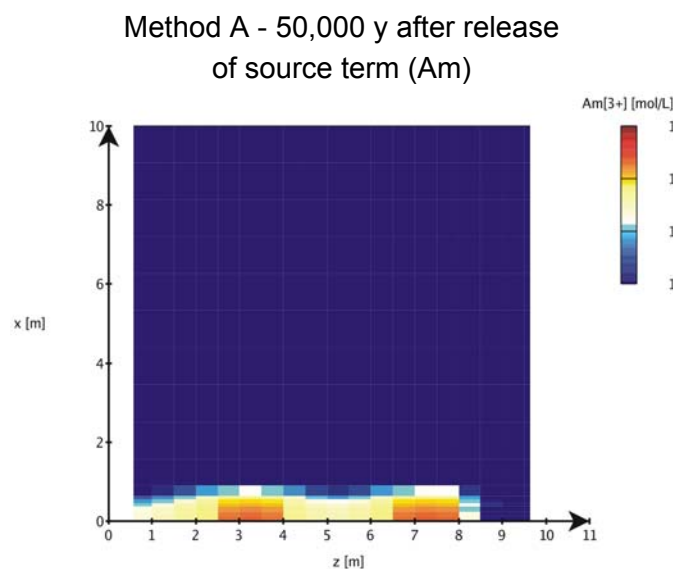


Figure 5.2.13: Task 12: Am migration modeling with 2D-cylindrical symmetry

5.2.4 Results from JRC

1D radial results are presented in Figure 5.2.14 for the release rates and concentrations.

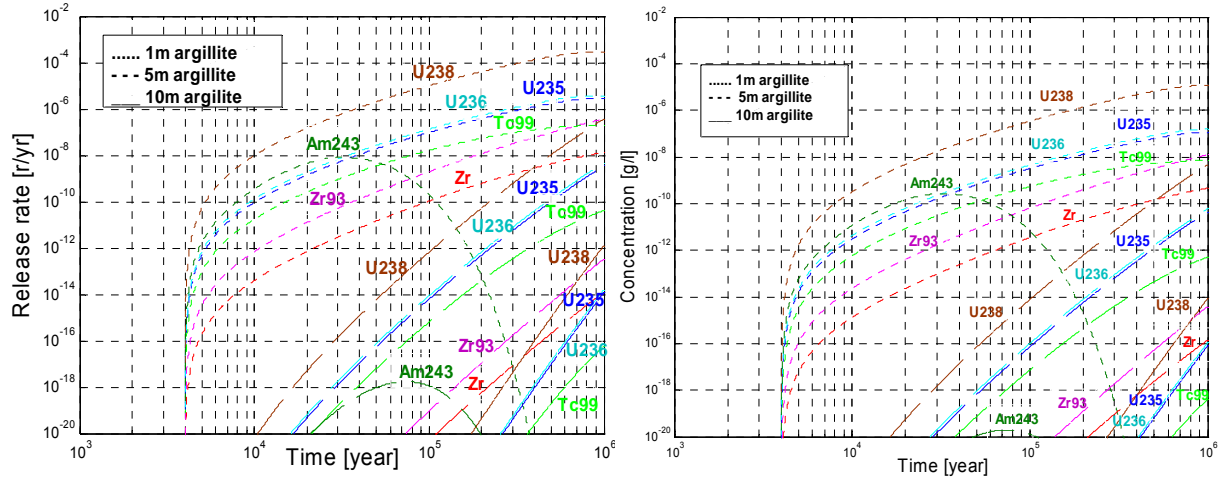


Figure 5.2.14: Release rates (left) and concentrations (right) in 1D radial direction, at 1 m (dot line), 5 m (dash line) and 10 m (solid line) through claystones

2D cylindrical calculations are presented in the form of two 1D plots in axial (Figure 5.2.15) and radial directions (Figure 5.2.16) for release rates as well as for concentrations.

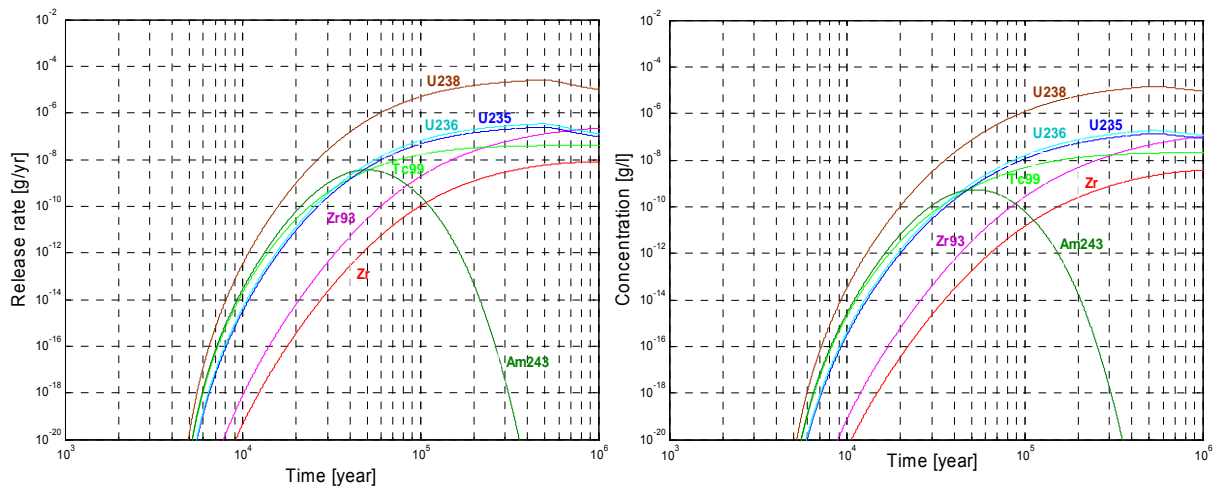


Figure 5.2.15: Release rates (left) and concentrations (right) in 2D axial direction, in the bentonite plug 1 m from the waste package

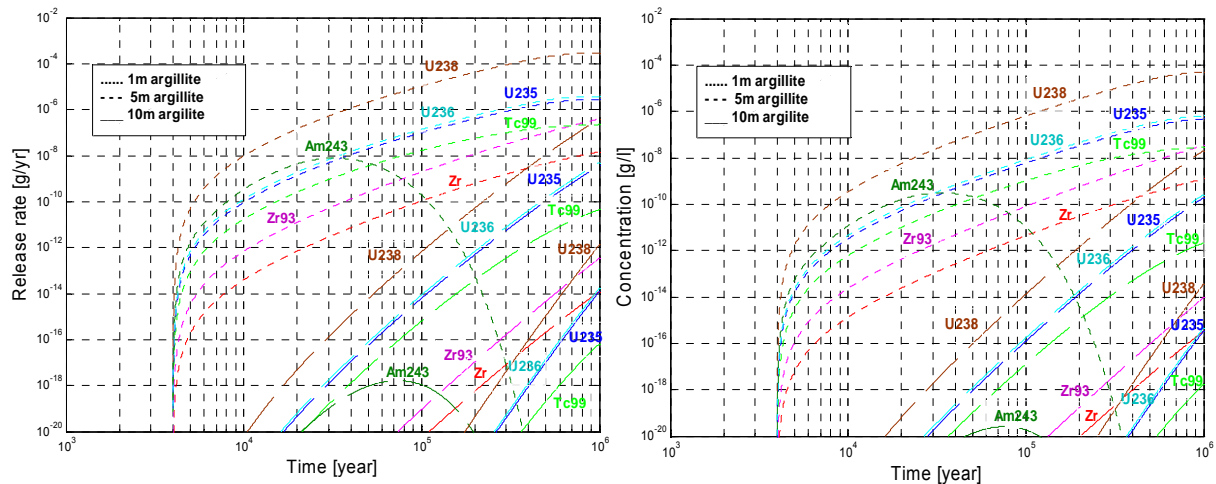


Figure 5.2.16: Release rates (left) and concentrations (right) in 2D radial direction, at 1 m (dot line), 5 m (dash line) and 10 m (solid line) through claystones

5.2.5 Results from SCK*CEN

In this exercise, a combination of sorption with a solubility limit is applied. Zr and Am are assumed to diffuse as cations.

5.2.5.1 Zr and Am inventory

The waste inventory is given in Table 2.2.3. A constant dissolution rate, in which the entire waste form (containing 1.2 kg Zr-93 and 0.22 kg Am-243) dissolves in 50,000 years, is assumed.

5.2.5.2 Process complexity and numerical simulation tools

Simple models

In these models linear reversible sorption described by a distribution coefficient (K_d) and/or a fixed concentration limit are included. Three cases are considered:

Case 1 (labelled as R in the figures): only sorption is accounted for. The same K_d values are used for the bentonite plug and the COx claystone. They are $100 \text{ m}^3/\text{kg}$ and $50.12 \text{ m}^3/\text{kg}$, for Zr and Am respectively.

Case 2 (labelled as SL in the figures): only a solubility limit is imposed. For Am, this limit is $4 \times 10^{-7} \text{ mol/l}$. For Zr, this fixed concentration limit includes competition with stable Zr:

$$\begin{aligned} [\text{Zr}] &= 2 \times 10^{-8} \text{ mol/l} * \text{fraction Zr-93 to total Zr} \\ &= 2 \times 10^{-8} \text{ mol/l} * 5.405 \times 10^{-2} \\ &= 1.08 \times 10^{-9} \text{ mol/l} \end{aligned}$$

Case 3 (labeled as SLR in the figures): sorption and solubility limit are both imposed.

Only case 3 results are shown in this report. Case 1 (sorption only, no solubility limit) and case 2 (solubility limit only, no sorption) results are presented in M4.1.17 report (SCK*CEN, 2009).



Complex models

These are thermodynamic models including surface sorption and ion exchange, for bentonite as well as for claystones. Thermodynamic data for montmorillonite surfaces are given in Table 6 of the benchmark definition. These data are applied for bentonite. However, the benchmark does not provide any information about which data to apply for claystones. Therefore, it was decided to take 33.4% of the values for montmorillonite as the claystone consist of 33.4% clay minerals according to Gaucher et al. (2004).

Two cases are examined:

Case 4, in which no competition with other elements is accounted for.

Case 5, for which beside the radio-isotopes Am and Zr, the waste also contains stable Zr, La, Ce, Pr, Nd, Sm and radio-isotopes Tc, U and Np. These will all compete for surface sites of clay minerals.

5.2.5.3 Overview of calculation cases

An overview of all calculation cases, indicating the geometry, the processes considered and the codes used is given in Table 5.2.1 and Table 5.2.2, for Zr and Am respectively. Note that in the thermodynamic cases (case 4 and 5), only sorption processes are calculated using thermodynamic equilibria and not the precipitation processes (due to lacking mineralogical data in the benchmark definition).

Table 5.2.1: Overview of calculation cases for Zr transfer

Task	Case	geometry	Solubility limit?	sorption on bentonite	sorption on C-O Clay (incl. EDZ)
Task 2	Case 1	1D radial	no		reference Kd: 1E+2 m ³ /kg
Task 2	Case 1	1D radial	no		reference Kd: 1E+2 m ³ /kg
Task 2	Case 2	1D radial	1.005E-7 kg/m ³		no
Task 2	Case 2	1D radial	1.005E-7 kg/m ³		no
Task 2	Case 3	1D radial	1.005E-7 kg/m ³		reference Kd: 1E+2 m ³ /kg
Task 2	Case 3	1D radial	1.005E-7 kg/m ³		reference Kd: 1E+2 m ³ /kg
Task 3	Case 3	1D axial	1.005E-7 kg/m ³	reference Kd: 1E+2 m ³ /kg	
	Case 4	1D radial	no	thermodynamic sorption model without competition	thermodynamic sorption model without competition
	Case 5	1D radial	no	thermodynamic sorption model with competition	thermodynamic sorption model with competition
Task 4	Case 1	2D radial	no	reference Kd: 1E+2 m ³ /kg	reference Kd: 1E+2 m ³ /kg
Task 4	Case 1	2D radial	no	reference Kd: 1E+2 m ³ /kg	reference Kd: 1E+2 m ³ /kg
Task 4	Case 2	2D radial	1.005E-7 kg/m ³	no	no
Task 4	Case 2	2D radial	1.005E-7 kg/m ³	no	no
Task 4	Case 3	2D radial	1.005E-7 kg/m ³	reference Kd: 1E+2 m ³ /kg	reference Kd: 1E+2 m ³ /kg
Task 4	Case 3	2D radial	1.005E-7 kg/m ³	reference Kd: 1E+2 m ³ /kg	reference Kd: 1E+2 m ³ /kg
Task 4	Case 3	2D radial	1.005E-7 kg/m ³	reference Kd: 1E+2 m ³ /kg	reference Kd: 1E+2 m ³ /kg

Legend:

	COMSOL Multiphysics 3.2
	PORFLOW 3.07
	PHREEQ-C

Table 5.2.2: Overview of calculation cases for Am transfer

Task	Case	geometry	Solubility limit?	sorption on bentonite	sorption on C-O Clay (incl. EDZ)
Task 2	Case 1	1D radial	no		reference Kd: 50.12 m ³ /kg
Task 2	Case 1	1D radial	no		reference Kd: 50.12 m ³ /kg
Task 2	Case 2	1D radial	9.72E-5 kg/m ³		no
Task 2	Case 2	1D radial	9.72E-5 kg/m ³		no
Task 2	Case 3	1D radial	9.72E-5 kg/m ³		reference Kd: 50.12 m ³ /kg
Task 2	Case 3	1D radial	9.72E-5 kg/m ³		reference Kd: 50.12 m ³ /kg
Task 3	Case 3	1D axial	9.72E-5 kg/m ³	reference Kd: 50.12 m ³ /kg	
	Case 4	1D radial	no	thermodynamic sorption model without competition	thermodynamic sorption model without competition
	Case 5	1D radial	no	thermodynamic sorption model with competition	thermodynamic sorption model with competition
Task 4	Case 1	2D radial	no	reference Kd: 50.12 m ³ /kg	reference Kd: 50.12 m ³ /kg
Task 4	Case 1	2D radial	no	reference Kd: 50.12 m ³ /kg	reference Kd: 50.12 m ³ /kg
Task 4	Case 2	2D radial	9.72E-5 kg/m ³	no	no
Task 4	Case 2	2D radial	9.72E-5 kg/m ³	no	no
Task 4	Case 3	2D radial	9.72E-5 kg/m ³	reference Kd: 50.12 m ³ /kg	reference Kd: 50.12 m ³ /kg
Task 4	Case 3	2D radial	9.72E-5 kg/m ³	reference Kd: 50.12 m ³ /kg	reference Kd: 50.12 m ³ /kg
Task 4	Case 3	2D radial	9.72E-5 kg/m ³	reference Kd: 50.12 m ³ /kg	reference Kd: 50.12 m ³ /kg

Legend:

	COMSOL Multiphysics 3.2
	PORFLOW 3.07
	PHREEQ-C

5.2.5.4 Kd/SL model

In this section, concentration profiles (Zr-93 and Am-243 concentrations as a function of distance) and Zr-93/Am-243 concentration in the observation sorption nodes as a function of time are shown for the different cases.

Zr-93

The following figures are shown and discussed for the Kd/SL model:

Figure 5.2.17: radial concentration profiles for Zr-93

Figure 5.2.18: axial concentration profiles for Zr-93

Figure 5.2.19: Zr-93 precipitate build-up in the waste zone

Figure 5.2.20: Zr-93 concentration at 1 m from the waste zone

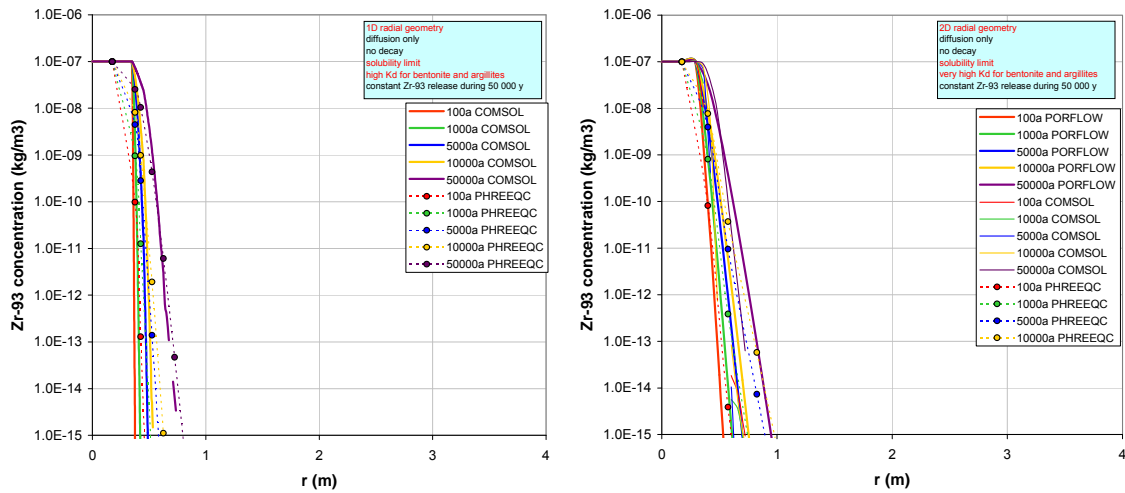


Figure 5.2.17: *Zr-93 radial concentration profiles for the Kd/SL model with linear sorption and solubility limit (left: 1D radial and right: 2D cylindrical)*

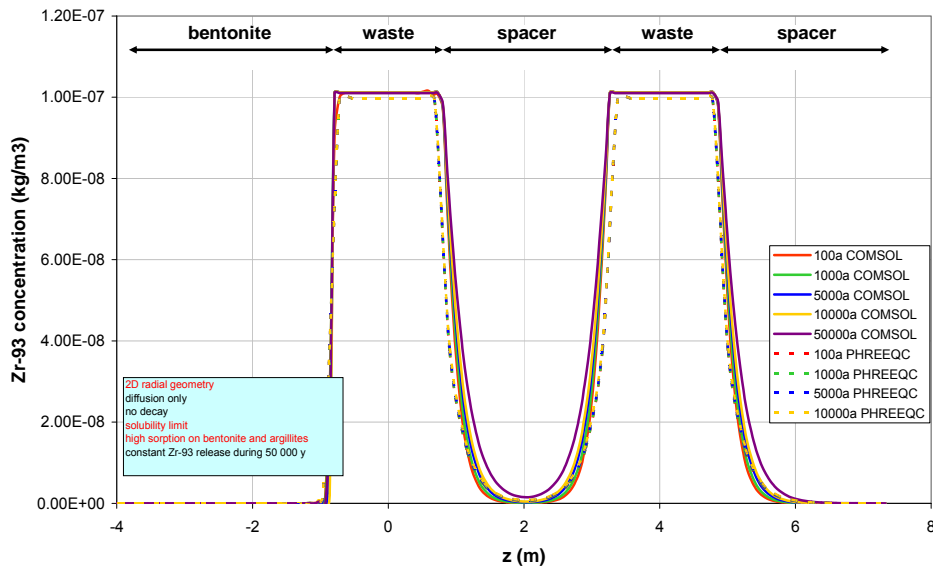


Figure 5.2.18: *Zr-93 axial concentration profiles for the simple model with linear sorption and solubility limit (2D)*

There seems to be a good agreement between COMSOL and PHREEQC predictions, although this case is difficult to evaluate. Combination of linear sorption and solubility limit gives extremely low concentrations (Figure 5.2.17 and Figure 5.2.18).

It was found that for exercise 2 the migration characteristics of the considered species are such that they are immobile, even for the relatively long timescales studied here. As a consequence, in most cases no meaningful concentrations were reached at the observation points defined in the benchmark. Therefore it is decided to show the build-up of precipitate (Figure 5.2.19) for the solubility limited cases. It is clear that the relative amount of Zr in the

vitrified waste is so high compared to its solubility limit that the latter is attained already in the first years of waste dissolution. Comparable figures are obtained for the 2D calculations.

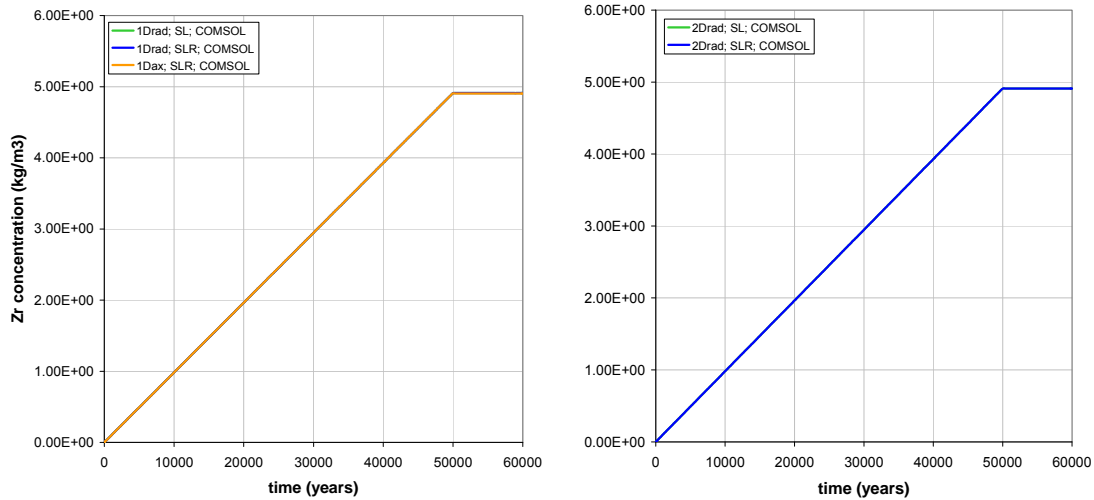


Figure 5.2.19: Zr-93 precipitate build-up in the waste zone for case 2 and 3, 1D radial (left) and 2D cylindrical (right) calculations.

Figure 5.2.20 shows the Zr concentration evolution at 1 m from the waste zone in the axial direction (Figure 5.2.20 right) and the radial direction (Figure 5.2.20 left). In case only the Zr solubility limit was modelled (without sorption), Zr is able to migrate in noticeable quantities in the near field. When sorption processes (here K_d) are included in the model, Zr is immobile and no signal is obtained at 1 m distance from the waste zone during the computed time span.

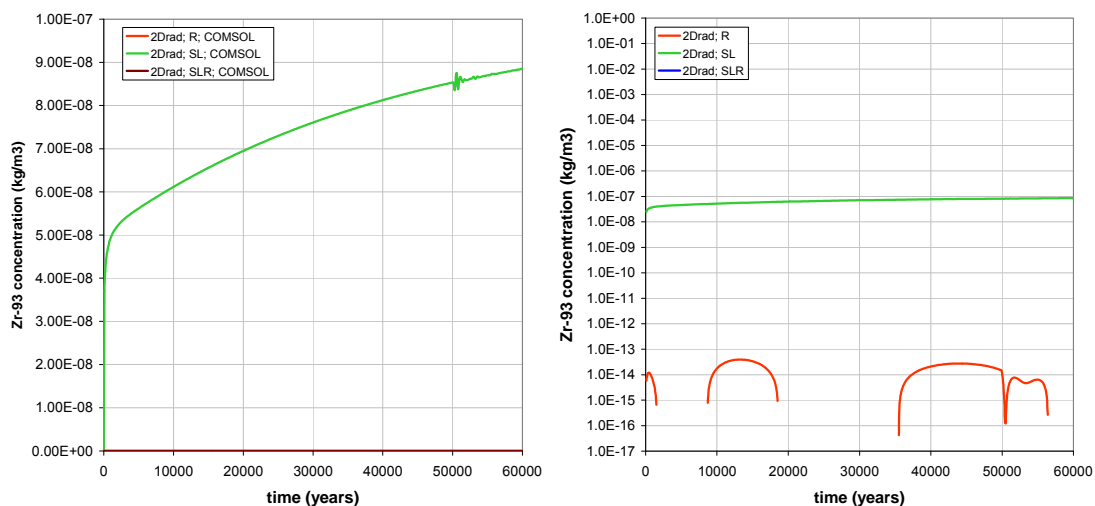


Figure 5.2.20: Zr-93 concentration at 1 m from the waste zone for the different cases (2D radial left and 2D axial right).

Am-243

The following figures are shown and discussed for the K_d/SL model:

Figure 5.2.21 radial concentration profiles for Am-243

Figure 5.2.22: axial concentration profiles for Am-243

Figure 5.2.23: Am-243 concentration precipitate build-up in the waste zone

Figure 5.2.24: Am-243 concentration at 1 m from the waste zone

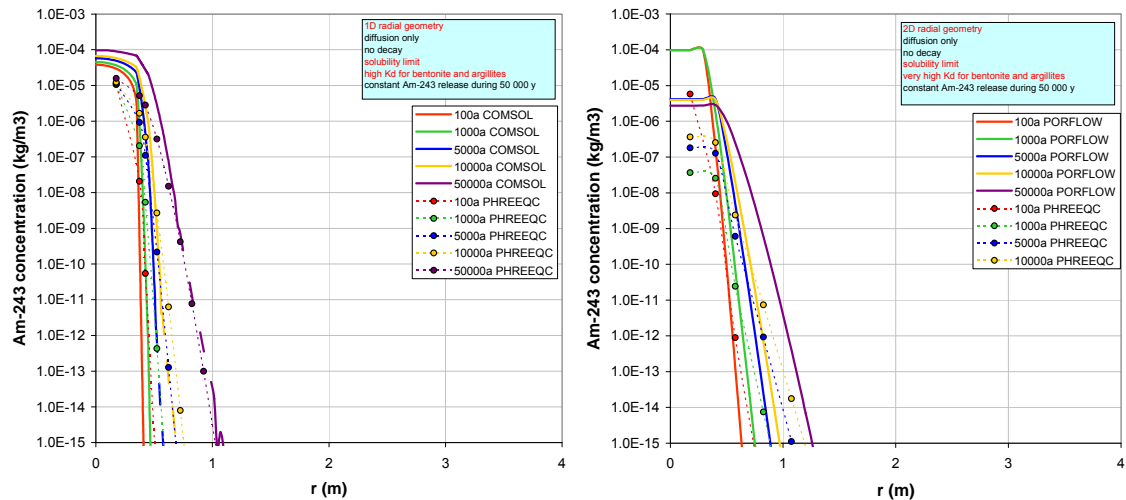


Figure 5.2.21: Am-243 radial concentration profiles for the simple model with linear sorption and solubility limit (1D and 2D)

The 2D radial model for Am gave a lot of stability and convergence problems in COMSOL. No results could be obtained. In PORFLOW, the code does not allow to implement a gradual dissolution (flux type source) combined with the implementation of a concentration limit (constant concentration type source). Hence, the whole inventory is available from the start when a concentration limit is defined (see Figure 5.2.21 right). While in PHREEQC the gradual dissolution results in increasing concentrations with time (until the solubility limit, which is not reached in this case), the PORFLOW results show solubility limited concentration profiles in the beginning, and decreasing concentrations in a later phase. These conceptual differences make it difficult to compare the PHREEQC and PORFLOW results.

Axial Am-243 concentration profiles for the 2D case are shown in Figure 5.2.22. As for the Zr migration exercise, the agreement between the codes for the 2D case is worse.

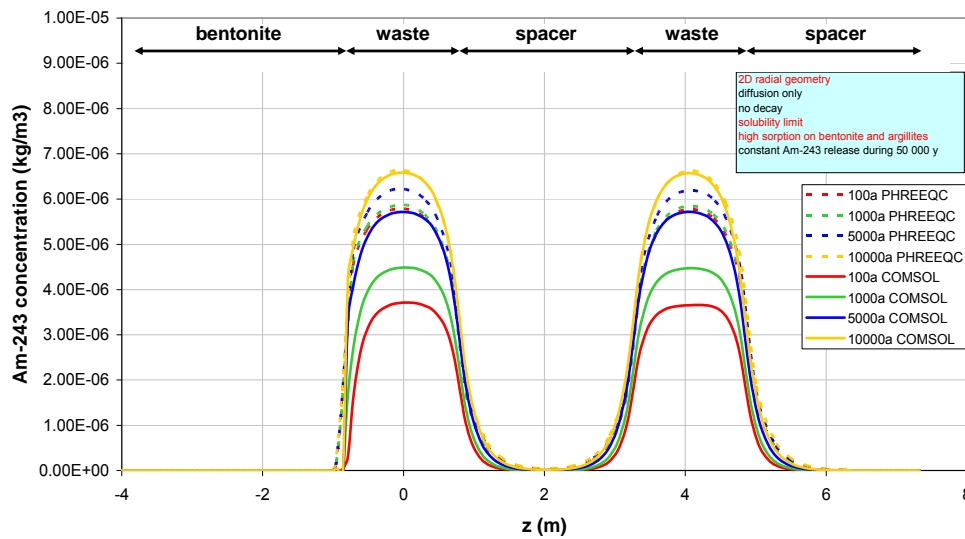


Figure 5.2.22: Am-243 axial concentration profiles for the simple model with linear sorption and solubility limit (2D)

Although COMSOL encountered some stability and convergence problems for the 2D Am transport simulations, output was obtained for the precipitate evolution in the waste zone. In Figure 5.2.23, the Am-243 precipitation build-up in the waste is shown for several radial 1D (left) and 2D calculation cases (right).

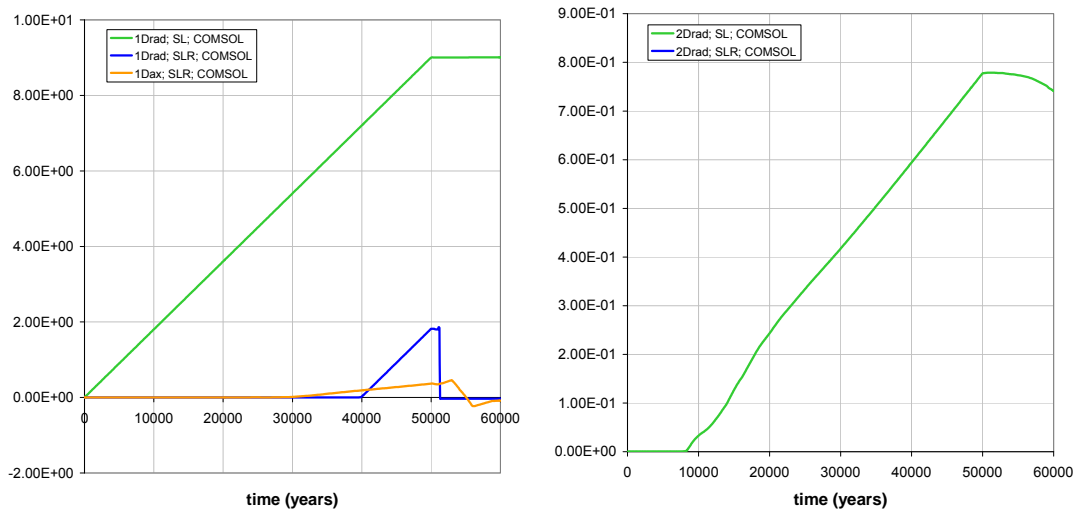


Figure 5.2.23: Am-243 precipitate build-up in the waste zone, for case 2 and 3. Left: 1D radial. Right: 2D calculation

Finally, Figure 5.2.24 shows the Am-243 concentration evolution at 1 m (radial and axial) from the waste in the 2D calculation case. When sorption is modelled, no meaningful results were obtained at that distance.

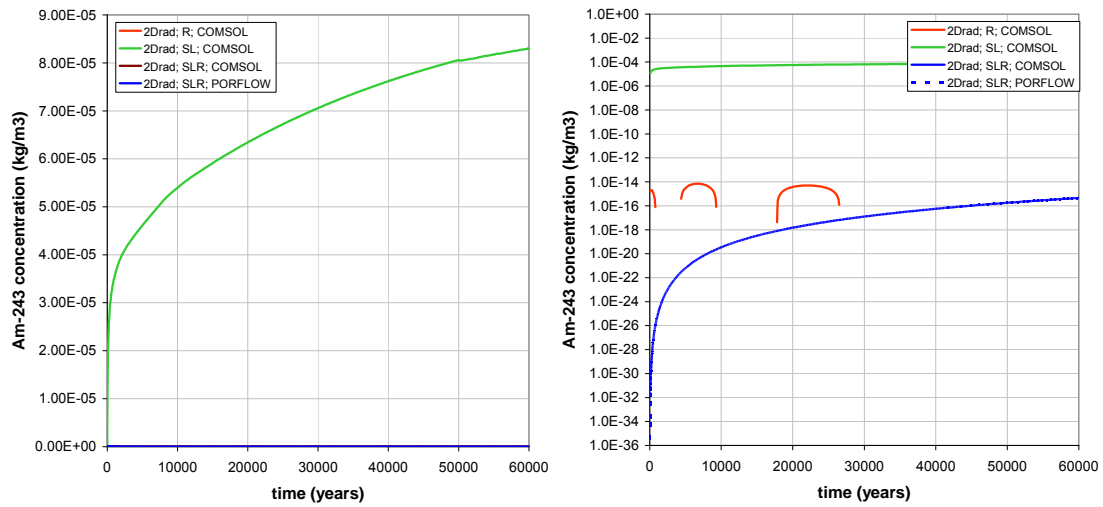


Figure 5.2.24: Am-243 concentration at 1 m from the waste zone for the 2D cases. Left: radial point, right: axial point

5.2.5.5 Thermodynamic model

Results for case 4 (thermodynamic model without competition) and Case 5 (thermodynamic model including competition with stable Zr, La, Ce, Pr, Nd, Sm, Tc, U and Np), are shown in Figure 5.2.25.

Results for the thermodynamic model without competition are very similar to those for the simple model implementing linear sorption only (case 1) and thus do not provide additional value. Concerning case 5, only sorption processes are calculated using thermodynamic equilibria and not the precipitation processes (due to lacking mineralogical data in the benchmark definition). It is clear that the competition for surface sites results in higher concentrations. This is the most pronounced for Zr-93.

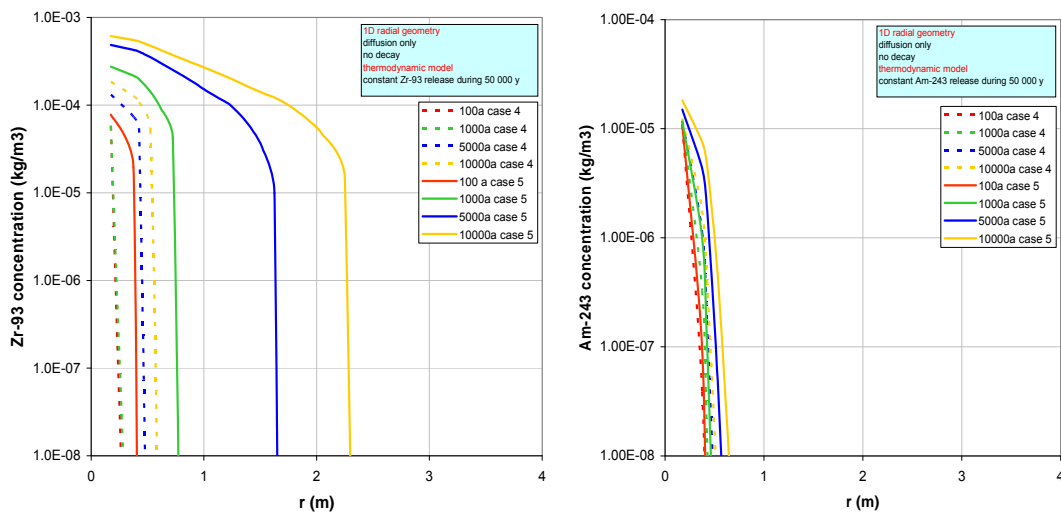


Figure 5.2.25: Zr-93 radial (left) and Am-243 (right) concentration profiles for the thermodynamic model (1D radial model)



5.2.5.6 Conclusions for exercise 2

Some conclusions for exercise 2 are as follows:

Imposing heavy sorption and low solubility in the same model run gives stability/convergence problems (COMSOL Multiphysics) and very long runs (all codes). This may require the application of smoothing functions and a more efficient solving strategy. However, this numerical optimisation process has not been performed.

Due to the proposed high K_d values, the output is not ideal for comparison: the concentrations are extremely low and there is no increase in radionuclide concentration at most of the observation points. Using radionuclide precipitation is a more useful output for model benchmarking. This shows that for exercise 2, upscaling of thermodynamic models to repository scale may not be appropriate (or that timescales are too short in this case to observe radionuclide migration in the simulations).

For the thermodynamic cases, it is important to consider competition effects as these might be non-negligible as was observed for Zr.

5.2.6 General comments

Some results were provided by Andra, CEA, IRSN and SCK*CEN.

Andra only performed calculations in radial 1D. They conclude that Kd/SL model is very conservative for Zr since a mineral precipitation is obtained for the full geochemical model. Conversely, Am migrates further with the thermodynamic model.

CEA didn't perform the full geochemical modelling and they went to the opposite conclusion: Kd/SL is conservative for Am and Zr concentrations are out of bounds.

IRSN also got various results for the thermodynamic model, depending on the controlling phase. They conclude that Kd/SL model is not conservative for both species.

SCK*CEN notes that there is an important competing effect when Zr transfer is modelled with the thermodynamic approach.

One can conclude that the necessary data for the thermodynamic model are not clearly known. This leads to an overestimation of Zr and Am transfer calculated with thermodynamic models. It is also necessary to solve the full geochemical model in order to identify the precipitation processes. Finally, Kd/SL data were not obtained in the *in-situ* conditions. These facts may explain the large differences between models for these radionuclides.



6 General discussions

The purpose of the present work was to model the migration of caesium (Cs), americium (Am) and zirconium (Zr) over a 50,000 y simulation period out a HLW-package into the surrounding bentonite and argillaceous host rock with different approaches such as constant K_D /SL, Langmuir isotherm and full thermodynamic model, in order to compare the particularities highlighted by these different methods. This study has been performed using the layout detailed in the benchmark definition (Andra, 2007).

Five participants took part to this benchmark, among which four led to important results allowing discussions and interpretations. Despite many data were proposed in the benchmark definition, the modelling approach was not described in enough details, thus allowing participants to use different geochemical models, different source term definitions and different numerical tools. Among all these differences, they all got to interesting conclusions developed and discussed in the present report.

Rather than trying to write an intricate general conclusion based the numerous calculations performed by every participants with different modelling approaches and simplifications, the conclusion written hereafter collects those written by participants, hence comparing and discussing sorption models. Some concluding statements then bring out similarities and discrepancies among these conclusions.

6.1 Participants' conclusions

6.1.1 *Andra's conclusions*

Simulations undertaken in this benchmark exercise show a great capacity of chemical-transport tools to simulate the radionuclide transfers with increasing complexity model (Kd/Langmuir/thermodynamic) with Phreeqc.

The calculated evolutions show that the Kd/SL model appears to be conservative for the Cs migration in the bentonite plug and that Cs migrates over the all plug in all cases, highlighting the need to explicitly describe the chemistry evolution of the opposite frontier over time (in contact with a concrete material) to enhance the thermodynamic simulations. In radial simulations, the Kd/SL appears to be no more conservative but Cs never migrates over distances higher than 6m for the Kd/SL model and 8 m for the thermodynamic one.

Zr is strongly retained with every considered models (Kd/SL and thermodynamic) very close to the waste package, since Zr never migrates over distances higher than 0.6 m in the bentonite plug and 1m in the claystone. It has to be mentioned that the mineral phase controlling the precipitation of Zr has to be precisely documented in the thermodynamic database to confirm such weak solubility limits.

As well as Zr, Am does not migrate over distances higher than 1 m in the bentonite plug and 6 m in the claystone. In both cases, the Kd/SL is not conservative. Actually, considering the



global radioisotope competition for the same exchange sites always lead to higher migration distances with the thermodynamic model.

The numerical tool present still some limitations, particularly concerning the geometry complexity (2D) or the resolution of numerical problems with the use of solid solutions, but also presents a great flexibility to refine the level of description following the final need of the simulation (phenomenological or preparatory simulations).

This benchmark exercise was the occasion to more efficiently analyze the simplification made in the performance assessment approach comparing to the phenomenological approach in order to draw safety margins.

6.1.2 CEA's conclusions

The results obtained with the Alliance platform (with Cast3m for generalized transport and Chess/Cast3m for reactive transfer) shows that for the Cs we can obtain consistent results between the three approaches in the axial case (Bentonite) in opposition to the radial case (Claystone plus EDZ). In opposition, the Zr simulations don't give which consistent results for the axial case. For the Am, the very high retention expected is observed on all the models and geometries.

In order to compare the simulations done with the thermodynamic models against simplest models as Kd or Langmuir, many simplifications have been done. Then we took into account the essential phenomenon in regard of the codes capabilities. The results show that the answer at the question "is the Kd model (with the considered values) upper bound?" is not unique in this benchmark. One essential cause can be the simplifications done.

Because of the gap of complexity between thermodynamic approach (which implies the use of reactive transport codes) and Kd approach (which can be used in generalized transport codes), it can be useful to describe more level of complexity for the thermodynamic model. Then more and more complicated computations can be done and compared in order to explain unexpected results. Also, if we had taken the same geometries, and exactly the same thermodynamic models, the comparisons between the different codes used in this benchmark could have been done.

6.1.3 IRSN's conclusions

The simulations performed in the present study indicate that globally, the constant K_D/SL modelling does not appear to be the most conservative method with the values chosen in the benchmark definition. Even if the order of magnitudes are not considerably different concerning the Cs and Am migration, the transfer of Zr highlighted strong discrepancies between the constant K_D/SL and full thermodynamic modelling. The calculated evolutions point out that:

- Cs migrates in the claystone from 6 m with constant K_D/SL model to 11 m with thermodynamic model, and over the whole bentonite plug in all cases,

- Am is restricted to an area close to the waste package (inferior to 1 m) with constant K_D /SL model and some cases treated with thermodynamic model, but may also migrate further under specific conditions. It is precisely worth mentioning that the choice of the pure phase controlling the studied radionuclide concentration, and also this of its competitive species, is fundamental in full thermodynamic modelling,
- Zr is also retained in an area close to the waste package in constant K_D modelling, whereas Zr is not sorbed at all in full thermodynamic modelling, leading to its transfer (only driven by diffusion) in the whole bentonite and host rock due to the lack of reliable data concerning Zr sorption.

To summarize, the present study highlighted that constant K_D /SL models can lead to results close to those obtained with thermodynamic modelling with considerably lower calculation times: the simulations performed are globally similar concerning the Cs migration, but a difference is noticed regarding to Am and especially Zr transfer. Parameters such as grid size refinement and symmetry are found to have a major influence on the K_D /SL constant modelling results: transfer processes are better described with a 2D-cylindrical or a 3D simulation grid, and a good compromise between calculation accuracy and timescale has been determined. Furthermore, most K_D values chosen for this work do not correspond to thermodynamic data, which can be explained either by the lack of consolidation of thermodynamic values (especially regarding to the sorption of radionuclides on the argillaceous host rock) or by a too high confidence in the K_D determination method.

6.1.4 SCK*CEN's conclusions

As the calculation cases were not unequivocally defined within the benchmark description (see Milestone M 4.1.2 (clay case) of the PAMINA project (Andra, 2007)), SCK*CEN chose to perform a wide range of calculations focussing on various levels of process complexity using the tools COMSOL Multiphysics, PORFLOW and PHREEQC. As such, all tasks defined in the benchmark definition have been performed, though based on a fairly simple description of the release of radionuclides from the waste (the source term). Furthermore, application of thermodynamic equilibrium for precipitation processes involving competition (part of exercise 2) could not be assessed due to lack of mineralogical data (not defined in the benchmark description). Nevertheless, the primary objective of this benchmark exercise was to elucidate whether or not the application of a more mechanistic description of the sorption process to model radionuclide migration on the repository scale provides any added value. In that respect, the following conclusions are drawn based on the studied cases:

- It is clear that the implementation of thermodynamic models for spatial scales and timescales (> 1M years) of relevance to a full performance/safety analysis remains practically not feasible in PHREEQC due to excessive computational times.
- For some cases (like e.g. Cs), a linear model is found to be sufficient to represent sorption. This is not surprising since the concentration range expected in the geosphere and even in the immediate vicinity of the waste packages (near field) is relatively small. For such diluted systems, there is no need to calculate sorption processes taking into account competitive aspects using thermodynamic models since

most isotherms are linear in the lower concentration range (e.g., up to 10^{-3} kg/m for Cs when using cation exchange competition model). Moreover, in the prevailing repository conditions, the isotherm is not expected to vary significantly as a function of the geochemical conditions on the species' migration path. Of course, it is acknowledged that these phenomena are element dependent and linked to the applied release model.

- Whenever the sorption behaviour is independent of variations in geochemical conditions (especially competition), sorption can be described by adsorption isotherms. Such isotherms (any shape) can be inserted into physical models. This avoids long runs usually inherent to geochemical codes (for the considered timescales).
- However, comparison of thermodynamic models with simple models for "intermediate" scales (repository near field) and relatively short timescales (compared to traditional PA timescales) can provide supporting information for how to choose adequate K_d values for the expected concentration range. Especially competition effects may be revealed more explicitly and could warrant for a more conservative choice of K_d .
- Finally, the comparison of results from conservative, simplified calculations with a more realistic (whether explicitly calculated thermodynamic approaches or just variant isotherm shapes) analysis could also demonstrate quantitatively the safety margin implicitly present in PA calculations through model abstraction.

6.2 General comments

Defining a benchmark with open technical means is difficult. For that reason all participants managed to model something allowing some qualitative discussions but it is impossible to compare their quantitative results. For instance, it isn't worth comparing the RN concentration at a given point and date. However all participants have validated their numerical tools and they have all plot the same data. For that reason it is possible to compare their discussions and it is tremendous to note that the same conclusions have been written by every participant:

- Differences between K_d/SL and thermodynamic models for Cs transfer modeling are relatively small. However K_d/SL model is not conservative. This can be either explained by geochemical changes in the near field (Andra) or K_d s measured in specific conditions
- Competing effect of Rb is low
- Modelling Zr and Am transfer is very difficult due to their very low solubility limits and huge K_d s. This led to significant differences between simple and thermodynamic results
- A full geochemical calculation is necessary for achieving an accurate RN transfer in the near field. For that purpose, thermodynamic databases and numerical tools have to be implemented
- In the scope of performance assessment calculations, the studied radionuclides have minor influence and the large scale transfer is not influenced by competition and geochemical changes. K_d/SL model remains the most appropriate as far as distribution coefficients (K_d) and solubility limits (SL) are measured in relevant situations.



References

- Andra (2005a) Référentiel de comportement des radionucléides et des toxiques chimiques d'un stockage dans le Callovo-Oxfordien jusqu'à l'homme - Site de Meuse/Haute-Marne. Rapport Andra N° C.RP.ASTR.04.0032.B
- Andra (2005b) Dossier 2005 argile - Référentiel du site de Meuse / Haute-Marne. Rapport Andra n° C.RP.ADS.04.0022.B
- Andra (2005c) Dossier 2005 argile – Tome Architecture et gestion du stockage géologique. Rapport Andra n° C.RP.ADP.04.0001.B
- Andra (2007) Pamina M 4.1.2 - Radionuclide migration in the near field (clay rock): First Benchmark specification for sensitivity analysis on “Kd” and “solubility limit” models / geochemical transport (Eric Giffaut, Alain Dimier, Laurent Trotignon, François Marsal, Christophe Serres, Karl-Fredrik Nilsson and Eef Weetjens)
- Andra (2009) Pamina M 4.1.18 - Contribution de l'Andra au benchmark sur la migration de radionucléides dans le champ proche (B. Cochapin)
- Arcos, D., Grandia, F. and Domènech, C. (2006). Geochemical evolution of the near field of a KBS-3 repository, Technical Report TR-06-16, SKB (S).
- Gaucher, E., Robelin, C., Matray, J.M., Négrel, G., Gros, Y., Heitz, J.F., Vinsot, A., Rebours, H., Cassagnabère, A., Bouchet, A., (2004) ANDRA underground research laboratory: interpretation of the mineralogical and geochemical data acquired in the Callovian-Oxfordian formation by investigative drilling. *Physics and Chemistry of the Earth* 29, 55-77.
- Gaucher, E. C., Blanc, P., Bardot, F., Braibant, G., Buschaert, S., Crouzet, C., Gautier, A., Girard, J. P., Jacquot, E., Lassin, A., Négrel, G., Tournassat, C., Vinsot, A., and Altmann, S., (2006a). Modelling the porewater chemistry of the Callovian-Oxfordian formation at a regional scale. *Comptes Rendus Geoscience* 338, 917-930.
- Gaucher et al. (2006b) 'Caractérisation géochimique des forages PAC et nouvelles modélisations THERMOAR', BRGM/RP-54416-FR
- Gaucher, E. C., Tournassat, C., Jacquot, E., Altmann, S., and Vinsot, A. (2007) Improvements in the modeling of the porewater chemistry of the Callovian-Oxfordian formation. *Clays. Natural & Engineered Barriers for Radioactive Waste Confinement*, Lille, France.
- Grambow B., Fattahi M., Montavon G., Moisan C., Giffaut E. (2006) Sorption of Cs, Ni, Pb, Eu(III), Am(III), Cm, Ac(III), Tc(IV), Th, Zr, and U(IV) on MX 80 bentonite: An experimental approach to assess model uncertainty. *Radiochemica acta*, **94**, pp 627-636
- IRSN (2009) Pamina M 4.1.19 - Modelling of radionuclide migration in the near field of a high-level waste disposal with HYTEC and MELODIE (François Marsal)



Lerouge, C., Michel, P., Gaucher, E. C., and Tournassat, C. (2006) A geological, mineralogical and geochemical GIS for the Andra URL: A tool for the water-rock interactions modeling at a regional scale. In: SKB (Ed.), FUNMIG - 2nd annual workshop, Stockholm-Sweden.

Sauzeat E., Guillaume D., Neaman A., Dubessy J., François M., Pfeiffert C., Pelletier M., Ruch R., Barres O., Yvon J., Villéras F. & Cathelineau M. (2001) Caractérisation minéralogique, cristallographique et texturale de l'argile MX80. Rapport Andra n° CRP0ENG 01-001, 82 p.

SCK*CEN (2009) Pamina M 4.1.17 - Contribution to reporting results of the clay benchmark (Eef Weetjens, Evelien Martens and Diederik Jacques)

Van der Lee J., De Windt L., Lagneau V., Goblet V. (2003) Module-oriented modeling of reactive transport with HYTEC. Computers & Geosciences 29, pp 265-275.

Van der Lee J. (2005) Reactive transport modelling with HYTEC Users guide and tutorial. Technical report LHM/RD/05/30, Ecole des Mines de Paris (France).